From bound states to the continuum

Calvin W. Johnson[1], Kristina D. Launey[2], Naftali Auerbach[3], Sonia Bacca[4], Bruce R. Barrett[5], Carl Brune[6], Mark A. Caprio[7], Pierre Descouvemont[8], Willem H. Dickhoff[9], Charlotte Elster[6], Patrick J. Fasano[7], Kevin Fossez[10], Heiko Hergert[10,11], Morten Hjorth-Jensen[10,11], Linda Hlophe[10], Baishan Hu[12], Rodolfo M. Id Betan[13], Andrea Idini[14], Sebastian König[15], Konstantinos Kravvaris[16], Dean Lee[10,11], Jin Lei[6], Pieter Maris[21], Alexis Mercenne[2], Kosho Minomo[11], Rodrigo Navarro Perez[1], Witold Nazarewicz[10,11], F. M. Nunes[10,11], Marek Ploszajczak[17], Sofia Quaglioni[18], Jimmy Rotureau[10], Gautam Rupak[19], Andrey M. Shirokov[20], Ian Thompson[18], James P. Vary[21], Alexander Volya[16], Furong Xu[12], Vladimire Zelevinsky[10,11], and Xilin Zhang[22]

[1]Department of Physics, San Diego State University, San Diego, CA 02182-1233, USA
[2]Department of Physics and Astronomy, Louisiana State University, Baton Rouge, LA 70803, USA
[3]School of Physics and Astronomy, Tel Aviv University, Tel Aviv 69978, Israel
[4]Institut für Kernphysik and PRISMA Cluster of Excellence, Johannes Gutenberg-Universität Mainz, 55128 Mainz, German
[5]Department of Physics, University of Arizona, Tucson, Arizona 85721
[6]Institute of Nuclear and Particle Physics, and Department of Physics and Astronomy, Ohio University, Athens, OH 45701, USA
[7]Department of Physics, University of Notre Dame, Notre Dame, IN 46556, USA
[8]Physique Nucleaire Theorique et Physique Mathematique, C.P. 229, Universite Libre de Bruxelles (ULB), B 1050 Brussels, Belgium
[9]Department of Physics, Washington University in St. Louis, MO 63130 USA
[10]National Superconducting Cyclotron Laboratory, Michigan State University, East Lansing, MI 48824
[11]Department of Physics and Astronomy, Michigan State University, East Lansing, MI 48824-1321
[12]State Key Laboratory of Nuclear Physics and Technology, School of Physics, Peking University, Beijing 100871, China
[13]Physics Institute of Rosario, S2000EZP Rosario, Argentina
[14]Department of Physics, Lund University, P.O. Box 118, S-22100 Lund, Sweden
[15]Inst. f. Kernphysik, TU Darmstadt, 64289 Darmstadt, Germany
[16]Department of Physics, Florida State University, Tallahassee, FL 32306, USA
[17]GANIL, CEA/DSM-CNRS/IN2P3, BP 55027, F-14076 Caen Cedex, France
[18]Lawrence Livermore National Laboratory, P.O. Box 808, L-414, Livermore, California 94551, USA
[19]Department of Physics & Astronomy and HPC Center for Computational Sciences, Mississippi State University, Mississippi State, MS 39762, USA
[20]Skobeltsyn Institute of Nuclear Physics, Moscow State University, Moscow 119991, Russia
[21]Department of Physics and Astronomy, Iowa State University, Ames, IA 50011, USA
[22]Physics Department, University of Washington, Seattle, WA 98195, USA

November 28, 2019

Abstract

One of the biggest and most important frontiers in nuclear theory today is to construct better and stronger bridges between bound state calculations and calculations in the continuum, in particular scattering and reaction theory, as well as teasing out the influence of the continuum on states near threshhold. This is particular challenging as most many-body calculations are in a bound state formalism, while reaction calculations are more commonly in a few-body formalism. Furthermore many-body and few-body formalisms often use different language and emphasize different properties. To build better foundations for these bridges, we present an overview of bound state and continuum methods and, where possible, point to current and possible future connections.

Contents

1 Motivation and context **3**
- 1.1 Experimental context . . . 4
- 1.2 Overview of facilities and experimental programs . . . 5
  - 1.2.1 Facility for Rare Isotope Beams (FRIB) . . . 5
  - 1.2.2 Astrophysics . . . 6
- 1.3 Atomic nuclei as open quantum systems . . . 7
- 1.4 Trade-offs . . . 8

2 Overview of few-body methods **9**
- 2.1 Relevant degrees of freedom and Effective field theory . . . 11
  - 2.1.1 Effective field theory . . . 11
  - 2.1.2 Halo EFT . . . 11
- 2.2 Dispersive optical model . . . 12

3 Overview of many-body methods **14**
- 3.1 No-core shell model . . . 15
  - 3.1.1 Continuum degrees of freedom in NCSM . . . 15
  - 3.1.2 J matrix approach (or HORSE, or Algebraic RGM) . . . 16
  - 3.1.3 Symmetry-adapted framework: Collective correlations and continuum . . . 17
- 3.2 Coupled Cluster and In-Medium Similarity Renormalization Group Methods . . . 18
  - 3.2.1 SRG Evolution of Interactions and Operators . . . 18
  - 3.2.2 Solving the Many-Body Problem with Decoupling Methods . . . 19
- 3.3 Lattice EFT and adiabatic projection method . . . 21
- 3.4 Berggren basis . . . 22
  - 3.4.1 Gamow shell model . . . 24
  - 3.4.2 No-core Gamow shell model approach . . . 25
  - 3.4.3 Using Berggren basis: pairing correlations and microscopic alpha decay . . . 25
  - 3.4.4 CC and IM-SRG with Berggren basis . . . 26
- 3.5 Self Consistent Green's functions . . . 27
- 3.6 Energy density functional and heavy nuclei . . . 28
- 3.7 Tails of wave functions: a challenge to many-body theory . . . 29

4 Connections **30**
- 4.1 Input from many-body calculations into few-body methods . . . 30
  - 4.1.1 Effective inter-cluster interactions (optical potentials) . . . 30
  - 4.1.2 Effective inter-cluster interaction based on the Green's function method for low energies: Results form the Coupled-cluster approach . . . 30
  - 4.1.3 Effective inter-cluster interaction based on the multiple scattering method for intermediate energies: Results based on the no-core shell model . . . 32
- 4.2 Sum rules and response functions based on bound state techniques . . . 32
- 4.3 Double charge-exchange transitions and the double Gamow-Teller resonance from the shell model . . . 33
- 4.4 Extrapolations from finite-volume calculations . . . 34

4.4.1 ANCs from finite-volume calculations 34
4.4.2 Busch formula 35
4.5 Time-dependent Basis Function method 37
4.6 Statistical reactions: Nuclear level densities 37

5 Conclusions: where we have been and where we are going 38

A Appendix: "How to" details 39
A.1 How to build a single-particle Berggren basis 40
A.2 How to build an effective nucleon-nucleus ('optical') potential via Green functions 45

1 Motivation and context

Rutherford discovered the atomic nucleus through scattering. Today we obtain data on nuclei through scattering and reactions experiments, either with other nuclei or electromagnetic probes, and via decays. Many if not most experiments measure *cross sections*, dictating the critical need for reliable and consistent quantum mechanical theories for calculating reaction observables.

Low-energy nuclear theory has been invigorated by the introduction and promulgation of novel, rigorous theoretical methods for many-body bound states, allowing for broadly successful *ab initio* calculations (see section 3). The low-energy community has also become aware of the need for similarly rigorous calculations for low-energy scattering and reaction theory, particularly for interpreting the results of experiment at the Facility for Rare Isotope Beams (FRIB) and rare isotope beam facilities around the world. There are only a handful of dedicated low-energy reaction theories, however, with far more effort going to structure calculations in bound state frameworks. In addition, current few-body reaction calculations often neglect the microscopic many-body structure of the target/projectile, while current many-body structure calculations typically limit or entirely neglect continuum degrees of freedom. In between are methods to connect structure calculations to reaction observables. These range from techniques for the calculation of electromagnetic and weak responses to microscopic derivations of effective nucleon-nucleus potentials.

This paper reports on the presentations and discussions of the 2018 Facility for Rare Isotope Beams Theory Alliance (FRIB-TA) workshop "From bound states to the continuum: Connecting bound state calculations with scattering and reaction theory". The goal of the workshop was to help develop tools to calculate reaction observables that are directly measured in experiments, primarily by expanding existing state-of-the-art few-body and many-body theories but also by motivating the development of innovative approaches that can build upon connections between these theories (Fig. 1). In particular, the main themes were: (1) to bridge from many-body theories based on bound state formalisms to continuum degrees of freedom, and (2) to expand few-body techniques to include microscopic degrees of freedom. This paper discusses scattering and reaction theory, bound state structure calculations, and especially work on the boundary. It summarizes the state of the art, with the aim to identify and lower the technical barriers to bridge between bound state calculations and the continuum.

The program recognized:

- The use of localized basis in many bound-state calculations and the need for theoretical advances that use hybrid degrees of freedom;
- The need to address collectivity, clustering, and non-resonant continuum;
- The need to replace current statistical methods in cases where reaction rates are dominated by low-lying resonances;
- The critical need for reliable effective inter-cluster interactions that can be employed in many currently available reaction codes used by theorists and experimentalists;
- The critical need for an accurate reproduction of thresholds (energy differences) and asymptotic normalization coefficients (ANC) – specifically, the goal is to obtain accurate energy differences, not necessarily accurate binding energies, and a proper handling of correlations in the nuclear wave functions, such as clustering, collectivity, and coupling to the continuum;
- The need for advancing approaches that combine *ab initio*/microscopic approaches, phenomenology, and experimental data;

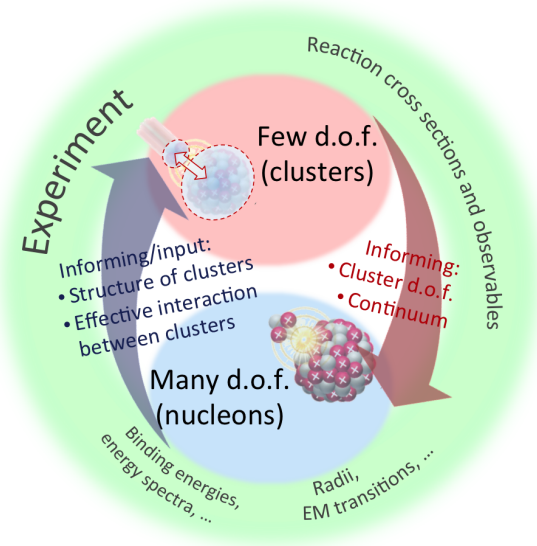

Figure 1: The goal of the FRIB-TA topical program was to help develop tools to calculate reaction observables that are directly measured in experiments, primarily by expanding existing state-of-the-art few-body and many-body theories but also by motivating the development of innovative approaches that can build upon connections between these theories.

- The important support of experiment that can provide measurements on a grid of the nuclear chart allowing for theoretical interpolations, with a focus on masses. In particular, theory may lead to smaller uncertainties if it interpolates between experimental data, instead of extrapolating to very neutron-rich nuclei.

The program further addressed: What are the accomplishments and limitations of each method? What does each method produce and at what energy regime? How well do these methods address important experimental questions? What are the pros and cons for using each continuum method with each bound state method? What are crucial technical details for getting started, e.g., in the Gamow-Berggren basis, how are the Berggren states chosen and how are they normalized? What are the current technical barriers for going further, e.g., convergence issues for applications in the no-core shell model, coupled clusters, etc. What are the most suitable microscopic methods for reactions with heavy nuclei? Are there benchmark calculations we can compare across methods?

1.1 Experimental context

While the driver for this paper is experiment, it is useful for us to identify two broad classes of experiments. The first we call *direct measurements*, where the quantity being measured is directly of physical interest. These include, for example, cross sections of interest to astrophysics, scattering phase shifts for constraining interactions, and excitation energies. The second are *interpreted* measurements, where one uses reactions or scattering to get at some other quantity of physical interest (Table 1.1). These include charge-exchange, transfer, breakup, and knockout reactions, Coulomb excitations, and so on. The interpretation of these experiments depend significantly upon the reaction theory used, and so robust interpretations require robust theory.

The nuclear physics community currently utilizes a diverse set of radioactive and stable beam facilities, and is eagerly anticipating the new opportunities for studying unstable nuclei which will be provided by FRIB. The types of reactions will include resonances, radiative capture, knock-out, transfer, charge-exchange and others, both on neutron-rich and proton-rich side. Current reaction models rely on phenomenology including phenomenological optical potential, valence shell-model calculations, R-matrix methods, and Glauber theory; fusion reactions in heavier nuclei use the Hauser-Feshbach model. An example for some of the challenges is illustrated in Fig. 2: while phenomenological optical potentials do well at high projectile energy, at low energies they fail to account appropriately for isolated resonances. To analyze and interpret data, theory with controlled approximations is needed, with uncertainties at least about 10%.

Reaction	Example	Nuclear information
Elastic Scattering	A(a,a)A ^{208}Pb(n,n)^{208}Pb	Extracts effective interactions (optical potentials), interaction radii, density distributions.
Inelastic Scattering	A(a,a′)A* ^{90}Zr$(\alpha,\alpha')^{90}$Zr*	Extracts electromagnetic transitions or nuclear deformation
Charge exchange	A(a,c)C ^{14}C(p,n)^{14}N	Studies beta decays and the weak interaction
Capture	A(a,γ)C ^{16}O$(\alpha,\gamma)^{20}$Ne	Determines resonance energies and widths
Breakup	d+^{90}Zr $\rightarrow^{90}$ Zr* + p + n	Extracts properties of loosely bound states
Knockout	A(a,a′b)B ^{16}O$(\alpha,2\alpha)^{12}$C	Probes structure of weakly bound nuclei
Pickup	A(a,c)C ^{90}Zr(d,p)^{91}Zr*	Extracts spin, parity and orbital occupancy in valence shells
Stripping	A(a,c)C ^{157}Gd$(^3$He$,\alpha)^{156}$Gd*	Extracts spin, parity and orbital occupancy in valence shells

Table 1: Examples of direct reactions and their role in extracting nuclear information.

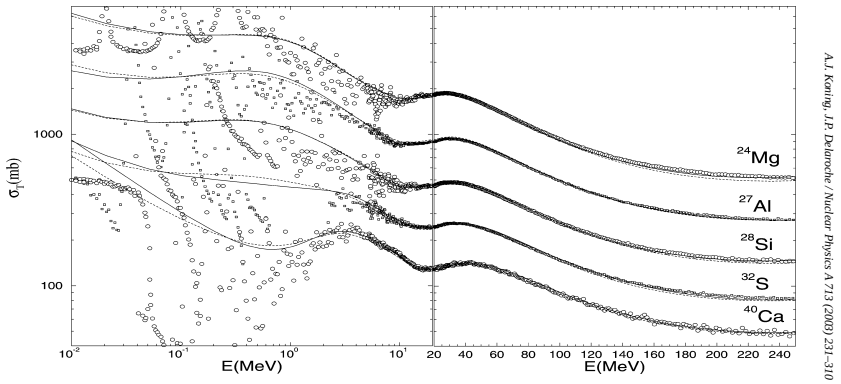

Fig. 2. Comparison of predicted neutron total cross sections and experimental data, for nuclides in the Mg–Ca mass region, for the energy range 10 keV–250 MeV. For more details, see Section 4.1.

Figure 2: Successful phenomenological optical potentials cannot address the low-energy regime where isolated resonances become important. Figure from A.J. Koning and J.P. Delaroche, Nucl. Phys. A 713 (2003) 231.

1.2 Overview of facilities and experimental programs

The facilities available to the U.S. nuclear science community have been recently summarized in two White Papers; see in particular Sec. 3 of Ref. [1] and Sec. 3.6 of Ref. [2]. The capabilities include radioactive and stable beams that vary in size from the large user facilities at Argonne National Laboratory and the National Superconducting Cyclotron Laboratory to small university laboratories. In addition, there are facilities which provide neutron and photon beams. These facilities are both specialized and complementary, and provide researchers with a broad suite of tools for addressing questions in nuclear physics.

1.2.1 Facility for Rare Isotope Beams (FRIB)

Present facilities are limited in their capability to produce nuclei far from the line of stability. Major progress in this area will be provided by FRIB, which is currently under construction at Michigan State University. Experimental capabilities at FRIB will include stopped beams, re-accelerated beams, fast beams, and isotope harvesting. The stopped beams are essentially unaccelerated beams that will be used for mass measurements, decay studies, and atomic spectroscopy. The re-accelerated beams will range in energy from 0.3 MeV per nucleon up to 12 MeV per nucleon.

The fast fragmentation beams will provide energies up to at least 200 MeV per nucleon. The isotope harvesting capability will provide for the collection of radioisotopes for applications and offline measurements. The re-accelerated and fast beam will be of particular interest to the nuclear reactions community. FRIB is expected to be ready for the first science experiments in 2021.

FRIB will be very well equipped for nuclear reaction studies. The Separator for Capture Reactions (SECAR) will be used to detect recoils from radiative capture reactions of interest to nuclear astrophysics. The Gamma-Ray Energy Tracking Array (GRETA) will perform high-resolution gamma-ray spectroscopy. The High Rigidity Spectrometer (HRS) is the key instrument for fast beams, as it will precisely measure the charged reaction products. Besides these instruments, there are several others, include active target detectors, a gas-jet target, neutron detectors, and other types of gamma-ray detectors. Since FRIB beam will be highly valuable, there is considerable incentive to design experiments that measure as many things as possible at one time, such as measuring elastic scattering and reactions simultaneously.

1.2.2 Astrophysics

Nuclear astrophysics is concerned with the origin of the elements and energy generation in astrophysics. The scenarios include the big bang, quiescent stellar burning, and cataclysmic events such as novae, x-ray burst, supernovae, and neutron star mergers. The state of the field and future U.S. plans for research in this area are summarized in a 2017 White Paper [1].

A priority for future work is to determine the nuclear physics which defines the r process, the source of many heavy nuclei, including gold and uranium [3]. The most important work will be mass measurements, which define neutron separation energies. Measurements of decay properties (half lives, β-delayed neutrons) is also very important. FRIB will be the key facility for this work, as it can produce many of the neutron-rich nuclei involved in the r process. These observables are related to the nuclear shell structure in the region, which will be the primary tool for interpreting measurements. There will certainly be cases where we want to understand (n,γ) cross sections in detail. These may be addressed by measurements of level density and γ-ray strength, or by measurements of (d,p) to deduce the properties of isolated levels.

Another focus area is radiative capture, which plays a particularly important role in nuclear astrophysics. The captured of charged particles [4] and neutrons [5] followed by the emission of one or more photons is important in the big bang, quiescent burning (e.g., solar fusion reactions and the s process) as well as explosive burning. The capture of charged particles by radioactive nuclei is studied using recoil separators, such as the Detector of Recoils And Gammas Of Nuclear reactions (DRAGON) separator at TRIUMF and the SECAR device at FRIB. For capture on stable nuclei, one may use separators or intense beams of protons or α particles in normal kinematics. Facilities for that latter include the Compact Accelerator System for Performing Astrophysical Research (CASPAR) at the Sanford Underground Research Facility as well the Laboratory for Experimental Nuclear Astrophysics (LENA) at Triangle Universities Nuclear Laboratory. For neutron capture, there are several dedicated neutron facilities [1, Sec. 3.4.1].

Many other types of reactions, including (p,α), (α,p), and (α,n), are important in nuclear astrophysics, and measurements of these are being vigorously pursued using stable and radioactive beams. These reactions, as well as radiative capture, may be further classified according to whether they are dominated by non-resonant (direct) processes, isolated resonances, or many resonances (statistical or Hauser-Feshbach regime). These regimes depend upon the mass, relevant excitation energy range, and nuclear structure of the compound nucleus.

Many critical reaction and decay rates in nuclear astrophysics cannot be measured directly, due to practical considerations such as very small cross sections, unavailability of beams, or the difficulty of measuring neutron-induced reactions on radioactive isotopes. A critical tool for nuclear astrophysics is thus indirect methods, which may be able to determine or constrain cross sections or decay rates by other measurements. One example is transfer reactions, which in favorable cases can determine excitation energies, spins, parities, and partial widths of resonant states. Another is charge-exchange reactions, which can determine weak interaction matrix elements. Much of the future work at FRIB and other facilities will involve indirect methods.

Indirect methods are critically reliant upon reaction theory for interpreting measurements and propagating uncertainties. At the present time, the theoretical tools are not always adequate. For example, the methods for analyzing transfer reactions to unbound states (the typical nuclear astrophysics scenario) are quite rudimentary. Even in the case of direct measurements, it is often the case that experiments alone do provide all of the needed information. A good example is the

^{7}Be(p, γ)^{8}B reaction, which is discussed below in this document. The experiments are unable to perform measurements at energies corresponding to the core of the sun, due to the small cross section. It is thus necessary to use experiment *and* theory to arrive at the best estimate for the stellar reaction rate.

1.3 Atomic nuclei as open quantum systems

One of the major goals of nuclear physics is the exploration of the drip lines, which are defined as the limit of nuclear stability with respect to the emission of one neutron or proton, and provide information on how many neutrons and protons can stick together. The main theoretical difficulty in the description of nuclei close to the drip lines and beyond, comes from the emergence of new effective scales associated with the increasing importance of couplings to continuum states as represented in Fig. 3. Indeed, couplings to continuum states are negligible in well bound states as a lot of energy would be required to break them apart, and so they exhibit well localized wave functions. However, weakly bound systems do not require much energy to break apart which translates into localized but extended wave functions, as if weakly bound systems were ready for the emission of one or more particles.

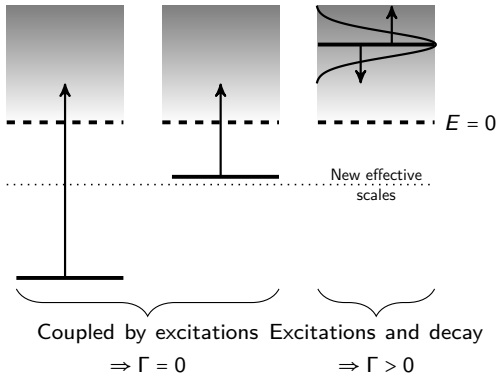

Figure 3: Three typical cases in quantum systems: a well bound state, a weakly bound state, and a decaying resonance state. In the first two cases, couplings between the discrete state and continuum states are only possible through excitations (below the particle emission threshold), while in the last case both excitations and decays are possible ways to couple to continuum states. Because of the strong continuum couplings in the last case, many continuum states have a structure very similar to the discrete state, which gives the characteristic energy dispersion or width observed experimentally.

Above the particle emission threshold, the situation is more complex. One particle or more can leave the system and consequently the process is intrinsically time-dependent. However, it is known experimentally that when scattering a neutron or a proton on a nucleus at low (positive) energies, there are some specific energies at which the absorption increases significantly, which give peaks of various widths in the cross section. This means that there exist some kind of structure in the continuum of positive energy many-body states, where the scattered nucleon spends a significant amount of time around the target before to leave it.

Emergence of near-threshold collectivization and clustering. – Coupling to the environment of scattering states and decay channels cannot be taken into account by an appropriate modification of the hermitian Hamiltonian of a closed quantum system. The matrix problem involving discrete and continuum states is complex-symmetric and leads to new phenomena such as, e.g., the resonance trapping [6, 7, 8, 9] and the super-radiance [10, 11], the multichannel coupling effects in reaction cross sections [12, 13] and shell occupancies [14, 15], the modification of spectral fluctuations [16], and the deviations from Porter-Thomas resonance widths distribution [9, 17, 18]. The appearance of collective states and clustering close to the corresponding cluster emission threshold is yet another consequence of the continuum coupling [19, 20]. Nuclear clustering is arguably one of the most mysterious nuclear phenomenon. Ikeda et al. [21] observed that α-cluster states can be found in the proximity of α-particle decay thresholds. This feature appears not to be a consequence of any specific feature of nuclear interactions because then the

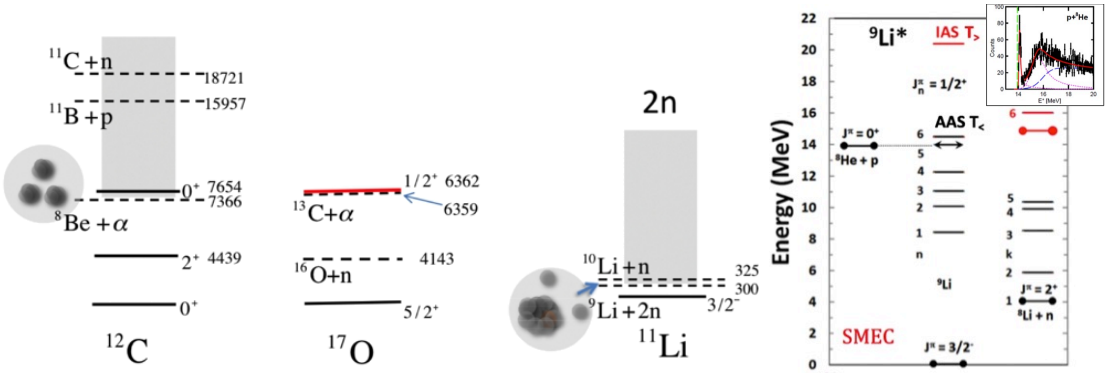

Figure 4: Various examples illustrating the emergence of nuclear clustering in the vicinity of the corresponding particle decay threshold. These include, e.g., Hoyle state 0_2^+ in ^{12}C, narrow near-threshold resonance $1/2_1^+$ in ^{17}O, halo ground state in ^{11}Li, and the collective splinter of the anti-analog resonance in ^{9}Li.

correlations and clustering in near-threshold states would appear at random. Hence, the origin of cluster (correlated) states in the proximity of cluster thresholds must be more general. It has been conjectured [19, 20] that the interplay between internal configuration mixing by interactions and external configuration mixing via decay channels leads to the new kind of near-threshold collectivity. Therefore, e.g., the 0_2^+ resonance in ^{12}C close to the α-particle emission threshold should carry an imprint of ^{8}Be+α clustering, whereas the $1/2_1^+$ resonance of ^{17}O in the vicinity the α emission threshold and above the neutron emission threshold should have the structure of ^{13}C+α cluster state and hence its lifetime should be long (Fig. 4). Similarly, the ground state of ^{11}Li should resemble the ^{9}Li+2n configuration of the nearest 2n-emission threshold rather than the ^{10}Li+n configuration of a more distant 1n-emission threshold, and the collectivity of $1/2_6^+$ neutron resonance in ^{9}Li should be caused primarily by the proximity of ^{8}He + p decay channel [22]. This generic phenomenon in open quantum systems explains why so many states, both on and off the nucleosynthesis path, exist "fortuitously" close to open channels.

The near-threshold correlations may have also a noticeable effect on electromagnetic transitions and moments, e.g., the E1 transition in ^{11}Be from a near-threshold $1/2_1^-$ state to the ground state $1/2_1^+$.

1.4 Trade-offs

No practical theory can cover every aspect. It is important therefore to understand and emphasize the strengths and weaknesses of various methods.

In many-body theories, the trade-offs usually involve degrees of freedom. In general the most particles included, the few degrees of freedom those particles can have. So for the lightest systems, one can describe with good accuracy both the long range and short range correlations. Such methods are often referred to as "exact methods", and include Faddeev(-Yakubovsky) approach [23, 24, 25, 26], hyperspherical harmonics method [27], and the Alt-Grassberger-Sandhas approach [28, 29], and are typically limited to $A \leq 5$. Beyond this, for light nuclei, examples include quantum Monte Carlo calculations, and the no-core shell model with various continuum extensions. For heavier nuclei, one can use coupled-cluster methods with many orbits and thus describe short-range correlations, but such methods work best at or near closed shells and best for ground states. Configuration-interaction methods can describe many excited states and work well away from closed shells, but for medium and heavy nuclei the number of tractable orbits becomes increasingly limited. In other words, *in order to treat some degree of freedom better, one must be willing to give up something else.* This principle is crucial to bridging the gap between sub-disciplines.

In scattering and reaction theories, similar principles apply. For example, few-body calculations can get highly precise results via the Faddeev equations and related methods, but at the price of ignoring internal degrees of freedom, or hoping those internal degrees of freedom can be robustly integrated out. There are other trade-offs as one goes to higher energy.

In other words, when bridging the gaps between disciplines, we have to ask, *what is it we really need* and, simultaneously, *what is it we are willing to give up?*

An example of this, discussed in more detail below, is the question of asymptotic behaviors. Correct asymptotic behavior is crucial for low-energy scattering and reactions, especially on weakly bound systems, and part of that correct behaviors involve energy thresholds such as the separation energy. But in most cases, *ab initio* calculations will not yield the energy threshold at the required accuracy. Therefore one must either give up, with eyes wide open, fully *ab initio* approaches, which undermines much of the current program in many-body physics, or perhaps find some clever way around the problem, for example through integral methods which can describe asymptotic behavior.

2 Overview of few-body methods

Few-body methods are of widespread use in the nuclear reaction community. For complex systems and/or heavy composites, it is understood that a full microscopic description of the reaction is not feasible. One then relies on the reduction of the scattering problem, inherently a many-body problem, to a problem involving only a few relevant degrees of freedom [30, 31] (Fig. 5). Once these degrees of freedom have been identified, specific formulations can be developed. Here we discuss the main methods currently in use in the field.

Figure 5: Few-body techniques rely on the reduction of the scattering problem, inherently a many-body problem, to a problem involving only a few relevant degrees of freedom.

Since our objective is ultimately to connect to experiment, the desired observables are cross sections, which can contain various levels of detail, for example energy distributions, angular distributions, etc. The cross sections can be constructed from the T-matrix for the process, which can generally be written in post form as [32]:

$$T^{exact} = \langle \chi_f^{(-)} \, |V| \, \Psi_i^{(+)} \rangle, \tag{1}$$

where $|\Psi_i^{(+)}\rangle$ represents the exact incoming wave, solution of the scattering equation:

$$H\Psi^{(+)} = E\Psi^{(+)} \tag{2}$$

with scattering boundary conditions $\Psi^{(+)}(R \to \infty) \equiv (F + TH^+)$. Here F represents the regular Coulomb wave and H^+ is the outgoing Hankel function [32]. The transition operator V is responsible for the reaction channel under study and $\chi_f^{(-)}$ is the outgoing distorted wave. If the many-body problem can be mapped onto a two-body problem, Eq. (2) is a trivial two-body scattering equation. However, most often one needs to consider more degrees of freedom and the solution of Eq. (2) rapidly becomes very challenging. Most nuclear probes are peripheral, and therefore a correct asymptotic treatment of the problem is critical. This can be a challenge for two reasons: a) standard bases used in many-body methods are bound state bases which perform poorly in expanding the asymptotics of scattering states and b) the long-range Coulomb force. As the projectile and/or target charge increases, the effect of Coulomb can become very large and the asymptotic properties of system may not be known analytically. Furthermore, as more degrees of freedom are included, there are several relevant thresholds (Q-values) that need to be taken into account. Observables are extremely sensitive to these thresholds, requiring a match to the experimental value of a few keV. When nuclei breakup into the continuum, the non-resonant continuum can be just as important at the resonant continuum, and final state interactions can have an important effect on phase-space. We briefly summarize below the few-body methods that have been developed to address these challenges.

One should keep in mind a number of important inputs needed for the few-body reaction theory. As mentioned above, Q-values are critical inputs. As opposed to many-body methods that rely on the NN-force, few-body methods rely on optical potentials, effective interactions between the relevant fragments, the dynamics of which have been determined to be important to describe the

process. In addition, for some processes one needs addition structure quantities such as overlap functions, transition densities, etc. Because it is hard to obtain the level of accuracy needed from many-body theoretical predictions, these quantities are either directly taken from data (such as the Q-values) or strongly constrained by data.

Traditionally in reaction theory, perturbation theory is used to expand the exact T-matrix into the well known distorted-wave Born (DWBA) series [32]. By retaining only the first and/or second terms of the expansion, a method referred to as DWBA, one avoids the complications of solving Eq. (2) exactly. While DWBA may still be preferred in the analysis of data, the theory community has long advocated for better methods, because DWBA is not reliable particularly when there is strong clustering and/or the proximity of breakup channels. A larger array of non-perturbative methods have been taking over the field in the last few decades. For the purposes of illustration, we focus here on three-body methods, although analogous theories are applicable to four-body scattering problems. Currently, there are no efforts to expand few-body methods in nuclear reactions to more than four-bodies, due to feasibility.

If the reaction A+a can be cast as a three-body problem $A+b+x$ where to a good approximation the projectile is well represented by $a = b + x$, the exact treatment of the scattering problem is provided by the Faddeev equations, which couple all rearrangement channels to all orders [33]. In the Faddeev method, an overcomplete basis spanning the three rearrangement channels is used and this ensures their separation in the asymptotic region. This is an important aspect of the method, since then we know how to impose the correct boundary conditions. In nuclear physics, the Faddeev equations are often solved in T-matrix form in momentum space [33, 34]. Examples of applications include the analysis of scattering and transfer of halo nuclei as well as other reaction channels [34, 35, 36]. Note that the solution of the Faddeev equations for systems with strong Coulomb becomes very challenging because the equations become non-compact [37]. Work to address this challenge using separable interactions is underway [38, 39, 40].

The continuum discretized coupled channels (CDCC) method for describing the reaction $A + a$ in terms of the three-body problem $A+b+x$ relies on the expansion of the three-body wavefunction in a couple set of eigenstates of the system $b + x$ [41]. These states include bound and scattering states. For practical reasons, the continuum is discretized, usually into energy bins and represented in terms of square-integrable *wave-packets* so that the resulting coupled-channel equations can be solved. As opposed to the Faddeev method, CDCC does not couple to all orders the rearrangement channels and therefore in some cases it cannot provide a complete picture of the reactions. However, for many cases in which rearrangement channels are not important, it offers the best alternative to the Faddeev method [42, 43]. Particularly for heavier systems and for reactions in which larger clusters are involved, when the current Faddeev methods fail, CDCC is the best alternative. Just in the last year, CDCC has been applied to a wide variety of cases, including the study of α yield in ^{6}Li induced heavy-ion reactions [44], the role of resonant states in fusion reactions [45] and the sensitivity of the NN-force in (d,p) reactions [46].

Both Faddeev and CDCC are computationally intensive. When the energy scales involved in the $b + x$ motion and the $A + a$ can be well separated, some non-perturbative approximations are used to reduce the problem without sacrificing accuracy. The adiabatic approximation consists of writing the problem as in CDCC, but neglecting the excitation energy in the $b + x$ sysytem [47]. By making all the eigenstates of the $b + x$ system degenerate with the ground state, the CDCC equations reduce to a simplified form which then can be solved parametrically in one of the variables [32]. One can also use the adiabatic approximation in particular reaction channels with enormous success [48, 49, 50]. Although primarily valid at higher energies, the adiabatic method for (d,p) performs well even at $E \approx 10$ MeV/A. Applications include the analysis of the comprehensive ^{10}Be(d,p)^{11}Be data [51, 52] and the extraction of $^{30}\mathrm{P}(n,\gamma)^{31}\mathrm{S}$ from the corresponding (d,n) reaction [53].

If the energy is large enough, then the Eikonal approximation may become appropriate [32]. The standard Eikonal model assumes that deviations from a straightline trajectory for the projectile can be neglected. Then, the effects of the interaction with the target are encapsulated into the so-called Eikonal phase. This phase $\phi(b)$ is readily computed per impact parameter from the integral over the projectile's path of the contributions of the interaction. Few-body eikonal theories for reactions are popular in the field due to their simplicity. Nuclear knockout reaction experiments have consistently over the years been interpreted with eikonal theory [54, 55]. In order to stretch the high-energy approximation, there also have been many studies to improve on the Eikonal descriptions (e.g., [56, 57]).

To add to the large body of work on three-body methods for reactions, the community has now been paying attention to the need to include excitations of one or more of the clusters in the scattering problem of $A + b + x$. Examples of these new developments are studies of breakup reactions including core excitation in CDCC [58, 59, 60, 61, 62] and Faddeev [63, 64]. Four-body extensions in reaction theory have also been pursued, particularly when considering two-nucleon halo projectiles (inherently three-body in structure) [65, 66] and reactions where both target and projectile are loosely bound [67].

The few-body reaction community has focused in developing increasingly sophisticated few-body theories that aim to solve the few-body problem very accurately. In contrast, uncertainties in the inputs to these theories are still ambiguously quantified. Recently, there has been some effort to use rigorous statistical methods to quantify the uncertainties in the reaction observables, associated with the optical potential, an essential input to any of these reaction theories. Examples focusing in the uncertainties in (d,p) reactions [68, 69] show that more work is necessary to fully understand, not only how to quantify the uncertainties, but also how to reduce them to the level needed so that, when combined with reaction data, one can extract the desired information.

2.1 Relevant degrees of freedom and Effective field theory

2.1.1 Effective field theory

A central idea in the effective field theory (EFT) formulation is the separation of the physics at a given energy scale of interest from the physics at the higher energy scale. At the energy scale of interest, once the degrees of freedom are identified no attempt at modeling the high energy scale physics is made. All the interactions allowed by the relevant symmetries are included. This is what is referred to as the model-independence of EFT interactions. Observables are expressed as an expansion in the ratio of low energy over the higher energy scale. This allows a systematic estimation of theory error from the higher order terms of the expansion that were not included in the calculation. Refs. [70, 71, 72] provide a comprehensive introduction to EFTs in various systems in nuclear and particle physics. Weinberg's pioneering work [73, 74] led to the construction of nucleon-nucleon interaction from an EFT of pion-nucleon interaction. It is worth emphasizing that EFT is an expansion in energy, and not in the number of particles. If the active number of particles is small then analytical methods are applicable. For larger systems with a large number of active particles, numerical methods such as EFT defined on a space-time lattice is more appropriate.

There are two aspects of Quantum Chromodynamics (QCD) that dominate low-energy physics, especially in light nuclei: (1) Chiral symmetry that dictates the lightness of pions, kaons, etas, and their interaction with nucleons. (2) Large scattering lengths and weakly bound systems that proliferate nuclear physics. Both of these aspects are consistently treated in the continuum and lattice formulations of EFT. This is important in establishing connections between QCD and nuclear interactions.

2.1.2 Halo EFT

Halo nuclei are weakly bound systems where the valance nucleons (usually one or two neutrons) are spatially decoupled from a tightly bound core. The matter radii measurements in helium and lithium isotopes by Tanihata et al. provided first experimental evidence for halo nuclei [75, 76]. These measurements challenged the conventional uniform density liquid drop model of atomic nuclei. ^{11}Li nuclei with just 11 nucleons has a matter radius ~ 3.3 fm that is comparable to lead nucleus with 208 nucleons. The large ^{11}Li matter radius is interpreted as resulting from two weakly bound valance neutrons forming a halo around a tightly bound ^{9}Li core [77].

Halo nuclei are characterized by small separation energies of the valance nucleons compared to the core excitation or breakup energy. This separation in energy scale is used to construct halo EFT. Refs. [78, 79] initiated the field of halo EFT. The review articles in Refs. [80, 81] describe various recent calculations of elastic scattering, electromagnetic captures and electromagnetic form factors. This formalism is also applicable to nuclear systems that have a cluster description at low energy such as the reaction $^{3}\mathrm{He}(\alpha,\gamma)^{7}\mathrm{Be}$ in terms of point-like ^{3}He and α clusters [82]. In halo EFT, the nuclear clusters and valance nucleons are treated as point-like particles that interact through short range forces. In this respect halo EFT is similar to pionless EFT [83, 84], and shares many calculational tools with it.

Halo EFT can provide important insight into capture reactions at astrophysical energies. Typically experimental measurements have to be extrapolated to low energies for big bang nucleosynthesis (BBN) and stellar burning calculations. Theoretical error estimates are crucial for these extrapolations. Halo EFT provides a systematic expansion where the cross sections are related to universal parameters that can be constrained by observables. The ^{7}Li$(n,\gamma)^8$Li reaction provides an example of this [85]. In Fig. 6, we show two potential model calculations that used the same Woods-Saxon form constrained by the same ^{8}Li binding energy input but differs from each other, and from data. In the halo EFT description, the p-wave ^{8}Li state requires two input at leading order (LO). These are usually fitted to the ^{8}Li binding energy and the corresponding p-wave effective range parameter ρ. The asymptotic normalization constant (ANC) is sensitive to ρ, and can greatly effect the overall size of the cross section. Reactions involving a p-wave bound state ^{7}Be$(p,\gamma)^8$B, ^{3}He$(\alpha,\gamma)^7$Be, ^{3}H$(\alpha,\gamma)^7$Li are impacted in a similar manner. The electric charge form factor of bound states can also be related to effective range corrections [84, 86]. Thus halo EFT can provide key physical insight into connections between physical observables in terms of universal parameters that are model-independent.

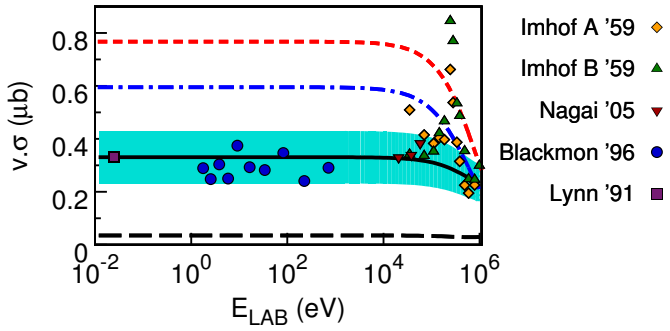

Figure 6: ^{7}Li$(n,\gamma)^8$Li capture cross section [85]. Black long-dashed and solid curves are the EFT results for the E1 capture to the excited state and the total E1 capture, respectively. The shaded area shows the estimated 30% EFT errors in the latter. The results of the potential model code CDXS+[87] using parameters from Model A [88] and Model B [89] are given respectively by the blue dot-dashed and red dashed curves. The references to the experimental data represented as colored dots are in Ref. [85].

In two-body systems, an important distinction between traditional potential models and halo EFT is the inclusion of electro-weak currents not constrained by Siegert theorem in the latter. A well known example from pionless EFT is the two-body axial current with coupling $L_{1,A}$ that is important in constraining solar neutrino-deuteron scattering cross section [90]. In the recent ^{3}He$(\alpha,\gamma)^7$Be cross section calculation [82], two-body currents not constrained by elastic scattering are found to contribute at LO. At the same time, due to the sensitivity of the ANC to the effective range ρ, a 10% change in the value of ρ can accommodate vanishing two-body current contribution in the energy region where data is available. However, at solar energies where data is lacking, the cross section with and without two-body corrections differ [82]. Halo EFT can provide meaningful error estimates in solar burning and BBN energy regime where data is lacking.

2.2 Dispersive optical model

The dispersion relation was recognized by Mahaux and Sartor as an important ingredient to link the energy domain of elastic scattering to the binding potential at negative energy which generates the levels of the nuclear shell model. Mahaux and Sartor developed the dispersive optical model (DOM) to provide this link. Their review paper is available in Ref. [91] and their approach has been later expanded by the St. Louis group with the aim to apply it also to unstable nuclei. In addition, more information related to experimental properties of the ground state has been included, in particular the description of the charge density has been incorporated by extending the analysis to include fully nonlocal potentials [92]. A recent review of this effort is available in Ref. [93] This approach has also been utilized to make predictions of the neutron skin of ^{48}Ca [94].

The dispersion relation for the self-energy is employed in its subtracted form

$$\begin{aligned} \text{Re}\ \Sigma_{\ell j}(r,r';E) &= \text{Re}\ \Sigma_{\ell j}(r,r';\varepsilon_F) \\ &- \mathcal{P}\int_{\varepsilon_T^+}^{\infty}\frac{dE'}{\pi}\text{Im}\ \Sigma_{\ell j}(r,r';E')\left[\frac{1}{E-E'}-\frac{1}{\varepsilon_F-E'}\right] \\ &+ \mathcal{P}\int_{-\infty}^{\varepsilon_T^-}\frac{dE'}{\pi}\text{Im}\ \Sigma_{\ell j}(r,r';E')\left[\frac{1}{E-E'}-\frac{1}{\varepsilon_F-E'}\right], \end{aligned} \tag{3}$$

where $\mathcal{P}$ is the principal value. The self-energy Σ is an effective one-body interaction between the particle (or hole) and the A-particle system, and is an exact representation of the Feshbach optical potential [95] generalized for both bound and continuum states [96, 97] (cf. Sec. 3.5).

The beauty of this representation was recognized by Mahaux and Sartor [91] since it allows for a link with empirical information both at the level of the real part of the non-local self-energy at the Fermi energy (probed by a multitude of HF calculations) and also through empirical knowledge of the imaginary part of the optical potential (constrained by experimental data) that consequently yields a dynamic contribution to the real part by means of Eq. (3). In addition, the subtracted form of the dispersion relation emphasizes contributions to the integrals from the energy domain nearest to the Fermi energy on account of the E'-dependence of the integrands of Eq. (3). Recent DOM applications include experimental data up to 200 MeV of scattering energy and are therefore capable of determining the nucleon propagator in a wide energy domain as all negative energies are included as well.

The importance of this formulation of an empirical representation of the nucleon self-energy is contained in its translation of experimental data into a theoretically accessible quantity. While the DOM assumes standard functional forms of the potentials, its parameters are constrained by data. The resulting information can therefore be used as an interface with *ab initio* approaches for the nucleon self-energy. An example is provided in Fig. 7 where the imaginary part of the central DOM self-energy of ^{40}Ca is compared for different ℓ-values with calculations based on the Faddeev random phase approximation (FRPA) [98, 93], one of the incarnations of the self-consistent Green's function approach.

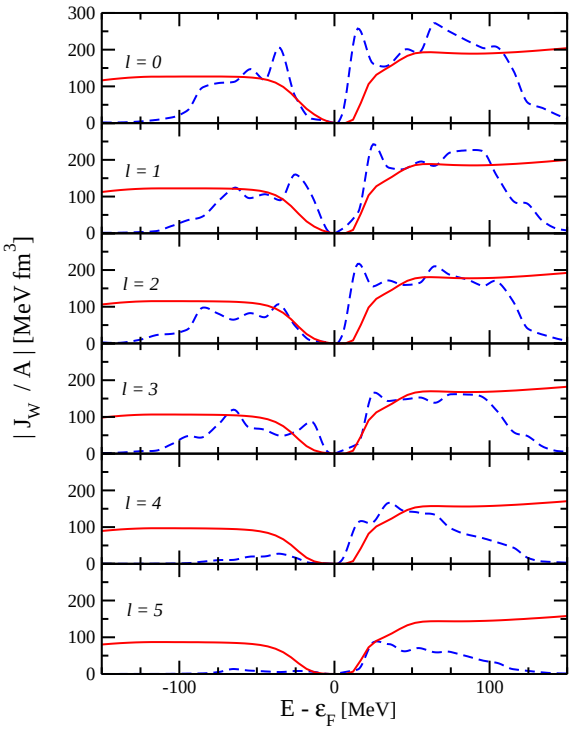

Figure 7: Comparison of volume integrals the imaginary part of a nonlocal implementation of the DOM for ^{40}Ca with *ab initio* FRPA calculations.

This comparison clearly demonstrates that a reasonable correspondence can be generated with theory and empirical results but also identifies the limitations that *ab initio* methods face. First it

should be noted that the FRPA result generate a self-energy that is a collection of many discrete poles. A phenomenological procedure is therefore required which assigns these poles a width that increases with distance to the Fermi energy. This will always be the case in all such calculations unless a continuum basis is employed. The inevitable finite configuration space also does not provide a good description beyond roughly 50 MeV away from the Fermi energy. Furthermore, the agreement for higher ℓ-values deteriorates rapidly. Such comparisons clearly demonstrate the usefulness of the DOM as a vehicle to assess the quality of theoretical approaches. A comparison with volume integrals obtained from multiple scattering approaches may provide better agreement at higher energy but most likely will fail at lower energy.

Finally, the DOM provides a new approach to the analysis of nuclear reactions, as it can provide distorted waves for protons and neutrons, as well as relevant overlap functions with their normalization (spectroscopic factors). Early applications already found such ingredients to provide a good description of transfer reactions [99]. More recently applications of the (d, p) reaction have been investigated with DOM potentials for ^{40,48,60}Ca in Ref. [100] generating physically more reasonable results as compared to those obtained with the global Koning-Delaroche potential because DOM potentials provide also a good description at negative energy. A very recent analysis including never before published data of the $^{40}\mathrm{Ca}(e, e'p)^{39}\mathrm{K}$ reaction also demonstrates that DOM ingredients provide all the necessary ingredients to accurately account for these data using the distorted-wave impulse approximation [101] at energies around 100 MeV for the outgoing proton. The spectroscopic factors provided for this analysis were constrained by other data and therefore provided a consistency check of their interpretation. The results furthermore demonstrate that the Nikhef analysis with separate phenomenological local potentials for bound and scattering states [102] slightly underestimated the values for spectroscopic factors by about 0.05.

3 Overview of many-body methods

There are a bewildering variety of many-body methods, though most of them draw from the same pool of theoretical tropes. To introduce them, we begin with the interacting shell model or just the shell model (SM), often called the configuration-interaction method in fields outside of nuclear physics. There are more powerful methods than the SM, several of which will be discussed below, but the SM is a conceptually straightforward paradigm, and some of its weaknesses with regards to the continuum are shared by other many-body methods.

The SM wave function is just an expansion in a basis $\{|\phi_\alpha\rangle\}$:

$$|\mathrm{SM}\rangle = \sum_\alpha c_\alpha |\phi_\alpha\rangle. \tag{4}$$

Unlike few-body methods, which typically work in relative (or Jacobi) coordinates, the SM wave function is usually in single-particle coordinates, that is the A-body wave functions are of the form $\phi_\alpha(\vec{r}_1, \vec{r}_2, \ldots, \vec{r}_A)$. The primary driver for this is the antisymmetry of fermions. Thus the basic element of SM wave functions are, either explicitly or implicitly, Slater determinants (or, more properly, their occupation-number representations), antisymmetrized products of single-particle wave functions, which is trivial in second quantization using fermion single-particle creation and annihilation operators. In relative coordinates, one must explicitly antisymmetrize by taking all possible permutations. We discuss some variants of the SM below. In additional to its conceptual simplicity, the SM can compute low-lying excited states nearly as easily as the ground state. As illustrated in Eq. (4), one conceptualizes the SM, as well as some other many-body methods, through the lens of the wave function; this is one of the conceptual gulfs between many-body and few-body methods, which frequently focus on the scattering or T-matrix. Equally foundational is the idea that one finds the coefficients c_α by a variational principle, minimizing the energy.

The coefficients also lead us to the primary disadvantage of the SM model: the lack of correlations in any given Slater determinant, so one must include many configurations, up to 24 billion in the largest calculations to date. Most variants on the SM, such as symmetry-adapted configuration-interaction SM and cluster-based SM, as well as alternatives such as coupled clusters (CC) and Green's function Monte Carlo (GFMC), build in correlations. This in turn has a cost, of course, of additional complexity or loss of flexibility (CC and GFMC must work harder to get excited states). In technical terms, any SM calculation includes many unlinked diagrams that must be cancelled, which in turn means the SM is not size-extensive, which CC is.

Single-particle coordinates have disadvantages, of which the primary one is that separation out of intrinsic or relative motion from center-of-mass motion is not trivial. Because of this it is difficult to truly identify relative cluster motion, for example the asymptotic behavior of a single particle (or alpha or other cluster) at a long distance from the remainder. This in turn leads to the simplifying assumption of boundary condition of wave functions vanishing at infinity. These problems drive several of the current methodologies for connecting to the continuum, such as the resonating group method (RGM) and related methods, and complex bases such as the Gamow-Berggren basis which imposes outward traveling boundary conditions.

3.1 No-core shell model

The basic idea of the no-core shell model (NCSM) is simply to treat all A nucleons in a nucleus as active, i.e., to write down the Schrödinger equation for A nucleons and then to solve it numerically. This approach avoids problems related to excitations of nucleons from the core, such as core-polarization effects, because there is no core, and being a non-perturbative approach, there are no difficulties related to convergence of a series expansion. It may also be formulated in terms of an intrinsic Hamiltonian, so as to avoid spurious center-of-mass (COM) motion.

The starting Hamiltonian

$$H = T_{\rm rel} + V = \frac{1}{A}\sum_{i<j}\frac{(\vec{p}_i - \vec{p}_j)^2}{2m} + \sum_{i<j}^{A}(V_{\rm NN})_{ij} + \sum_{i<j<k}^{A}(V_{\rm 3N})_{ijk} + \ldots + V_{\rm Coulomb}, \tag{5}$$

where m is the nucleon mass, V_{NN} is the nucleon-nucleon (NN) interaction, V_{3N} is the three-nucleon interaction, and $V_{\rm Coulomb}$ is the Coulomb interaction between the protons. There is no restriction on the V_{NN} and V_{NN} interactions used, without any restriction, typically interactions that are derived in the chiral effective field theory [103, 104, 105, 106], meson-exchange theory [107], or inverse scattering HORSE formalism [108, 109] (see Sec. 3.1.2). The NCSM uses a harmonic oscillator (HO) single-particle basis that allows preservation of translational symmetry of the nuclear self-bound system, even if single-particle coordinates are utilized. This is possible as long as the basis is truncated by a maximal total HO energy of the A-nucleon system [or selected according to SU(3) symmetry, as discussed in Sec. 3.1.3]. The NCSM employs a large but finite harmonic oscillator (HO) basis.

The NCSM champions light nuclei due to its computational efficacy, but is limited by the explosive growth in computational resource demands with increasing number of particles and size of the spaces in which they reside. To address this, the NCSM framework has been extended to heavier nuclei by using truncating schemes as in the Importance Truncation NCSM [110] and Monte Carlo NCSM [111], by using a symmetry-adapted basis (see Sec. 3.1.3), and by re-introducing the core with theoretical methods designed to treat the many-body correlation effects of the core in a non-perturbative manner, such as deriving effective interactions for a valence shell from NCSM [112], coupled cluster method (CC), and In-medium Similarity Renormalization Group (IMSRG) (see Sec. 3.4.4).

3.1.1 Continuum degrees of freedom in NCSM

One way to address the long-distance behavior of nuclear wave function and to introduce coupling to the continuum is by using a basis that explicitly considers cluster degrees of freedom. This can be done through a combination of the NCSM with the Resonating Group Method (RGM) [113, 114, 115]. In the RGM [116], nucleons are organized within different groups, or clusters, "resonating" through the intercluster exchange of nucleons. This antisymmetrization between the different clusters guarantees the Pauli exclusion principle, which along with the consideration of internal structure for the clusters, is one the most important features of the approach. In the case of two clusters $(A-a)$ and a, the cluster states for a channel ν are defined as $|\Phi_{\nu r}\rangle = |A-a\rangle \otimes |a\rangle Y_\ell(\hat{r}_{A-a,a})\frac{\delta(r-r_{A-a,a})}{r r_{A-a,a}}$ for a relative distance between the clusters $r_{A-a,a}$. The nuclear wave function is given in terms of the cluster states

$$|\Psi\rangle = \sum_\nu \int_r dr r^2 \frac{g_\nu(r)}{r}\hat{\mathcal{A}}\,|\Phi_{\nu r}\rangle \ , \tag{6}$$

with unknown amplitudes $g_\nu(r)$ that are determined by solving by the integral Hill-Wheeler equations (that follow from the Schrödinger equation):

$$\sum_\nu \int dr r^2 \left[H_{\nu'\nu}(r,r') - E N_{\nu'\nu}(r',r)\right] \frac{g_\nu(r)}{r} = 0. \tag{7}$$

Here, $H_{\nu'\nu}(r',r) = \langle \Phi_{\nu' r'} | \hat{\mathcal{A}} H \hat{\mathcal{A}} | \Phi_{\nu r} \rangle$ is the Hamiltonian kernel and $N_{\nu'\nu}(r',r) = \langle \Phi_{\nu' r'} | \hat{\mathcal{A}} \hat{\mathcal{A}} | \Phi_{\nu r} \rangle$ is the norm kernel, where $\hat{\mathcal{A}}$ is the antisymmetrizer. The kernels are computed using the microscopic wave functions of the clusters that can be obtained, e.g., in the NSCM. Once the kernels are computed, Eq.(7) can then be solved using a microscopic R-matrix approach [117, 118], the code for which is publicly available [119].

A hybrid basis approach, the no-core shell model with continuum (NCSMC) [120, 121], uses mixed shell-model and RGM basis to achieve a faster convergence [122].

Another way to include the continuum in the NCSM framework is to start with a continuum single-particle basis, such as the Gamow-Berggren basis (see Sec. 3.4.2).

3.1.2 J matrix approach (or HORSE, or Algebraic RGM)

The J-matrix formalism in scattering theory was originally developed in atomic physics [123] utilizing the so-called Laguerre basis which is a Sturmian-type basis for the Coulomb problem. A generalization of this formalism utilizing either the Laguerre or the harmonic oscillator bases was suggested in Ref. [124]. Later the harmonic-oscillator version of the J-matrix method was independently rediscovered in nuclear physics [125, 126, 127, 128]. The J-matrix with oscillator basis is sometimes also referred to as an *Algebraic Version of RGM* [125, 126] or as a *Harmonic Oscillator Representation of Scattering Equations* (HORSE) [129].

Within the HORSE approach, the basis function space is split into internal and external regions. In the internal region which includes the basis states with oscillator quanta $N \leq \mathbb{N}$, the Hamiltonian completely accounts for the kinetic and potential energies. The internal region can be naturally associated with the shell-model space. In the external region, the Hamiltonian accounts for the relative kinetic energy of the colliding particles only (and for their internal Hamiltonians if needed) and its matrix takes a form of an infinite tridiagonal matrix of the kinetic-energy operator (plus the sum of eigenenergies of the colliding particles at the diagonal if they have an internal structure). The external region represents the scattering channels under consideration. If the eigenenergies E_ν, $\nu = 0, 1, \ldots$, and the respective eigenvectors of the Hamiltonian matrix in the internal region are known, one can easily calculate the S-matrix, phase shifts and other parameters characterizing the scattering process (see, e. g., Refs. [124, 129, 130, 131]).

The HORSE formalism was successfully utilized in numerous studies of the nuclear continuum with two- and three-body open channels in cluster models either with phenomenological intercluster interactions (see Ref. [132] and references therein) or within the RGM framework (see Refs. [133, 134, 135, 136, 137] and references therein). The inverse scattering HORSE formalism was also developed [138, 139, 140, 141, 142, 143] and utilized for designing high-quality NN interactions JISP6 and JISP16 [109] describing the NN scattering data and deuteron properties together with observables in light nuclei. However, an extension of the NCSM to the states in the continuum by a direct implementation of the HORSE formalism seems to be unpractical since it requires a calculation of all spurious-free NCSM eigenstates of a given spin-parity which is impossible in modern large-scale NCSM studies. This drawback can be overcome by the use of a specific Lanczos-type reformulation of the HORSE method [144], which has not been implemented yet. Another option is to use the so-called Single-state HORSE (SS-HORSE) approach [145, 146, 147, 148] which makes it possible to calculate the low-energy S-matrix and resonance energies and widths by a simple analysis of the dependence of the lowest NCSM eigenstate of a given spin-parity on parameters defining the many-body NCSM basis space, the oscillator frequency $\hbar\Omega$ and the basis truncation boundary $N_{\max}$. The NCSM-SS-HORSE approach was successfully applied to the studies of the $n\alpha$ scattering [145, 146] and the resonance in a system of four neutrons (tetranetron) [149]. Both the Lanczos-type HORSE formalism [144] and the SS-HORSE [145, 146, 147] extensions of the NCSM as well as HORSE-RGM applications [150] are prospective for future studies of nuclear reactions.

3.1.3 Symmetry-adapted framework: Collective correlations and continuum

Built upon the *ab initio* NCSM framework, the symmetry-adapted framework exploits exact and approximate symmetries of the nuclear many-body dynamics (reviewed in Ref. [151, 152]). The symmetry is utilized to construct the basis states, that is, the model space is reorganized to a symmetry-adapted (SA) basis that respects the symmetry. Hence, calculations are not limited *a priori* by any symmetry and employ a large set of basis states that can, if the nuclear Hamiltonian demands, describe a significant symmetry breaking. In particular, the symmetry-adapted no-core shell model (SA-NCSM) [152, 153], has achieved significantly reduced model spaces without compromising the accuracy for various observables, and has accommodated nuclei beyond the light species, as well as modes of enhanced deformation and spatially extended clustering (Fig. 8) [154, 155, 156, 157]. The model is founded on efficacious techniques of group theory and uses symmetry-adapted (SA) bases, based on the SU(3) symmetry group and its extension, the symplectic $\mathrm{Sp}(3,\mathbb{R})$ group, associated with deformation, vibrations and rotations. Such symmetries were first recognized by Bohr & Mottelson [158], followed by the seminal work of Elliott [159, 160, 161] and the microscopic no-core formulation by Rowe & Rosensteel [162, 163]. Earlier applications, which have been typically limited to just a few basis states and symmetry-preserving interactions, have provided successful descriptions of dominant collective features of nuclei – from the lightest systems [164, 165], through intermediate-mass nuclei [166, 167, 152], up to strongly deformed nuclei of the rare-earth and actinide regions [163, 168, 169, 170]. An important result is that dominant features of nuclei are indeed found to track with SU(3) and Sp(3,R) symmetries and naturally emerge from first-principle considerations [152, 153]. A major advantage of the SA-NCSM is that the SA model space can be down-selected to a subset of SA basis states that describe equilibrium and dynamical deformation, and within this selected model space the spurious center-of-mass motion can be factored out exactly [171, 172]. Another major advantage is the use of group theory, including the Wigner-Eckart theorem and group-theoretical algorithms.

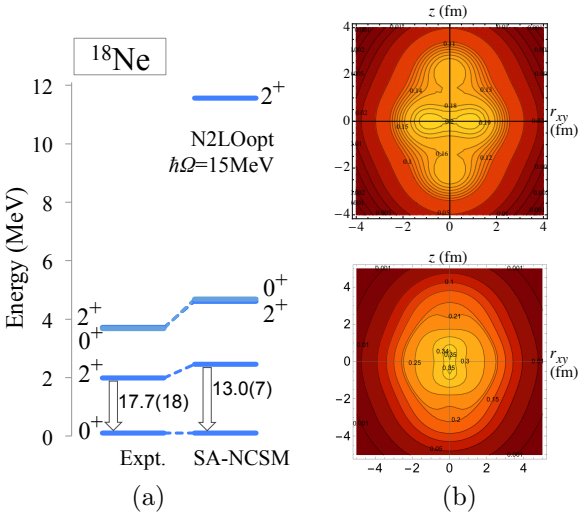

Figure 8: *Ab initio* SA-NCSM calculations using the chiral $\mathrm{NNLO_{opt}}$ [173] NN interaction. (a) Energy spectrum of ^{18}Ne in 9 HO major shells, along with the $B(E2;2^+ \rightarrow 0^+)$ strength in W.u. reported for 33 shells. (b) Density profile of the ground state of ^{20}Ne (top) and ^{48}Ti (bottom). Simulations are performed on the Blue Waters system. Figure adapted from Ref. [157].

SU(3)-scheme basis. – The many-nucleon SU(3)-scheme basis states are constructed using efficient group-theoretical algorithms [174, 175]. For a total of N HO quanta, the SU(3) symmetry further classifies the states according to the distribution of these quanta in the x, y, and z directions. Hence, a pair of quantum numbers can be introduced, $(\lambda\,\mu)$ with $\lambda = N_z - N_x$ and $\mu = N_x - N_y$, where $N_x + N_y + N_z = N$, and they, together with the total intrinsic spin S, label the states. E.g., $N_x = N_y = N_z$, or equally $(\lambda\,\mu) = (00)$, describes a spherical configuration, while N_z larger than $N_x = N_y$ ($\mu = 0$) indicates prolate deformation.

$\mathrm{Sp}(3,\mathbb{R})$-scheme basis. – The symplectic $\mathrm{Sp}(3,\mathbb{R})$ symmetry provides a further organization of the nuclear model space, and underpins the many-nucleon $\mathrm{Sp}(3,\mathbb{R})$-scheme basis states (reviewed in Refs. [151, 176, 152]). The main feature is that, within a symplectic configuration, $L = 0$ and $L = 2$ particle-hole excitations are driven by the total kinetic energy operator (or equally, the nuclear monopole moment that describes the "size" of the nucleus) and quadrupole moment (that describes the deformation of the nucleus). Indeed, operators that preserve the symplectic symmetry (do not mix symplectic configurations) include the monopole and quadrupole moment operators, the many-body kinetic energy, generators of rigid and irrotational flow rotations, and

the total orbital momentum L. Using Sp$(3,\mathbb{R})$-scheme basis is not as straightforward as the SU(3)-scheme basis, as there are no known Sp$(3,\mathbb{R})$ coupling/recoupling coefficients. The SA-NCSM with Sp$(3,\mathbb{R})$-scheme basis resolves this by diagonalizing an Sp$(3,\mathbb{R})$ symmetry-preserving operator calculated in the SU(3) basis [153]. The resulting Hamiltonian matrix is drastically small in size and its eigensolutions, the nuclear energies and states, can be calculated without the need for supercomputers. Alternative methods build the symplectic basis recursively, as outlined in Refs. [177, 178, 179], and later generalized to a no-core shell-model framework in Refs. [180, 181, 151] and in the *ab initio* symplectic no-core configuration interaction model (SpNCCI) [182, 183]. *Ab initio* SA-NCSM calculations reveal the predominance of only a few symplectic configurations in low-lying nuclear states in isotopes up through the calcium region – this implies that these states are typically made of only one or two equilibrium nuclear shapes (deformed or not) with associated vibrations and rotations [181, 152, 153].

In order to converge long-range properties of the nucleus, *i.e.*, those which depend up on the "tails" of the nuclear wave function, it is necessary, in the context of an oscillator basis, to include orbitals with large numbers of radial nodes and thus many oscillator quanta. Indeed, in a symplectic basis, once the dominant symplectic configurations contributing to the nuclear wave function are identified, the calculation can be extended, within these configurations, to include basis states with many more oscillator quanta than would be possible in a traditional NCSM calculation. In this way, one can accommodate collective correlations that are essential to account for deformation, as well as include small but critical configurations from the continuum. Such a pattern is encouraging for possible use of the SA framework to provide the structure component of reaction calculations.

3.2 Coupled Cluster and In-Medium Similarity Renormalization Group Methods

3.2.1 SRG Evolution of Interactions and Operators

Much of the progress in nuclear structure theory in the past decade has been enabled by the use of Effective Field Theory (EFT) and Renormalization Group (RG) methods. Two- and three-nucleon interactions from chiral EFT have become the standard input for *ab initio* structure theory — see Refs. [184, 185, 186, 187] for reviews and discussions of open issues. RG methods are a natural companion to EFT models, because they allow one to smoothly dial the *resolution scale or cutoff* of a theory. In principle, they could be used to rigorously connect various EFTs of the strong interaction by systematically integrating out degrees of freedom (high-momentum modes, composite particles, etc.), possibly starting from QCD. In practice, applications are typically simpler but nevertheless extremely useful: By lowering the resolution scale of input chiral two- and three-nucleon forces, we decouple their low- and high-momentum modes and greatly accelerate the convergence of few- and many-body methods that rely on Hilbert space expansions. This decoupling is achieved by means of a continuous unitary transformation, which we implement via the operator flow equation

$$\frac{d}{ds}H(s) = [\eta(s), H(s)]\,. \tag{8}$$

To decouple momenta, we construct the generator of the transformation using the relative kinetic energy,

$$\eta(s) \equiv [\frac{\vec{k}^2}{2\mu}, H(s)]\,. \tag{9}$$

Clearly, η would vanish – and the SRG evolution would stop – if the Hamiltonian were diagonal in momentum space. In applications, it is convenient to parameterize the flow by $\lambda \equiv s^{-1/4}$. From Eqs. (8) and (9), it is clear that λ has the dimensions of momentum. Its meaning is illustrated in Fig. 9 (a): the figure shows the SRG evolution of a two-nucleon Hamiltonian matrix in momentum space, and λ measures the width of diagonal band. In other words, it limits the momentum that the interaction can transfer in an NN scattering process to $|\vec{k} - \vec{k}'| \lesssim \lambda$. Thus, λ can be identified with the resolution scale of the evolved Hamiltonian.

The benefits of using the SRG to decouple low- and high-momentum physics in nuclei do come at a cost: the evolved nuclear Hamiltonian will contain induced many-body operators, even if we start from a two-body interaction. Numerically, the effect of induced interactions is demonstrated in Fig. 9 (b), which shows the evolution of ^{3}H ground-state energies that have been calculated with a family of SRG-evolved chiral NN and NN+3N interactions (see Ref. [188] for details). If we

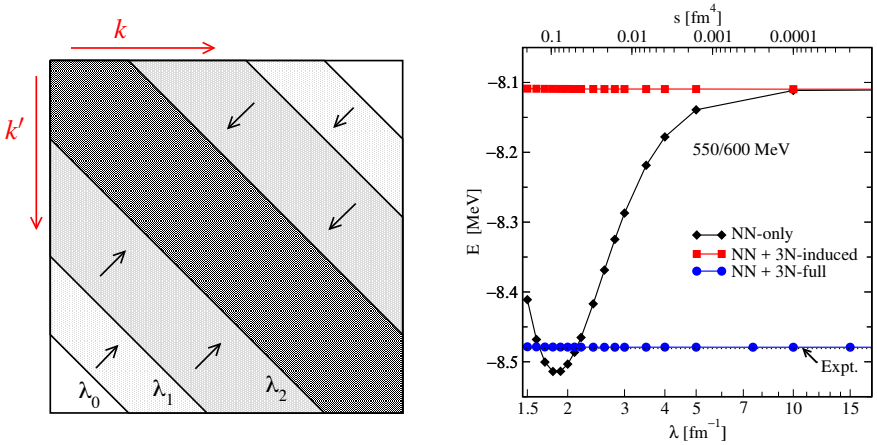

(a) (b)

Figure 9: SRG evolution of nuclear Hamiltonians. (a) Schematic view of the SRG evolution in momentum space. (b) Ground state energy of ^{3}H as a function of the flow parameter λ for chiral NNLO NN and $NN+3N$ interactions (see Ref. [188] for details). NN-only means initial and induced $3N$ interactions are discarded, $NN+3N$-induced takes only induced $3N$ interactions into account, and $3N$-full contains initial $3N$ interactions as well. The black dotted line shows the experimental binding energy [189]. Data for the figure courtesy of K. Hebeler.

neglect the induced three-body terms in the evolved interaction and the SRG generator, the energy varies by 5–6% as we evolve the Hamiltonian over a typical range of λ values (NN-only). If we include induced 3N interactions, the unitarity of the transformation is restored and the energy no longer varies with λ. Note that the NN+3N-induced results now match the ground-state energy we would have obtained with the unevolved NN interaction, while the NN+3N-full results are obtained from a consistently evolved NN+3N starting Hamiltonian that was fit to reproduce experimental triton data [184, 185, 190]).

Given that this example shows the importance of tracking induced interactions, one may ask whether the added complexity of dealing with 3N (and possibly higher) many-body forces makes RG evolving the Hamiltonian worthwhile at all. The answer to that question is affirmative, because the induced interactions will still be of low-momentum/low-resolution character — their improved convergence behavior in many-body calculations (far) outweighs the increased complexity of the Hamiltonian. Moreover, a hierarchy of many-nucleon forces naturally appears in Chiral EFT anyway, because its degrees of freedom are composite objects like nucleons and pions rather than quarks.

Another important consequence of working with SRG and chiral EFT is that *all operators of interest* must be constructed and RG-evolved consistently to ensure that observables like expectation values or cross sections remain invariant under specific choices of calculation schemes and resolution scales (see, e.g., Refs. [191, 192, 193, 194, 195]). This will be especially important when we work to connect nuclear structure and reaction theories. The SRG provides us with a useful diagnostic in these efforts: As discussed for Fig. 9, truncations of the SRG flow can lead to a violation of unitarity that manifests as a λ-dependence of calculated observables. We can use this dependence as a tool to assess the size of missing contributions, although they have to be interpreted with care [191].

3.2.2 Solving the Many-Body Problem with Decoupling Methods

The Coupled Cluster (CC) method and the In-Medium SRG (IMSRG) avoid the basis size explosion by avoiding the construction of the Hamiltonian matrix altogether, and hence can reach heavy nuclei.Instead, they use similarity transformations that act on the operator directly and decouple specific states or groups of states from the rest of the Hamiltonian matrix in an implicit fashion.
IMSRG. – We start with a general one- plus two-body Hamiltonian, which can be written in

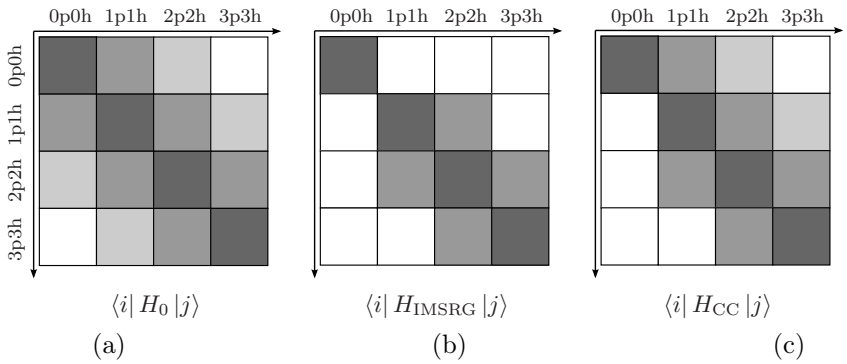

Figure 10: Decoupling of particle-hole excitations from a 0p0h reference state: the schematic matrix representation of the initial Hamiltonian H_0 (a) and the transformed Hamiltonians obtained from IMSRG (b) and CC (c), respectively (see text).

second quantization as

$$H = E + \sum_{ij} f_{ij}\{a_i^\dagger a_j\} + \frac{1}{4}\sum_{ijkl}\Gamma_{ijkl}\{a_i^\dagger a_j^\dagger a_l a_k\}\,. \tag{10}$$

The parentheses indicate that the strings of creation and annihilation operators have been *normal ordered* with respect to a reference state, which is typically a Slater determinant constructed from harmonic oscillator or Hartree-Fock orbitals (see Refs. [196, 197, 198] for details). After normal ordering, E is the energy expectation value of the reference state, while f and Γ are the *in-medium* mean-field Hamiltonian and residual two-nucleon interaction, respectively.

Figure 10 (a) shows the matrix representation of the Hamiltonian in the basis consisting of our reference Slater determinant and its particle-hole excitations. Note that H is band diagonal because it can at most couple npnh states to $(n \pm 2)$p$(n \pm 2)$h states. The goal of the IMSRG is to decouple the one-dimensional block in the Hamiltonian matrix that is spanned by our reference state Slater determinant (labeled 0p0h in Fig. 10) from all excitations, using the flow equation (8). In principle, we can use a suitably chosen reference to target different eigenstates, e.g., by taking references which are expected to have the largest overlap with the target (see Chapter 10.3 of Ref. [198]). In practice, we usually target the ground state by using a Hartree-Fock Slater determinant as our reference.

To achieve the desired decoupling, we use $H \equiv H_d + H_{od}$, where H_{od} denotes the part of H that we want to suppress, and H_d defines the desired Hamiltonian at the end of the IMSRG flow. In the free-space SRG discussed in Sec. 3.2.1, we decoupled momentum scales by by choosing $H_d = \vec{k}^2/2\mu$ and driving interaction matrix elements that couple states with $|\vec{k} - \vec{k'}| \gtrsim \lambda$ to zero. Here, we need to suppress

$$H_{od} \equiv \sum_{ph} H_{ph}\{a_p^\dagger a_h\} + \frac{1}{4}\sum_{pp'hh'} H_{pp'hh'}\{a_p^\dagger a_{p'}^\dagger a_{h'} a_h\} + \text{H. c.}\,, \tag{11}$$

which are the terms of H that couple the reference Slater determinant to 1p1h and 2p2h excitations, respectively. In analogy to the free-space SRG, we define the generator

$$\eta(s) \equiv [H_d(s), H_{od}(s)] = [H_d(s), H(s)] \tag{12}$$

to evolve the Hamiltonian operator and implicitly transform it to the matrix representation shown in Fig.10 (b). We note that this will not only decouple the ground state from excitations, but also eliminate the outermost band in the Hamiltonian matrix, which makes the evolved Hamiltonian an attractive input for subsequent configuration interaction or equation-of-motion approaches (see, e.g., Refs. [199, 200, 201]).

In most IMSRG applications to date, we truncate all operators at the two-body level, which defines the so-called IMSRG(2) scheme. Since we work with normal-ordered operators, the omission of induced three-body terms causes much smaller issues than in the free-space SRG: We are only truncating residual 3N interactions, while in-medium contributions to the zero-, one-, and two-nucleon parts of the Hamiltonian are accounted for. For more details about the method, we refer our readers to Refs. [196, 197, 198].

CC method. – In contrast to the IMSRG, the Coupled Cluster method decouples sectors of the Hamiltonian matrix through a non-unitary similarity transformation. Traditionally, the discussion of CC focuses on the correlated wave function, for which the ansatz

$$|\Psi_{CC}\rangle = e^T |\Phi\rangle \tag{13}$$

is introduced. Here, T is the so-called cluster operator, which is defined as

$$T = \sum_{ph} t_{ph}\{a_p^\dagger a_h\} + \frac{1}{4}\sum_{pp'hh'} t_{pp'hh'}\{a_p^\dagger a_{p'}^\dagger a_{h'} a_h\} + \dots\,, \tag{14}$$

and $t_{ph}, t_{pp'hh'}, \dots$ are the cluster amplitudes (see, e.g., Refs. [202, 203, 198]). In practical applications, the cluster operator is usually truncated to include up to 2p2h (CC with Singles and Doubles, or CCSD) or some of the 3p3h terms (CCSDT, including Triples). Acting on a Slater determinant reference state, e^T admixes arbitrary powers of such correlated few-particle, few-hole excitations. Note, however, that the cluster operator T is not anti-Hermitian because it lacks de-excitation operators, and therefore e^T is not unitary.

The cluster amplitudes are determined by demanding that the similarity transformed Hamiltonian,

$$H_{CC} \equiv e^{-T} H e^T\,, \tag{15}$$

does not couple the reference to 1p1h and 2p2h states. Defining $|\Phi_{h\dots}^{p\dots}\rangle = \{a_p^\dagger \dots a_h \dots\}\,|\Phi\rangle$, the decoupling conditions lead to the following system of non-linear equations:

$$\langle\Phi|\, e^{-T} H e^T\, |\Phi\rangle = E_{CC}\,, \tag{16}$$

$$\langle\Phi_h^p|\, e^{-T} H e^T\, |\Phi\rangle = 0\,, \tag{17}$$

$$\langle\Phi_{hh'}^{pp'}|\, e^{-T} H e^T\, |\Phi\rangle = 0\,. \tag{18}$$

Here, E_{CC} is the CC approximation to the ground-state energy, which corresponds to the upper left entry in H_{CC}'s matrix representation, as shown in Fig. 10 (c). The other blocks in the first column of the matrix vanish because of the CC equations.

As a consequence of the non-unitarity of the CC transformation, care must be taken when one evaluates observables using the CC wave function, or uses the non-Hermitian H_{CC} (cf. Fig. 10) as input for subsequent diagonalization. In this regard, the CC methods are less convenient than unitary transformation methods like the IMSRG. An advantage of CC over a unitary method is that the Baker-Campbell-Hausdorff series appearing in Eqs. (16)–(18) terminates at finite order because of the properties of the cluster operator, while additional truncations must be used in unitary approaches.

3.3 Lattice EFT and adiabatic projection method

Lattice EFT is a numerical method for calculating nuclear properties exactly in a periodic box from an EFT defined on a space-time lattice. Lattice methods for field theory was introduced by Wilson in the context of QCD [204]. Lattice methods for nuclear *ab initio* calculations from an EFT were introduced in Ref. [205]. In lattice EFT, one starts with an initial state wave function $|\psi_0\rangle$ (a Slater determinant) and evolves it in Euclidean time τ as $\exp(-\tau H)|\psi_0\rangle$ with the microscopic Hamiltonian H derived from EFT interactions. The exponential behavior of the partition function $\mathcal{Z} = \langle\psi_0|\exp(-\tau H)|\psi_0\rangle$ at large Euclidean times allows one to extract information about ground and excited state energies. Expectation values of observable $\mathcal{O}$, including higher order energy corrections, can be calculated as $\langle\psi_0|\exp(-\tau H/2)\mathcal{O}\exp(-\tau H/2)|\psi_0\rangle/\mathcal{Z}$. The review article [206] describes the implementation of lattice EFT for few- and many-body calculations. Both the pionless EFT and chiral formulation in the so called Weinberg power counting on a space-time lattice are described in detail there. The lattice EFT calculations are performed by Monte Carlo simulations over possible field configurations between the initial and final states.

The lattice EFT methods have been applied to a wide range of systems from few nucleons to $A \sim 30$ [207, 208]. The first accurate *ab initio* calculation of the Hoyle state energy was performed in lattice EFT [209]. Beyond static properties, reaction cross sections can be calculated using lattice methods. At low energy one usually considers the reactions $a(b,c)d$, $a(b,\gamma)c$ where a, b, c, d are nuclear clusters and γ a photon. Two recent algorithmic developments – adiabatic projection method and pinhole algorithm – allow for *ab initio* reaction calculations in lattice EFT.

In the adiabatic projection method [210], an initial trial state $|\vec{\boldsymbol{R}}_0\rangle$ approximating two nuclear clusters with separation $\vec{\boldsymbol{R}}_0$ is evolved with the microscopic Hamiltonian as $|\vec{\boldsymbol{R}}_\tau\rangle = \exp(-\tau H)|\vec{\boldsymbol{R}}_0\rangle$. Energy measurements with normalized wave functions determines the adiabatic Hamiltonian as $H_a = (\langle\vec{\boldsymbol{R}}'_\tau|\vec{\boldsymbol{R}}_\tau\rangle)^{-1}\langle\vec{\boldsymbol{R}}'_\tau|H|\vec{\boldsymbol{R}}_\tau\rangle$. The Hamiltonian H_a defined in the cluster coordinates has matrix dimensions $L^3 \times L^3$ whereas the microscopic Hamiltonian is $L^{3(A-1)} \times L^{3(A-1)}$ for an A-body system. The cluster Hamiltonian H_a is applicable at energies below the breakup of the nuclear clusters. It includes all deformation and polarizations of the clusters in the presence of other clusters from an *ab initio* calculation, without any modeling. The α-α s- and d-wave scattering phase shifts calculated from the 8-body Hamiltonian using the adiabatic projection method is shown in Fig. 11. Details of the calculations are in Ref. [211].

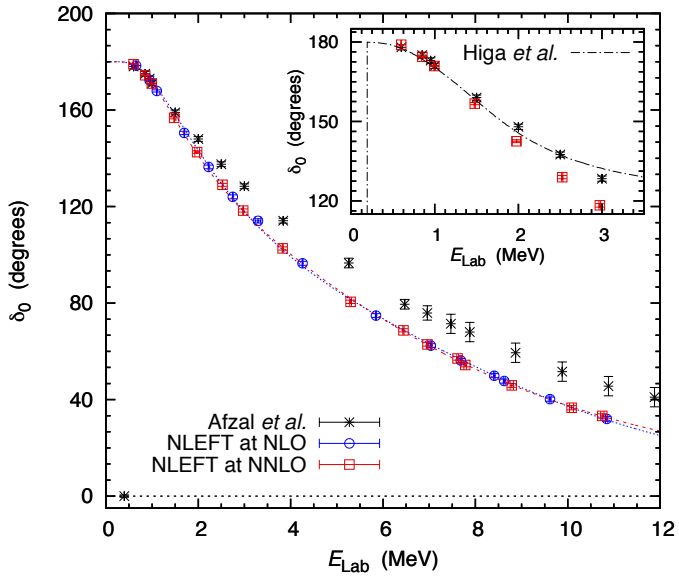

Figure 11: α-α s-wave elastic scattering phase shift from an *ab initio* lattice EFT calculation [211].

In the lattice EFT calculations, the particle locations in an atomic nuclei are not accessible. This deficiency has been remedied now with the introduction of the pinhole algorithm [212]. An opaque screen with A pinholes is inserted in the middle of the Euclidean time steps. The location, and spin-isospin labels of the pinholes are selected by the nuclear distribution in the simulation as determined by the microscopic interaction. This is implemented by inserting in the middle of the time step the A-body density operator $:\rho_{\alpha_1,a_1}(\boldsymbol{r}_1)\cdots\rho_{\alpha_A,a_A}(\boldsymbol{r}_A):$ with spin label α_i and isospin label a_i, respectively. Once the location of the nucleons $\vec{\boldsymbol{r}}_i$s are calculated from the pinholes, the center-of-mass location $\vec{\boldsymbol{R}}_{\rm c.m.}$ is determined by minimizing $\sum_{i=1}^{A}|\vec{\boldsymbol{R}}_{\rm c.m.} - \vec{\boldsymbol{r}}_i|^2$. The nucleon distributions were calculated for carbon isotopes ^{12}C, ^{14}C, ^{16}C; and accurately reproduced experimental measurements where available [212]. For example, the lattice EFT calculation for the ^{14}C charge radius 2.43 ± 0.07 fm is compatible with data 2.497 ± 0.017 fm [213] within the error bars.

3.4 Berggren basis

To address the challenges of describing nuclei as open quantum mechanical systems (Sec. 1.3), the quasi-stationary formalism has been developed, where the state of a many-body system in the continuum is described as a stationary wave with outgoing boundary conditions. While this formalism has been first introduced in 1884 [214], it has been introduced in nuclear physics by G. Gamow in 1928 [215]. The same idea was introduced in atomic physics by A. F. J. Siegert in 1939 [216].

Tore Berggren [217, 218] developed, at the end of the sixtieth, a complex-energy basis for applications to nuclear systems. In the Berggren basis (detailed in appendix A.1), bound states, resonances, and discretized complex-energy scattering states are all treated at the same footing, which is especially suitable for the description of loosely bound nuclei. This last attribute makes the Berggren representation easy to implement in already existing codes using well localized basis

states, as harmonic oscillator or Gaussian basis functions. Existing published codes provide the building blocks, i.e. bound states, resonant states and complex energy scattering states, which are eigenfunction of a given mean-field [219, 220, 221] and would substitute the localized basis. While dealing with divergent radial wave function or complex energy scattering state required some extra skill, in addition to the increased computational complexity, the gain of using the Berggren basis is that the single-nucleon asymptotic is well reproduce.

The key of the quasi-stationary formalism is that in the case of decaying resonances, the complex eigenenergies can be written as

$$E = E_0 - i\frac{\Gamma}{2} \quad \Rightarrow \quad T_{1/2} = \frac{\hbar}{\Gamma}\ln(2), \tag{19}$$

where the real part corresponds to the energy position of the resonance (the peak in the scattering cross section) and the imaginary part is associated to the energy dispersion or width of the resonance (width of the peak). The width can then be used to get the lifetime of the resonance. In short, the quasi-stationary formalism gives an access to the structure quantum systems in the continuum without using a time-dependent approach, by providing the energy positions and widths of resonances simultaneously. The price to pay for describing an intrinsically time-dependent process in a time-independent approach is that some of the solutions are not square-integrable anymore as shown in Fig. 12. While the bound state shown in Fig. 12 has a localized wave function that

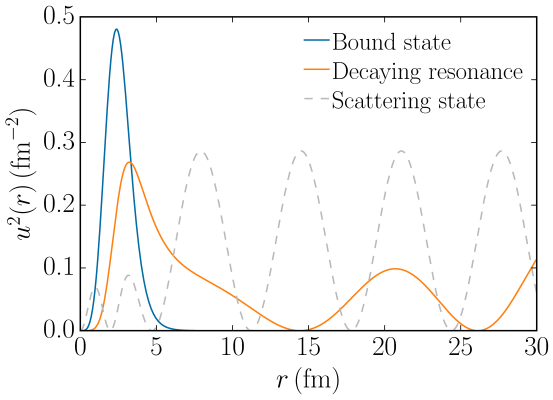

Figure 12: Typical bound state, decaying resonance, and scattering radial wave functions. The scattering and decaying resonance wave functions are not normalizable in the usual sense (Hilbert space norm).

falls off at large distances, the scattering state wave function has a plane-wave shape, and the decaying resonance has a localized inner part but also an external part that oscillates and grows to infinity, proportionally to the decay width. In fact, resonant and scattering states are not part of the Hilbert space, and they find their place in quantum mechanics when it is defined in the rigged Hilbert space [222, 223, 224].

The Berggren basis is a versatile tool that has been used in several nuclear many-body approaches (Fig. 13), starting with the Gamow shell model (GSM) [225], in the density matrix renormalization group method for open quantum systems or Gamow-DMRG [226, 227], as well as in the coupled cluster (CC) method [203]. It has also been used in the particle-plus-rotor model for atomic and nuclear physics problems [228], and was recently used in the Gamow coupled-channel approach in Jacobi coordinates [229] to solve the three-body problem. The configuration interaction approaches are currently limited to about ten particles (a core with about ten valence particles in GSM and the G-DMRG method, or ten active particles in no-core calculations), while the CC or IMSRG approaches can reach a hundred active particles, but only around (sub-)closed shell nuclei plus or minus one or two particles. The main issue with all these structure approaches, is that while in principle they take into account channel couplings through the configuration mixing thanks to the Berggren basis, it is not clear how to distinguish individual decay channels. As a consequence, these approaches cannot provide partial decay widths or any reaction observable. In order to circumvent this problem and access reaction observables in Berggren-based approaches, two possibilities are available (Fig. 13, right panel). The hard way is the extension of the many-body structure formalism to the resonating group method (RGM) where reaction channels are defined explicitly, similarly to what was done in the no-core shell model [230]. This strategy was adopted in the GSM+RGM (also referred to as coupled-channel Gamow shell model, GSM-CC) and allows to compute reactions observables directly from the many-body calculations [231, 232, 233, 234, 235]. The second way is to generate an effective potential for the "target" from many-body structure

calculations [236, 237, 238, 239, 240] using the many-body Green function formalism [241] (cf. Sec. 4.1.2).

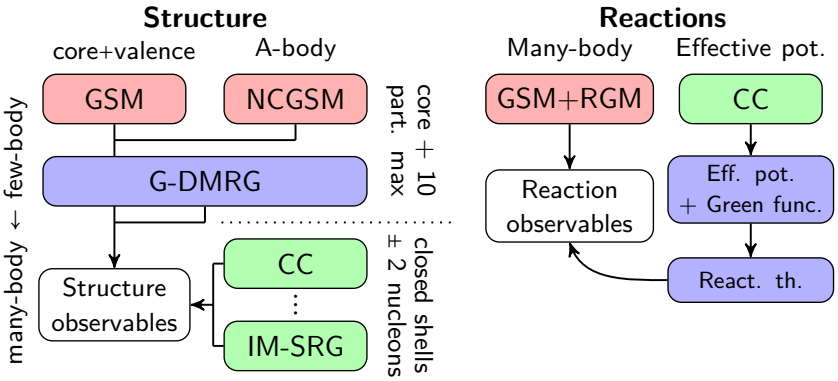

Figure 13: Snapshots of the methods using the Berggren basis for structure (left) and reaction (right) calculations. On the left, several methods are missing such as the particle-plus-rotor model or the Gamow coupled channel in Jacobi coordinates. On the right, the current strategies to obtain reactions observables can be divided in two groups: the use of RGM cluster basis as an extension of structure calculations and the effective potentials methods.

3.4.1 Gamow shell model

Early attempts to reconcile discrete and continuum aspects of nuclear many-body problems have been based on the projection formalism [242, 243] and lead to the development of the continuum shell model (CSM) [244, 245] and, more recently, the shell-model embedded in the continuum (SMEC) [246, 247, 248] which provides a unified approach to low-energy nuclear structure and reactions. In SMEC, one couples eigenstates of the phenomenological SM Hamiltonian with relevant reaction channels to describe the level spectroscopy and the reaction cross sections in the same many-body formalism [249] (Fig. 14).

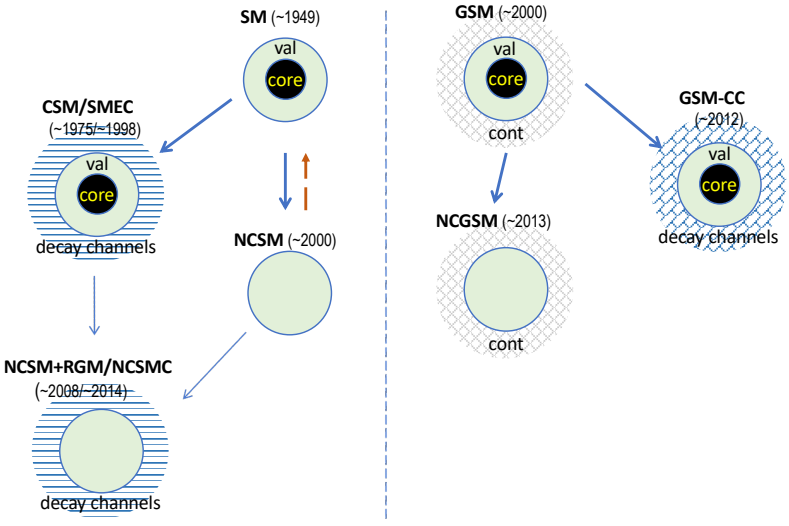

Figure 14: Recent evolution of paradigms in the low-energy nuclear structure and reaction theory from closed to open quantum systems.

First open quantum system formulation of the nuclear SM, respecting unitarity at the particle emission threshold(s), has been achieved in Gamow shell model (GSM) [250, 251, 252, 253]. The many-body states in GSM are given by the linear combination of Slater determinants defined in the Berggren ensemble of single-particle states. Reaction channels are not explicitly identified so

GSM in this Slater determinant representation is the tool for spectroscopic studies of bound and unbound states and their decays. Most numerical applications of the GSM have been done by separating an inert core and using the cluster orbital shell model [254] relative variables in the valence space. In this way, spurious center-of-mass excitations are removed.

The solution of an eigenvalue problem involving the continuum states is an acute numerical problem. As in the standard SM, the dimension of the many-body valence space increases catastrophically with the number of valence nucleons and the size of the single-particle basis. In GSM, each single-particle state of the discretized scattering contour becomes a new shell in the many-body calculation. Moreover, the use of Berggren ensemble implies complex-symmetric matrices for the representation of the hermitian Hamilton operator. To achieve convergent results, the density matrix renormalization group (DMRG) approach, first introduced to overcome the limitations of the Wilson-type renormalization group to describe strongly correlated 1D lattice systems with short-range interactions [255], has been extended for non-Hermitian systems and applied to solve the configuration-interaction problem of the GSM [256, 257]. As the properties of shells in the non-resonant continuum vary smoothly along the scattering contour, the GSM+DMRG approach is well suited to optimize the size of the scattering space and achieve completeness in GSM calculations.

For the description of scattering properties and reactions, the entrance and exit reaction channels have to be identified. This can be achieved in GSM by expressing wave functions in the complete basis of the reaction channels (in a procedure that is based on the RGM described in Sec. 3.1.1). This coupled-channel representation of the Gamow shell model (GSM-CC) has been recently applied for various observables involving one-nucleon reaction channels, such as the excitation function and the proton/neutron elastic/inelastic differential cross sections [231, 232, 233], or low-energy proton/neutron radiative capture reactions [234, 235]. Channels in these reactions are given by the initial/final GSM eigenvectors of $(A-1)$-body system coupled to proton/neutron in the continuum states. Resulting A-body wave functions are antisymmetrized and the separation of core and valence particles allows the GSM-CC to be applied in medium-heavy and heavy nuclei. One should stress that channels in GSM-CC are build by GSM wave functions which respects the unitarity at the decay thresholds of each cluster subsystem. The extension of the GSM-CC approach to reactions involving cluster reaction channels, such as deuteron or α-particle reaction channels, has been recently developed as well [258]. In particular, the calculated center-of-mass differential cross sections of the ^{4}He(d,d) elastic scattering in the GSM-CC [258] reproduces both the resonance spectrum of ^{6}Li, the phase shifts and the elastic scattering cross sections with a similar precision as the NCSMC [122]. However, GSM-CC can be applied to study the elastic scattering and transfer reactions involving many-nucleon projectiles whose composites cannot be reached in the NCSMC approach.

3.4.2 No-core Gamow shell model approach

More recently, following the progress in the NCSM and in constructing realistic nuclear interactions rooted in chiral effective field theory, the strategy pioneered by the continuum shell model has been further extended to *ab initio* description of structure and reactions within the no-core shell model coupled with the resonating-group method (NCSM/RGM) [113, 115], and the no-core shell model with continuum (NCSMC) [120, 121]. For the studies of resonant states in light nuclei, the no-core Gamow shell model (NCGSM) formulation has been recently successfully applied to investigate the resonant states of Helium and Hydrogen isotopes and the existence of tetraneutron [259, 260].

3.4.3 Using Berggren basis: pairing correlations and microscopic alpha decay

Pairing. – An alternative to the many-body basis truncation is to consider an effective interaction which keeps a subsets of all possible correlations, as for example pairing. Of special interest may be the constant pairing interaction which admits exact solutions. Since the realization that pairing effects [261] were important in nuclei system [262], it has been incorporated as a simplified model interaction to describe nuclear properties [263]. An overcoming formulation of the approximate solution of the pairing Hamiltonian, which conserves the number of particles, was proposed by Richardson shortly after pairing emergences [264]. A resurgence of Richardson approach happened at 2000 [265]; since then it has been recognized as a valuable model to study nuclear systems [266, 267, 268]. The application to pair correlation involving the resonant continuum has been introduced in Ref. [269] through the Gamow states. The proper treatment of the continuum must include the correlations with the resonant and non resonant part of the continuum spectrum of

energy. Subsequently, an overarching formulation which includes the full continuum, was introduce in Ref. [270] through the continuum level density. By modeling the resonant contribution with Breit-Wigner distribution and by rotating the contour to the imaginary energy axis, one separates explicitly the resonant and non-resonant contribution from the pairing interaction. Figure 15 (a) shows the relative contribution of the bound, resonant and nonresonant continuum in the drip-line nucleus ^{22}C. The analytic extension to the complex energy plane shows that the Berggren basis emerges naturally in the conserving particle number solution of the pairing Hamiltonian. For the derivation of the Richardson equations in the Berggren basis, see [271, 272]. This can be applied to studies of loosely bound nuclei, and also unbound nuclei. For example, the study of the unbound nucleus ^{28}C in the Gamow basis [270], produces a natural width for the ground states energy (which real part is positive.)

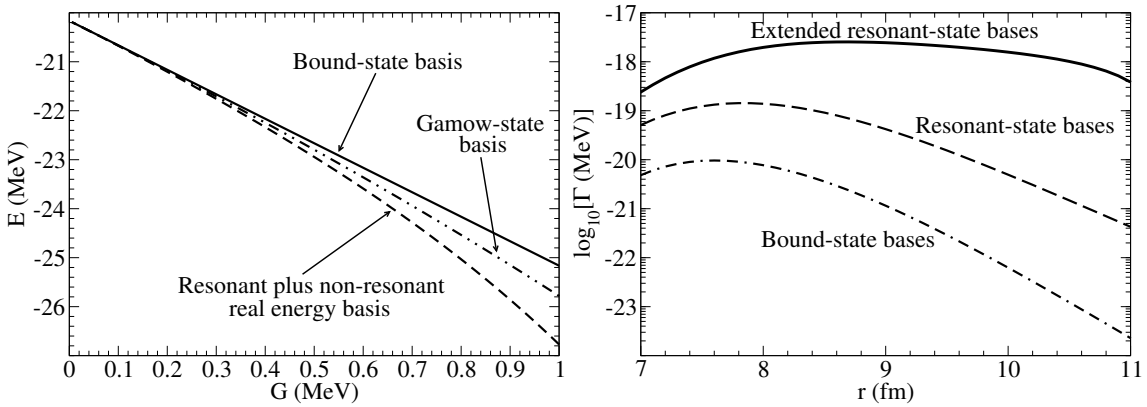

Figure 15: (a) Assessment of the bound states and the continuum in the ground state energy of the drip-line nucleus ^{22}C as a function of the pairing strength G. (b) Assessment of the continuum in the alpha decay calculation in ^{212}Po.

Microscopic alpha decay. – One of the biggest challenges in the microscopic description of nuclear drip-line physics is the proper assessment of the asymptotic behavior of the many-body wave function. This is particularly relevant in the description of the alpha decay since, from the R-matrix formalism, the absolute width results from the product of two functions which both depend on the radial coordinates, i.e. penetrability and reduced width [273]. Alpha decay has been traditionally describe in harmonic oscillator basis [274, 275, 276] with the limitation that asymptotic tail were not properly describe, which is reflected by the fact that the absolute width strongly depends on the radial coordinate. Since the Berggren basis properly includes the continuum, and then also the proper behavior of the radial coordinate asymptotically, one expects that the product of the two functions becomes independent of the radial coordinate.

From a pure microscopic stand point, i.e. without the explicit inclusion of a cluster, the clusterization of the four nucleons has to be built from the single-particle model spaces and the nucleon-nucleon interactions. The implementation of the Berggren bases, both in proton an neutron representation, allows the use of an extended basis that includes as many resonant continuum states through the Gamow resonances. Figure 15 (b) shows the behavior of the absolute width Γ as the single-particle model space increases from a representation which includes only bound states, resonant states, and finally an extended resonant-state bases, when a schematic separable force is used [277]. The plateau of the 2 fm width around the surface of the nucleus can only be achieved by using the Berggren basis. A proper treatment of the microscopic alpha decay in the vicinity of the drip-line nuclei should take into account all nucleon-nucleon correlations, e.g., with a suitable effective interaction in the continuum [278] or similar to Ref. [279] with applications to the superallowed alpha decay in ^{104}Te in the proton drip-line region.

3.4.4 CC and IM-SRG with Berggren basis

The complex-energy Gamow-Berggren framework has been recently merged with the IMSRG approach that uses a chiral EFT force [280]. The Gamow IMSRG has been successfully applied to neuron-rich carbon isotopes with significant results, e.g., pointing to a halo structure for the dripline nucleus ^{22}C. Some interesting resonant excited states are predicted, which would be valuable for fu-

ture experiments. However, there are still some issues needed to be solved in the Gamow-Berggren calculations. The complex resonant Berggren wave functions are not square integrable, which results in problems in the direct calculations of nuclear radii and electromagnetic transitions. The long-range Coulomb interaction is also difficult to be handled, due to the non-integrability of resonant wave functions. Though one can write an intrinsic Hamiltonian with the center-of-mass motion removed, the spurious center-of-motion excitation in the Gamow-Berggren wave functions is not easy to be treated, because usually the Woods-Saxon or Hartree-Fock basis is used, instead of the harmonic oscillator basis in which the spurious center-of-motion excitation can be removed by using the Lawson method [281]. One may use the so-called cluster-orbital shell-model framework to avoid the spurious center-of-mass excitation in the Gamow-Berggren many-body wave functions [254, 282]. However, in the *ab initio* types of the Gamow calculations, the transformations of realistic nucleon-nucleon interactions to the cluster-orbital shell-model scheme are very difficult to be handled. In addition, the Gamow numerical computations are performed with complex numbers and complex functions, therefore one needs to pay special attentions on the convergences of complex-number calculations. Due to the existence of scattering channels, the model space of a Gamow calculation can be huge, which requires substantial computer resources. Additionally, the stability of the Gamow numerical computations might be an issue, particularly for the imaginary parts of the resonance or continuum results. Nevertheless, the Gamow calculations provide a powerful tool to calculate the structure and reactions of bound, weakly-bound and unbound systems.

3.5 Self Consistent Green's functions

Green's functions are a representation of the solutions to a time-independent Hamiltonian H [241],

$$G(\alpha,\beta;t-t_0) = -\frac{i}{\hbar}\sum\!\!\!\!\!\!\int u_n(\alpha)u_n^*(\beta)e^{-\frac{i}{\hbar}\varepsilon_n(t-t_0)}, \tag{20}$$

represents a non-local, one-body, time-dependent Green function relevant for a single-particle problem. The integral sum runs over n eigenstates of the spectrum with eigenvalues ε_n and eigenfunctions u_n, and α,β are relevant complete sets of quantum numbers (*e.g.* $\boldsymbol{r},\boldsymbol{r'}$, $\boldsymbol{k},\boldsymbol{k'}$ or harmonic oscillator quantum numbers n,n',ℓ,j). Imposing $t > t_0$, that is causality in time–forward propagation, the time–dependent Green function can be rewritten through the Fourier transform of the Heaviside $\Theta(t-t_0)$. This generates the spectral representation of the forward Green function,

$$G(\alpha,\beta;E) = \sum\!\!\!\!\!\!\int \frac{u_n(\alpha)u_n^*(\beta)}{E-\varepsilon_n+i\eta}, \tag{21}$$

with $\eta \to 0$.

In the nuclear many-body problem, the reference state is usually the ground state of a doubly closed shell nucleus. Therefore, a particle can be both added to and removed from the ground state. It is important to consider both forward propagating and backward propagating Green functions, reducing to the familiar Källén–Lehmann spectral representation [283, 284]. That is, for a nucleus of A nucleons,

$$G(\alpha,\beta;E) = \sum \frac{u_p(\alpha)u_p^*(\beta)}{E-(E_p^{A+1}-E_0^A)+i\eta} + \frac{v_h(\alpha)v_h^*(\beta)}{E-(E_0^A-E_h^{A-1})-i\eta}. \tag{22}$$

The eigenvalues E_p^{A+1} and E_h^{A-1} correspond to the eigenstates of the particle $(A+1)$ configuration and the hole $(A-1)$ configuration, respectively. The particle and hole amplitudes u_p, v_h are given by,

$$u_p(\alpha) = \langle\psi_0^A|a_\alpha|\psi_p^{A+1}\rangle, \qquad v_n(\alpha) = \langle\psi_0^A|a_\alpha^\dagger|\psi_h^{A-1}\rangle, \tag{23}$$

with a_α and $a_\alpha^\dagger$ representing the addition and removal operator for the chosen basis $\{\alpha\}$.

The Green function can, in principle, be constructed with every many-body method from densities and eigenstates (cf. Sec. 4.1.1 and Appendix A.2). However, Green functions are directly used to solve the many-body problem following a diagrammatic expansion scheme [285, 286, 287]. The expansion will determine the many–body approximation used and the physics included in the self-energy, therefore in the propagator.

Starting from a general time-independent Hamiltonian, e.g., containing a two and three-body Hamiltonian,

$$H = T + V_{\rm NN} + V_{\rm 3N}, \tag{24}$$

the application of diagrammatic rules reduce it to a one-body effective interaction, that is referred to as the irreducible self-energy $\Sigma^\star$. A direct diagrammatic expansion can be employed, or, alternatively the equation of motion for the single-particle propagator can be utilized to generate its coupling to the two-particle propagator, *etc.* Particular schemes to sum infinite-order contributions have been implemented for infinite systems with full self-consistency. In the case of the ring-diagram approximation for the polarization propagator, one recovers the so-called *GW* approximation [288] which has found ample application in condensed matter physics. Ladder diagram summation are particularly relevant for nuclear systems and have been successfully implemented with full self-consistency at finite temperature for different realistic interactions (see e.g. Ref. [289]). Finite temperature calculations avoid consideration of pairing solution although these can be incorporated as well [290].

A related method used to calculate self-consistent ab-initio Green functions uses the Algebraic Diagrammatic Construction (ADC) [291, 286]. It is an automated way to include orders of perturbation into the definition of the irreducible self-energy,

$$\Sigma^\star(E) = \Sigma^\infty + \widetilde{\Sigma}(E), \tag{25}$$

where Σ^∞ is the static, energy independent part arising from mean-field like contributions, including an eventual external static potential, and $\widetilde{\Sigma}(E)$ is the energy-dependent part arising from correlations. The procedure uses the Dyson equation making the calculation of the propagators non-perturbative. In particular, the Dyson equation,

$$G = G^0 + G^0\Sigma^\star G, \tag{26}$$

is solved iteratively to obtained the dressed propagator G, from the bare propagator G^0 over the single-particle vacuum as defined in Eq. (22). One of the important properties of Green functions, is the dispersion relation (derived from the Kramers-Kronig relation) that connects real and imaginary part of the self-energy (see Sec. 2.2).

3.6 Energy density functional and heavy nuclei

Although *ab initio* many-body methods have increased their range of applicability throughout the nuclear chart in recent years, the majority of nuclei remain out of reach for these type of methods. The nuclear energy density functional (EDF) formalism remains the most microscopic approach available for heavy isotopes [292]. The EDF approach enforces a simple wave function for the nuclear system, like a Slater determinant in Hartree-Fock (HF) theory. This is in contrast to *ab initio* approaches that explicitly include the many-body correlations of the system into the wave function. In order to recover these correlations, the many-body Hamiltonian is constructed as a density dependent functional with parameters adjusted to reproduce a collection of nuclear structure properties. The main advantage of a mean field approach like EDF is that the resulting framework scales well with the number of particles. This makes EDF a reliable tool to study FRIB relevant systems like neutron rich nuclei close to the drip-line.

In HF theory the contribution of the two-body interaction $V_{NN}(\boldsymbol{r})$ to the total energy can be obtained by contracting the two-body potential matrix elements with the density matrix. This can be expressed in relative ($\boldsymbol{r}$) and center of mass ($\boldsymbol{R}$) coordinates as

$$\begin{aligned} E^{NN} = \frac{1}{2}\mathrm{Tr}_1\mathrm{Tr}_2 \int d\boldsymbol{R} \int d\boldsymbol{r} \langle \boldsymbol{r}\sigma_1\tau_1\sigma_2\tau_2 | V_{NN}(\boldsymbol{r}) | \boldsymbol{r}\sigma_3\tau_3\sigma_4\tau_4 \rangle \\ \times \left[\rho_1\left(\boldsymbol{R}+\frac{\boldsymbol{r}}{2}\right)\rho_2\left(\boldsymbol{R}-\frac{\boldsymbol{r}}{2}\right) - \rho_1\left(\boldsymbol{R}-\frac{\boldsymbol{r}}{2},\boldsymbol{R}+\frac{\boldsymbol{r}}{2}\right)\rho_2\left(\boldsymbol{R}+\frac{\boldsymbol{r}}{2},\boldsymbol{R}-\frac{\boldsymbol{r}}{2}\right) P_{12}^{\sigma\tau} \right], \end{aligned} \tag{27}$$

where the traces indicate summation over the spin σ and isospin τ quantum numbers and $P_{12}^{\sigma\tau}$ is an exchange operator. While in principle a realistic NN interaction can be used in Eq. (27) to calculate the HF energy, the non-local nature of the densities in the exchange term makes the calculations rather involved. In practice, interactions with specific symmetries are developed to deal with this non-localities, like the contact terms of a Skyrme functional or the Gaussian functions of a Gogny interaction. In such cases parameters are adjusted to reproduce nuclear structure data.

The phenomenological nature of this approach makes the implementation of systematic improvements, both in the description of experimental data and in predictive power, rather complicated. While additional terms can be added to the EDF to reduce difference between theory and

experiment, it is hard to define a clear hierarchy among the different terms for a general functional. EFT approaches introduce such kind of systematic improvements by relying on an order by order low momentum expansion from which a multi-nucleon interaction can be extracted. In practice two and three-body interactions are derived from the EFT expansion with some low energy constants adjusted to reproduce few-body observables.

In order to implement the systematic order by order improvements of EFT into the EDF framework [i.e., use a chiral interaction in Eq. (27)], the non-local densities can be treated with a density matrix expansion (DME). The DME approach can be considered analogous to a Taylor expansion in the sense that it expands a non-local density in terms of a local density and its derivatives

$$\rho\left(\boldsymbol{R}+\frac{\boldsymbol{r}}{2},\boldsymbol{R}+\frac{\boldsymbol{r}}{2}\right)\approx\sum_{n=0}^{n_{\max}}\Pi_n(kr)\mathcal{P}_n(\boldsymbol{R}) \tag{28}$$

where the Π_n functions are determined by the DME variant, $\mathcal{P}_n$ denote derivatives of the local density and the arbitrary momentum scale k is usually chosen to be the Fermi momentum k_F.

This DME approach has recently been fully implemented in [293] with a chiral two pion exchange potential including Δ resonances [294]. Although this EDF is microscopically constrained, a phenomenological contribution to the EDF is still necessary to recover the many-body correlations. Nevertheless, this implementation presents an improvement, in terms of describing experimental nuclear structure data, over previous purely phenomenological approaches like UNEDF2 [295]. Furthermore, a systematic improvement can be observed when comparing theoretical calculations of nuclear masses at different chiral orders with measured values.

3.7 Tails of wave functions: a challenge to many-body theory

An example of the challenges as one goes from bound state calculations to reactions and other calculations in the continuum are the tails of wave functions. In principle the tails are simple: they depend upon the separation energy ("slope") and the asymptotic normalization coefficient (ANC) ("amplitude"). The separation energy is an example of the sensitivity of such calculations to energies. The ANC can be, at least in principle, calculated through an integral over the interior of the nucleus, but this method still has to be fully implemented in many-body methods in occupation space [296].

As a specific example, consider the astrophysically important reaction ^{7}Be+p $\rightarrow^8$B+γ. The separation energy for the ground state of ^{8}B is only 137 keV, and in the core of the Sun, the Gamow reaction peak is around 20 keV. To give an idea of the importance of the long range tail, approximate the p-wave ground state wave function by an exponential, $\exp(-\kappa r)$, where $\kappa=\sqrt{2mE_s/\hbar^2}\sim 0.08$fm, where E_s is the separation energy (137 keV), and the scattering state by $\sin kr$ where $k\sim\sqrt{2mE_G/\hbar^2}\sim 0.03$fm, where E_G is the Gamow peak energy of 20 keV. This of course ignores Coulomb. For an E1 transition, then, the integrand looks like $r^2\exp(-\kappa r)\sin(kr)$. Even ignoring the scattering state, the E1 $\times$ the loosely bound state *peaks* at around 25 fm. To get the integral to converge, one has to integrate out beyond 100 fm.

Of course, if one can extract accurately the ANC and the separation energy, one can then compute the integral correctly. The problem then becomes, can one extract from theory both the separation energy and the ANC with sufficient accuracy.

Now here is one of the "cultural" differences between many-body theory and reaction theory, at least for weakly bound systems. Scattering and reaction theory, especially for weakly bound systems, depend crucially upon the asymptotics, which depend in turn on getting both relative energies such as the separation energy right, and on getting the amplitude (ANC) of the asymptotic wave function correct as well. Many-body theorists are well aware that their models generally do poorly on the asymptotics of the wave functions.

But getting the tails right is a tricky business. It is not simply enough to go beyond harmonic oscillator states. Radial wave functions derived from Woods-Saxon potentials, Hartree-Fock, or Coulomb-Sturmian will in general also not have the correct asymptotic behavior – they will be simply less grossly violating than harmonic oscillator.

The reason is that the asymptotic behavior does not arise from the one-body wave functions we build the wave functions from, but is an A-body effect: it is the behavior of the relative wave function between a single proton or neutron and the remaining $A-1$ body system. For any cluster decomposition, such as $d+(A-2)$ or $\alpha+(A-4)$ the problem is the same.

And here we have the clash of cultures. Even representing the 'distance' between a single nucleon, or a cluster of nucleons, and the center of mass of the remnant in a fully antisymmeterized many-body formalism is very difficult to define. Most attempts to do so are either (a) in a relative, Jacobi-coordinate system, where one can make the distances explicit (but these are limited to about 6 particles at most) (b) some explicitly clusterized model where one can place clusters a specified distance apart, such as Fermion Molecular Dynamics, or the group-theoretical methods which can "boost" clusters.

Another approach is to use integral relations, which relate scattering amplitudes and ANCs to integrals over the bulk of the wave function via Green's functions. The advantage of such approaches is that they are much less sensitive to the tails of the wave functions but can still get scattering information correct. Such methods have been applied to GFMC and hyperspherical harmonic calculations, but also work with a general many-body approach.

4 Connections

4.1 Input from many-body calculations into few-body methods

4.1.1 Effective inter-cluster interactions (optical potentials)

Exact solutions for the scattering problem have only been formulated and carried out for few-nucleon systems. Todays most advances in exact scattering calculations have been carried out for the four-nucleon system [297, 298, 25, 299]. Applying this approach to nuclear reactions has been and still is isolating important degrees of freedom, thus reducing the many-body problem to a few-body problem, and solving the few-body problem exactly [300].

Isolating important degrees of freedom means projecting onto a reduced Hilbert space and thus creating effective interactions between the degrees of freedom that are treated either exactly or with 'controlled' approximations. Since the 1960's (or earlier) such effective interactions have been constructed by fitting relevant experimental data with usually complex functions, leading to the well known phenomenological optical model potentials (see e.g. [301, 302, 303, 304]), which are local and energy-dependent. While the large body of phenomenological work may keep some place in practical applications, an overarching goal is to construct such effective interactions from the same first principles that govern the advance in many-body approaches to nuclear structure.

The effective interaction between a nucleon and a nucleus is one of the most important ingredients for reaction theories. Theoretical formulations have been introduced early on by Feshbach, leading to the Green's function formulation [96]. The theoretical approach to elastic scattering of a nucleon from a nucleus, pioneered by Watson [305, 306], made familiar by Kerman, McManus, and Thaler [307] and being refined further as the spectator expansion [308] leads to a multiple scattering expansion that can employ structure and reaction contents on equal footing in an order by order fashion. Both approaches start from a many-body Hamiltonian employing two- and three-nucleon forces.

4.1.2 Effective inter-cluster interaction based on the Green's function method for low energies: Results form the Coupled-cluster approach

The computation of a many-body propagator can be used to generate an effective interaction between the few sub-systems (clusters) that participate in a reaction process (e.g., nucleon-nucleus optical potential). An ideal framework for constructing nucleon-nucleus optical potential, is the Green function propagator. This is the propagator related to the $A+1$ and $A-1$ system with respect to the A system, and the self-energy Σ arising from the Dyson equation, see Eq. (26), is the desired effective potential [97]. The Green function can be calculated self-consistently form first principles [286] or constructed from a phenomenological approach [309] (cf. Sec. 3.5). It can eventually be built also using solutions from other many-body methods [238].

For the CC method (Sec. 3.4.4), the matrix elements of the corresponding Green's function

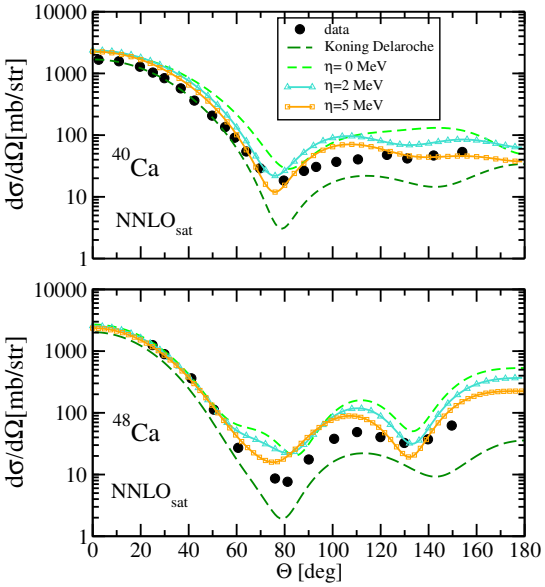

Figure 16: Differential elastic cross section for ^{40}Ca(n,n)^{40}Ca at 5.17 MeV (top) and ^{48}Ca(n,n)^{48}Ca at 7.81 MeV (bottom) calculated with the NNLO$_{\rm sat}$ interaction. Calculations are shown for $\eta = 0, 2, 5$ MeV. Results obtained using the phenomenological Koning-Delaroche potential are shown for comparison. Data points are taken from [311] (errors on the data are smaller than the symbols).

reads

$$G^{CC}(\alpha,\beta,E) \equiv \langle\Phi_{0,L}|\overline{a_\alpha}\frac{1}{E-(\overline{H}-E^A_{gs})+i\eta}\overline{a^\dagger_\beta}|\Phi_0\rangle + \langle\Phi_{0,L}|\overline{a^\dagger_\beta}\frac{1}{E-(E^A_{gs}-\overline{H})-i\eta}\overline{a_\alpha}|\Phi_0\rangle. \quad (29)$$

where $\overline{a_\alpha} = e^{-T}a_\alpha e^T$ and $\overline{a^\dagger_\beta} = e^{-T}a^\dagger_\beta e^T$ are respectively, the similarity-transformed annihilation and creation operators. $\langle\Phi_{0,L}|$ is the left eigenvector associated with the gs of $\overline{H}$ ($\overline{H}$ being not Hermitian has left- and right-eigenvectors [310, 203]). By definition, the parameter η is such that in the physical limit $\eta \to 0$. In practice, the Green's function (29) is calculated by working in the complex Berggren basis [217, 225] which (i) enables the description of bound, resonant and scattering states of the A and $A \pm 1$ nuclei and (ii) removes numerical instability associated with the poles of the Green's function.

Figure 16 shows calculations for the neutron elastic cross sections for ^{40}Ca and ^{48}Ca calculated with the optical potential obtained by inverting the Dyson equation fulfilled by the Green's function calculated at the CCSD level. Calculations were performed using the NNLO$_{\rm sat}$ chiral interaction [312] (which contains both NN+3NFs terms) which reproduces the binding energy and charge radius for both systems [313, 314]. Results are shown for respectively 5.17 MeV and 7.81 MeV in order to compare with available experimental data. In both cases, one expects the calculated optical potentials to have a finite imaginary part which reflects the loss of flux in the elastic channel. More precisely, in the case of neutron scattering on ^{40}Ca at $E = 5.17$ MeV, there is a potential absorption due to excitation of ^{40}Ca to its first excited state $E(0^+) = 3.35$ MeV or second excited state $E(3^-) = 3.74$ MeV. However, the calculated optical potentials yield a negligible value for the absorption in all partial waves [315]. This indicates that correlations beyond the singles and doubles truncation level in the CC method are needed to account for the absorption due to the target excitation. A similar situation occurs for the neutron scattering off ^{48}Ca at 7.81 MeV.

As shown in Fig. 16, one could artificially increase absorption by considering finite values of η instead of taking the limit $\eta \to 0^+$. When η increases, the elastic scattering cross section decreases with a more pronounced relative reduction at larger angles and the agreement with data improves. Angular distributions calculated with the phenomenological Koning-Delaroche potential [311] are also shown for comparison in Fig. 16.

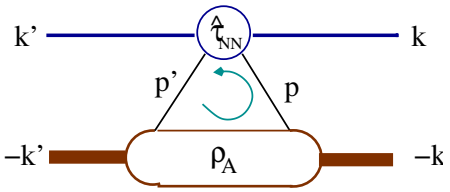

Figure 17: Schematic illustration of the effective (optical) potential $\hat{U}(\mathbf{k}', \mathbf{k})$ for the single scattering term in the the multiple scattering approach, where the momenta $\mathbf{k}$ and $\mathbf{k}'$ are the initial and final momenta of the projectile in the frame of zero total nucleon-nucleus momentum, $\hat{\tau}$ is the NN t-matrix. The same nucleon-nucleon NN interaction is used to calculate the nuclear density ρ_A of the target.

4.1.3 Effective inter-cluster interaction based on the multiple scattering method for intermediate energies: Results based on the no-core shell model

The spectator expansion is constructed within a multiple scattering theory predicated upon the idea that two-body interactions between the projectile and the target nucleons inside the nucleons play a dominant role. Thus, the first order term involves two-body interactions between the projectile and one of the target nucleons (represented by a one-body density matrix), the second order term involves the projectile interacting with two target nucleons and so forth. While the original spectator expansion [308] referred to expanding the many-body transition amplitude, it is more natural in the spirit deriving an effective interaction between the projectile and the target nucleus to expand the effective potential operator [316] in terms of active particles.

Current implementations of this expansion are based on two active particles leading to an effective potential schematically given in Fig. 17 and meaning that a one-body density matrix and a two-nucleon transition amplitude determine the effective nucleon-nucleus interaction [239], which is nonlocal as well as energy-dependent. We want to emphasize that now the one-body density matrix and the two-nucleon transition amplitude are derived from the same underlying nucleon-nucleon interaction [317]. Figure 18 shows the angular distribution of the differential cross section and the analyzing power for ^{4}He and ^{16}O at 200 MeV laboratory projectile kinetic energy with the effective interaction calculated as desribed in [239] and consistenly based in the NNLO$_{\rm opt}$ chiral interaction from [173].

It should also be pointed out that the many-body character of the free Green's function treated in [239] in the extreme closure approximation in principle connects even the first order of the effective potential to a two-body density matrix if one wants to include the effect of other nucleons in the nucleus on the struck target nucleon. In a mean-field picture this effect was estimated in [318] and found to be important only at energies below 100 MeV projectile kinetic energy. Similarly, in the lowest order two-body antisymmetry is achieved through the use of two-body t-matrices which are themselves antisymmetric in the two "active" variables (corresponding to the weak binding limit in [319]). For the next order, requiring two-body densities, three "active" variables need to be antisymmetrized, an effect which has been estimated in [320] and found small in the regime of 200 MeV projectile energy. Genuine three-nucleon force effects will only enter in the next order of the spectator expansion and also require two-body densities as well as solving a three-body problem for the three active nuclei. However, useful insights into the size and energy dependence of those contributions may already be obtained by an approximate solution.

4.2 Sum rules and response functions based on bound state techniques

Response functions to an electroweak probe and the response function moments, called sum rules, can be obtained without explicitly solving for the final eigenstates, by utilizing an indirect method, the Lorentz integral transform (LIT) method [323, 324]. The method transforms the problem into one that can be solved by a many-body bound-state technique. For example, many-body approaches previously used include hyperspherical harmonics, coupled-cluster method [325], and the symmetry-adapted no-core shell model [326]. The LIT method allows for calculating response functions using smaller model spaces in the many-body calculations by achieving fast-converging LIT transforms as compared to a slow-converging discretized response function. The LIT method has been applied to, e.g., nuclear responses for electromagnetic and weak operators [324], nuclear

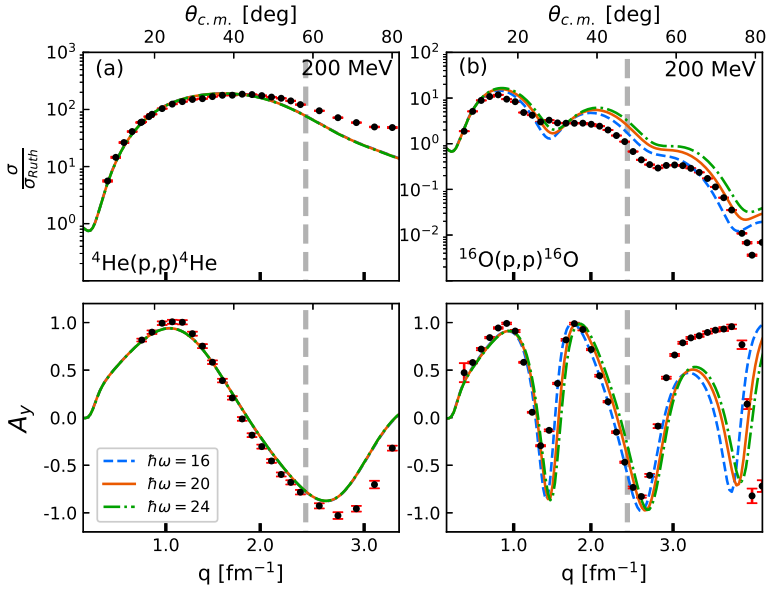

Figure 18: The angular distribution of the differential cross section divided by the Rutherford cross section and the angular distribution of the analyzing power for elastic proton scattering from ^{4}He (left panels) and ^{16}O (right panels) at 200 MeV laboratory kinetic energy as function of the momentum transfer and the c.m. angle calculated with the NNLO$_{\rm opt}$ chiral interaction [173]. For the ^{4}He calculations $N_{\rm max} = 18$ is employed, while for the ^{16}O $N_{\rm max} = 10$. The values of $\hbar\omega$ are given in the legend. The data for ^{4}He at 200 MeV are taken from Ref. [321] while the data for ^{16}O at 200 MeV are taken from Ref. [322]. The dashed vertical line in each figure indicates the momentum transfer $q = 2.45$ fm^{-1} corresponding to the laboratory kinetic energy 125 MeV of the np system up to which the NNLO$_{\rm opt}$ chiral interaction was fitted.

electric dipole polarizability [327, 328], and nuclear polarization effects for muonic atoms [329]. Alternatively, to calculate sum rules, the Lanczos sum rule (LSR) method (see, e.g., [330, 331] and references therein) is especially suitable for computing the low-lying energy spectrum that contains the peaks of electromagnetic transitions, such as electric monopole, dipole, and quadrupole transitions (e.g., see Ref. [326]).

4.3 Double charge-exchange transitions and the double Gamow-Teller resonance from the shell model

The double charge-exchange (DCX) processes are a promising tool to explore nuclear structure and in particular the study of two-body correlations in nuclei. In the 1980s, the DCX reactions using pion beams produced in the three meson factories at LAMPF, TRIUMF, and SIN were performed successfully providing interesting nuclear structure information. At present, there is a renewed interest in DCX reactions, to a large extent due to the extensive studies of double beta ($\beta\beta$)-decay, both the decay in which two neutrinos are emitted ($2\nu\beta\beta$) and neutrinoless double beta decay ($0\nu\beta\beta$). In DCX and $\beta\beta$-decay, two nucleons are involved. The pion, however, interacts weakly with states involving the spin and the pion DCX reactions do not excite the states involving the spin, such as the double Gamow-Teller (DGT) state. The DGT strength is an essential component of the $\beta\beta$-decay transitions. It was suggested in the past that one could probe the DGT state and hopefully the $0\nu\beta\beta$ decay using DCX reactions with light ions. At present DCX reactions are performed using light ions. There is a large program called NUMEN in Catania where reactions with ^{18}O, and ^{18}Ne have been performed. The hope is that such studies might shed some light on the nature of the nuclear matrix element of the $\beta\beta$-decay and serve as a "calibration" for the size of this matrix element. These DCX studies might also provide new interesting information about nuclear structure. One of the outstanding resonances relevant to the $0\nu\beta\beta$ decay is the double Gamow-Teller (DGT) resonance suggested in the past. At RIKEN, there is a DCX program using ion beams with the hope to observe the DGT states and other nuclear structure properties. At

Osaka University, the new DCX reactions with light ions were used to excite the double charge exchange states and compare to the pion DCX reaction results. One additional peak appeared in the cross section suggesting that it is a DGT resonance.

In the present research [332], the DGT transition strength distributions in even-A calcium isotopes are calculated in the full fp-model space using the nuclear shell model code NuShellX@MSU. The single Gamow-Teller operator is applied two times sequentially on the ground state of the parent nucleus to obtain the DGT strength. The properties of the DGT distribution are examined and limiting cases when the SU(4) symmetry holds or when the spin orbit-orbit coupling is put to zero, are studied. The DGT sum rules were used here as a tool to determine whether in our numerical calculations most of the DGT strength is found. The nuclear shell model wave functions of the initial ground state, $J = 1^+$ intermediate states, and $J = 0^+, 2^+$ final states were computed using the shell model using the FPD6 and KB3G interactions. The maximum number of intermediate states was 1000. The calculations were done for up to 5000 final states. This was enough to exhaust almost the total strength.

We comment on the question of quenching of GT strength, sometimes phrased as the renormalization of the GT operator. The single GT strength is reduced considerably, $30 - 40\%$ quenched. The origins of this quenching is still a puzzle. Two basic mechanisms were introduced. The quenching in charge exchange reactions is with respect to strength in the main peaks of the GT resonance. It is suggested that the rest of the strength is strongly fragmented and spread out at energies several tens of MeV above the main peaks. The nuclear force mixes the 1p-1h configurations that make up the GT state with 2p-2h configurations, leading to fragmentation of strength. There are experimental attempts to locate this strength but the results so far are not conclusive. The second possibility is that the missing GT strength is due to the coupling of the GT state to the internal excitation of the nucleon, namely to the Δ resonance, removing the strength to a high energy of about 300 MeV excitation. (Of course, there is the possibility that both mechanisms could contribute.) The quenching of the GT strength would affect the DGT strength as well and probably to a larger extent. The $\beta\beta$-decay, as already mentioned, is directly related to the DGT strength. The transition operator of the $2\nu\beta\beta$ is the same as the DGT operator. In the case of the $0\nu\beta\beta$ the transition operators have in addition to the DGT operator also a spatial dependence. The quenching will affect both types of $\beta\beta$-decay transitions. However, the effect on the $0\nu\beta\beta$ may be different than for the $2\nu\beta\beta$, depending on the quenching mechanism. By studying the stronger DGT transitions, in particular, the DGT giant resonance experimentally and theoretically, the calculations of $\beta\beta$-decay nuclear matrix elements can be calibrated to some extent. Nowadays the ion DCX reactions have been discussed mainly in the context of $0\nu\beta\beta$, however, the ion DCX reaction itself is a new probing tool of nuclear structure, in particular of spin degrees of freedom. The DGT resonance is just one example. Because two nucleons participate in the DCX reactions, one can expect that the nucleon-nucleon interaction and correlations can be probed, including nuclei that are far from the stability region. It is important to derive a DCX reaction theory that will enable to incorporate the microscopic description of the DGT strength in order to calculate cross sections.

4.4 Extrapolations from finite-volume calculations

4.4.1 ANCs from finite-volume calculations

As pointed out previously, ANCs are in principle observables, but difficult or impossible to measure directly. Usually one has to rely on their inherent connection to low-energy scattering properties, encoded, e.g., in the parameters of the effective range expansion. The latter is typically how ANCs enter in Halo EFT calculations, where the EFT expansion allows for their systematic correlation with other parameters. However, this does not allow to predict ANCs based on microscopic interactions.

An interesting possibility to obtain direct theoretical predictions of ANCs is given by finite-volume calculations as they are performed not only in lattice QCD but also in lattice EFT. With the latter approach, which is by now able to simulate sizable number of nucleons and also include the Coulomb interaction [211, 333, 212], it could be possible to extract ANCs relevant for reactions like α+^{3}He or ^{7}Be+p in the future, based on simulations of ^{7}Be and ^{8}B, respectively.

The key idea behind extracting ANCs from the volume dependence of bound states goes back to a result by Luscher, who derived in Ref. [334] that an s-wave bound states of two interacting particles with reduced mass μ, generated by an interaction with finite range R, is shifted in energy when it is enclosed in a cubic box with periodic boundary conditions. Denoting the length of this

box by L, the volume dependent binding energy shift of the state is

$$\Delta B(L) = -3|C|^2 \frac{\mathrm{e}^{-\kappa L}}{\mu L} + \mathcal{O}\big(\mathrm{e}^{-\sqrt{2}\kappa L}\big)\,, \tag{30}$$

where $\kappa = \sqrt{2\mu B}$ is the binding momentum of the state and C denotes the ANC. Equation (30) is valid for $L \gg R$, and the exponential form as well as the ANC occurring in the expression for the energy shift directly reflect that it is the *asymptotic* (long-range) properties of the state that govern the volume dependence, and not the short-range details of the interaction. While we focus here on the cubic periodic case as it occurs in lattice calculations, we note that the same basic principle applies more generally, e.g., to infrared extrapolations of harmonic oscillator basis, where the model-space truncation has been shown to impose an effective hard-wall boundary condition [335, 336, 337, 338]. What makes Eq. (30) so useful is that it directly relates the *infinite-volume* quantities κ and C to the volume dependent energies, allowing, in the simplest case, a combined extraction of both from a calculation at merely two different volumes. In practice, however, given in particular that lattice simulations typically involve stochastic noise, it is better to have more volumes available to perform a more sophisticated fit.

While Eq. (30) is limited to two-body s-wave states, it has been shown to hold in a more general form also for bound states with angular momentum. Specifically, Refs. [339, 340] derived that for a two-body state with angular momentum ℓ, the energy shift is

$$\Delta B^{(\ell,\Gamma)}(L) = \alpha\left(\tfrac{1}{\kappa L}\right) |C|^2 \, \frac{\mathrm{e}^{-\kappa L}}{\mu L} + \mathcal{O}\big(\mathrm{e}^{-\sqrt{2}\kappa L}\big)\,, \tag{31}$$

where Γ labels a representation of the cubic group (thus taking into account that the periodic box breaks the spherical symmetry of the infinite-volume system), and $\alpha(x)$ is a known polynomial, tabulated in Ref. [340], that depends on ℓ and Γ. Reference [341] further generalized the relation to the case of bound states comprised of more than two particles. Most relevantly to the present discussion, this work shows that the exponential scale governing the asymptotic volume dependence of a given state is associated with the nearest breakup threshold, with the shift still overall proportional to the associated ANC if the breakup is into two particles. Importantly, this result is true regardless of whether or not the state is described in an effective two-body halo picture.

4.4.2 Busch formula

The Busch formula was originally derived in Ref. [342] to connect the energy spectrum of a two cold atom system confined in a harmonic potential trap to their s-wave scattering phase shift. Various works have followed [343, 344, 345, 346], including generalizing it to the cases of higher partial waves [345, 346]. The formula can be written as

$$p^{2l+1} \cot \delta_l\,(p) \quad = \quad (-1)^{l+1} (4\mu\omega)^{l+\frac{1}{2}} \frac{\Gamma\left(\frac{3}{4} + \frac{l}{2} - \frac{E}{2\omega}\right)}{\Gamma\left(\frac{1}{4} - \frac{l}{2} - \frac{E}{2\omega}\right)}\,, \tag{32}$$

where $p \equiv \sqrt{2\mu E}$, E is the eigenenergy associated with the trap frequency ω (for a particle with mass m, the potential is $\frac{1}{2}m\omega^2\vec{r}^2$), l as the partial wave, δ_l is the corresponding phase shift, and μ is the two-body reduced mass. The formula was applied in low-energy nuclear physics to study a nucleon-nucleon system [346] and a three-nucleon system [347]. The formula is only exact when ω approaches zero; the correction at finite ω was missing and increases with ω [346]. In the framework of Halo-EFT, we have shown that in the low energy region, where the short-distance details of the two-cluster interaction are not resolved, the correction can be expressed in terms of the Taylor expansion [348]:

$$\sum_{i=0}^{\infty}\sum_{j=0}^{\infty} C_{i,j} \left(\frac{b^{-4}}{\Lambda^4}\right)^i \left(\frac{p^2}{\Lambda^2}\right)^j \quad = \quad (-1)^{l+1} \left(\frac{4\mu\omega}{\Lambda^2}\right)^{l+\frac{1}{2}} \frac{\Gamma\left(\frac{3}{4} + \frac{l}{2} - \frac{E}{2\omega}\right)}{\Gamma\left(\frac{1}{4} - \frac{l}{2} - \frac{E}{2\omega}\right)}\,, \tag{33}$$

$$\text{with } \left(\frac{p}{\Lambda}\right)^{2l+1} \cot \delta_l\,(p) \quad = \quad \sum_{j=0}^{\infty} C_{i=0,j} \left(\frac{p^2}{\Lambda^2}\right)^j\,. \tag{34}$$

Λ is introduced as a reference momentum scale to make the parameters $C_{i,j}$ dimensionless, and is the high-momentum scale of the theory; $b \equiv 1/\sqrt{\mu\omega}$ is the infrared length scale of a harmonic potential.

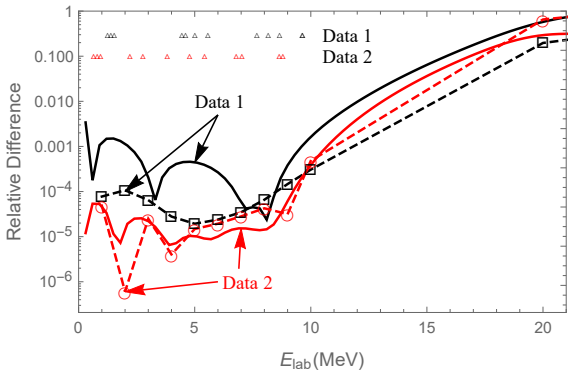

Figure 19: Relative error of the predicted NN scattering phase shift in $^1S_0$ channel vs laboratory energy. Two different eigenenergy "data" sets are used (inset): Data-1 with $\omega = 6, 3, 1, 0.9, 0.8$ MeV, and Data-2 with $\omega = 1, 0.9, 0.8, 0.6$ MeV (data with $\omega \approx 1$ MeV from [346]; data with $\omega = 6, 3$ from [349]). The open symbols are the true difference (dashed curves to guide the eye), and the solid curves represent our estimated 1-σ error bar. Both data sets have 12 eigenenergies.

Following Ref. [346], we tested the improved-Busch formula by studying a two-nucleon system in the $^1S_0$ channel. Fig. 19 shows how precisely the low-energy phase-shift can be predicted using the improved formula truncated to a finite series. In order to fix the unknown $C_{i,j}$ coefficients, Bayesian inference is applied to analyze the eigenergies [346, 349] calculated by the NCSM as data. The Bayesian analysis can provide robust error estimation [350]: here it is due to the formula-truncation error as the *ab initio* calculations relative error of 10^{-6} is at least one order of magnitude smaller. Note that the high-energy scale in terms of $E_{\rm lab}$ is on the order of 10 MeV as set by the one-pion exchange [346] (for N-α scattering this high-energy scale is around 20 MeV); in the low-energy region, the predictions agree quite well with the exact results, and interestingly the estimated error and the true deficiency are consistent [350]. Adding more data points would improve precision further, because larger data set allows the series in Eq. (33) to be truncated at a higher order. However, a consistent treatment requires rigorous estimate for the *ab initio* results uncertainties, which could be comparable to the series truncation error.

The (improved) Busch formula shows an effective way to connect bound state physics to the continuum ones, by first separating them (here, by using a background potential). In a potential trap, the continuum physics is reduced, and the *ab initio* method can be applied to compute energies and other properties associated with the "compacted" system. The Halo-EFT, as a cluster-based theory, is designed to focus on the continuum physics, with its unknown parameters dictated by the underlying short-distance physics. Our strategy is matching the two different frameworks through computing physical observables such as eigenenergies. The simplification in the two-cluster system is that through matching, the eigenenergies can be directly related to the phase shifts, as shown by the (improved) Busch formula. The next step is to generalize this strategy to more complicated systems, including inelastic channels and reactions, and systems with more than two clusters. The formula bears similarity to the Luscher formula [351], as used intensively and being generalized [352, 353] in the Lattice QCD community to extract hadrons scattering information from the system eigenenergies in periodic boundary conditions (cf. Sec. 4.4.1). It would be also interesting to compare the improved Busch formula with the infrared extrapolation procedure commonly used by the low-energy *ab initio* community [336], which is based on the relationship between the eigenenergies in a hard-sphere boundary condition and the scattering phase shift.

In our Halo-EFT work [354, 355, 356, 357] on $^7{\rm Be}\,(p,\gamma)^8\,{\rm B}$, we found that the dependence of the S factor at zero energy on the ANCs (C), elastic scattering length (a), inelastic channel contribution strength ε_1, and two-body current contribution ($\overline{L}$), can be linearized as

$$\begin{aligned} S(0) &= 35.76 C^2_{(^3P_2)} \left[1 - 0.002670 a_{(^3S_1)}(1 + 0.9095\varepsilon_1 - 0.3632\overline{L}_1)\right] \\ &\quad + 35.76 C^2_{(^5P_2)} \left[1 - 0.002670 a_{(^5S_2)}(1 - 0.3632\overline{L}_2)\right] + 2.337 \left(C^2_{(^3P_2)} + C^2_{(^5P_2)}\right). \quad (35) \end{aligned}$$

All the variables carry units in terms of proper powers of fm, except $S(0)$ in terms of eV b. (In the derivation, the ^{8}B ground state is 0.1370 MeV below the ^{7}Be+p threshold.) The correlation between $S(0)$ and the squared ANCs follows from the dominance of the one-body external direct

capture, and it is similar to earlier results, e.g., Refs. [358, 359, 360, 361]. We also found that changing the ^{8}Be binding energy by 1 keV, while fixing all C, a, and $\overline{L}$, changes the $S(0)$ by 1% [356, 357].

4.5 Time-dependent Basis Function method

The *ab initio* time-dependent Basis Function (tBF) method solves non-perturbative and time-dependent problems in quantum mechanics. For an initial demonstration problem, this method is applied to the Coulomb excitation of the deuteron by an impinging heavy ion [362].

The tBF is designed to utilize NCSM solutions directly for a limited set of reactions (such as COULEX) in its initial formulation. The *ab initio* NCSM solves the many-body Schrödinger equation for the bound states of nuclei treating all nucleons on an equal footing and uses nucleon-nucleon and three-nucleon interactions derived from chiral EFT.

4.6 Statistical reactions: Nuclear level densities

Many nuclear reactions (in the laboratory, in technological applications, and in astrophysics) can be successfully understood only if the level density of the final states in continuum is reliably evaluated. The importance of the level density for undertstanding nuclear structure and reactions was realized in the first years of nuclear physics. Bethe, Landau and Frenkel were the first to put the foundation of our current approaches. The main line of the research was based on the Fermi-gas models for the nucleus. Here the nuclear states were treated as combinations of the particle-hole excitations and their counting essentially was reduced to the distribution of excited constituents over the single-particle levels near the Fermi-surface.

The next steps were related to introducing particle correlations seen in pairing effects and collective states of vibrational and rotational character. The single-particle states were determined self-consistently with the use of semi-empirical models or more advanced density functional approaches. The collective states were added with the help of the random phase approximation and construction of rotational bands. Collective excitations, especially in deformed nuclei, lead to the so-called collective enhancement of the level density at relatively low energy. In experimental analysis, the level density of the "back-shifted" Fermi-gas formula is mostly used, as a function of neutron N and proton Z numbers, excitation energy E, and total spin projection M,

$$\rho(E,N,Z,M) = \frac{1}{12\sqrt{2}a^{1/4}(E-\Delta)^{5/4}\sigma}\, e^{2\sqrt{a(E-\Delta)}-M^2/2\sigma^2}. \tag{36}$$

The level density for spin J can be restored as the difference of ρ for $M = J$ and $M = J+1$. The main parameter a, the back-shift Δ, supposedly due to pairing, and the spin cut-off parameter σ usually require empirical adjustments.

Microscopic approaches are often based on the shell model (configuration-interaction approaches). These approaches either produce exact diagonalization of very large Hamiltonian matrices, currently with dimensions up to 10^{11}, or use statistical Monte Carlo methods based on the same matrices and a selected part of the matrix elements that includes the most coherent interactions (see, e.g., [363, 364, 365]). An inherent weak point here is the necessary truncation of orbital space as otherwise the diagonalization becomes practically impossible. However, the experience shows that a shell-model exact diagonalization can predict well the observed level density up to excitation energy about 15 MeV, or even further on, which is sufficient for many applications. The advantage of the shell model is in the exact treatment of all parts of interactions, including non-collective collision-like incoherent matrix elements. Such matrix elements are responsible for a smooth and wider shape of the total level density (each matrix element of this type adds quadratically to a width of the level density while these parts of the interaction are missed in other methods). The total level density in the shell-model space is the Gaussian function, as predicted by the random matrix theory (the down-going part describes just the model rather than realistic physics). One can extract thermodynamic properties of the system (entropy, temperature, single-particle occupation numbers, etc.) and justify the ideas of quantum chaos in real systems with no random elements (see, e.g., [366, 367, 368, 369, 370, 371, 372]).

Based on the chaotic properties of many-body dynamics with sufficiently strong interactions, the statistical procedures were worked out avoiding the diagonalizattion of prohibitively large matrices. The "moments" method uses only first two Hamiltonian moments which can be read

from the matrix itself [373, 374, 375, 376]. This was successfully used for nuclei in *sd* and *pf* shells; with special precautions, the results coincide with those of complete diagonalization when the latter is practically possible.

Practically all current theoretical and experimental results for the level density are well described by the "constant temperature model" (CTM) with an exponential form different from that in eq. (36),

$$\rho(E) = \text{const}\, e^{E/T}. \tag{37}$$

In contrast to the original interpretation of this model as a manifestation of the pairing phase transition, the shell-model analysis shows that this description remains valid, with the same T, when pairing is excluded and even for anti-pairing (repulsive interaction). The parameter T in Eq. (37) is not an actual temperature kept constant while the system undergoes a phase transition. Instead, this is similar to the limiting temperature at high energy with the exponentially rising number of resonances when the system has a crossover to quark-gluon or string state. Such a behavior is known for the bag model of particle physics. In nuclei it marks the gradual transition to quantum chaos where the thermodynamic temperature of the initial stage,

$$T_{\text{t-d}} = T[1 - e^{-E/T}], \tag{38}$$

reaches the value predicted by the bulk Gaussian curve.

In practice, the parameter $1/T$ characterizes the rate of increase of the level density at low energy. Among many silicon isotopes, the lowest T belongs to ^{28}Si with $N = Z$, due to the presence of isospin 0 states. The parameter T falls down if the single-particle levels are degenerate (the largest rate of chaotization for degenerate orbitals). The model predicts collective enhancement in the deformed case and the specific J-dependence. The results for the best parameters for all *sd* nuclei and all J-classes are tabulated [377]. The generalization to heavier nuclei is in preparation. The main theoretical problems are (i) to understand better the nature of the CTM and to give predictions for its parameters and their A- and J-dependence and (ii) to find ways for overcoming computational difficulties in going to heavier nuclei (see, e.g., [378, 379, 377, 380]).

5 Conclusions: where we have been and where we are going

The past quarter century has seen a resurgence in microscopic nuclear many-body theory, in particular in the development and application of a host of *ab initio* techniques. But many challenges remain, in particular in coupling the detailed many-body calculations to reactions and other physics in the continuum.

Of particular importance are applications to medium and heavy nuclei, which are and will be of interest to current and upcoming radioactive ion beam facilities. Coupled-cluster methods, including CC with a Gamow-Berggren basis, can address isotopes near closed shells. IMSRG can address open-shell nuclides, but cross-shell calculations are currently still difficult, and how to address tails of wavefunctions is not yet fully understood. The SA-NCSM approach is using symmetry-adapted bases, especially SU(3) and symplectic Sp(3,R) bases, which can describe open-shell, deformed medium-mass nuclei, and rigorously encode the important physics of deformation and kinetic energy.

Some open topics:

- How the effective NN interaction is modified in weakly-bound/unbound states;
- Pairing correlations in the vicinity of drip lines and close to the particle emission threshold in particle stable nuclei;
- Violation of mirror and isospin symmetries by the continuum coupling - astrophysical consequences;
- Coupling of collective and single-particle motion in the continuum, including the correct treatment of tails;
- Changes, if any, in γ-selection rules for in- and out- band transitions in resonance bands with respect to those known in stable nuclei;
- Specific near-threshold phenomena in γ- and particle-decay

- New kinds of multi-nucleon correlations and clustering in the vicinity of particle emission thresholds, e.g., ^{3}He and ^{3}H clustering vs ^{4}He clustering; similarity and differences;
- Role of coalescing resonances (exceptional points) in nuclear spectroscopy and reactions;
- Finally, merging *ab initio* models with phenomenology or experimental data.

Most of these problems are equally important both for experimentalists and theorists.

There are several potential paths from many-body theory to the continuum. For example, one could take the path from many-body theory $\rightarrow$ fully microscopic (NCSMC, R-matrix, tBF, etc.). Such a path would be "fundamental" but is extremely difficult because of the overwhelming number of degrees of freedom.

Alternately, one can attempt to decouple or integrate out most of those pesky degrees of freedom. For example, a second path is from many-body theory$\rightarrow$ effective ('optical') potential. This aligns with many "phenomenological" calculations of reactions today, but remains full of potential pitfalls, such as accounting properly for (or confirming where it is negligible) the Pauli principle, etc.

A third, related path, also rooted in current practice, is from many-body theory $\rightarrow$ structure parameters, e.g., 'spectroscopic factors'. This is practical, and can be useful for some indications of the uncertainties in many-body calculations. But spectroscopic factors, while useful, are model dependent and not a real observables [381].

Of course, as always, the path forward may be none of the above. We hope this somewhat stitched-together and of necessity incomplete paper will be a resource to the community–for example, in the Appendices, where we give more details about how to construct a Gamow-Berggren basis and optical potentials–showing where we are, where we want to be, and perhaps inspiring the new ideas and hard work needed to make progress.

Acknowledgements

This work covers material discussed at a workshop sponsored by the Facility for Rare Isotope Beams Theory Alliance.

This material is based upon work supported by the U.S. Department of Energy, Office of Science, Office of Nuclear Physics, under Award Numbers DE-FG02-95ER-40934, DE-FG02-03ER41272, DE-SC0013365, and by the National Science Foundation, Award Numbers PHY-1613362, PHY-1912643, PHY-1811815, OIA-1738287, PHY-1913728, and by the Deutsche Forschungsgemeinschaft (DFG, German Research Foundation) – Projektnummer 279384907 – SFB 1245. This research used resources of the National Energy Research Scientific Computing Center (NERSC), a U.S. Department of Energy Office of Science User Facility operated under Contract No. DE-AC02-05CH11231. We thank Anna McCoy for valuable input into the discussion of the SpNCCI framework.

A Appendix: "How to" details

A.1 How to build a single-particle Berggren basis

The general idea of the quasi-stationary formalism can be summarized as follows for the one-body problem: One starts with the time-independent Schrödinger equation for a given partial wave (39) and one looks for the solutions that are regular at the origin as defined in Eq. (40) and with outgoing boundary conditions as defined in Eq. (41).

$$\frac{\partial^2 u_\ell(k,r)}{\partial r^2} = \left(\frac{\ell(\ell+1)}{r^2} + \frac{2m}{\hbar^2} V(r) - k^2 \right) u_\ell(k,r). \tag{39}$$

$$u_\ell(k,r) \underset{r\sim 0}{\sim} C_0(k) r^{\ell+1}. \tag{40}$$

$$u_\ell(k,r) \underset{r\to\infty}{\sim} C_+(k) H^+_{\ell,\eta}(kr) + C_-(k) H^-_{\ell,\eta}(kr) \tag{41}$$

Two kind of solutions come out of the quasi-stationary problem and both can have real or complex eigenenergies. The resonant solutions, also called Gamow or Siegert states, are associated with discrete energies and are poles of the S-matrix. They are often called just "poles". The scattering solutions correspond to the nonresonant (continuum) states and have continuous energies.

A convenient way to look at the resonant solutions of the quasi-stationary problem is to look at the position of their momenta in the complex momentum plane as shown in Fig. 20.

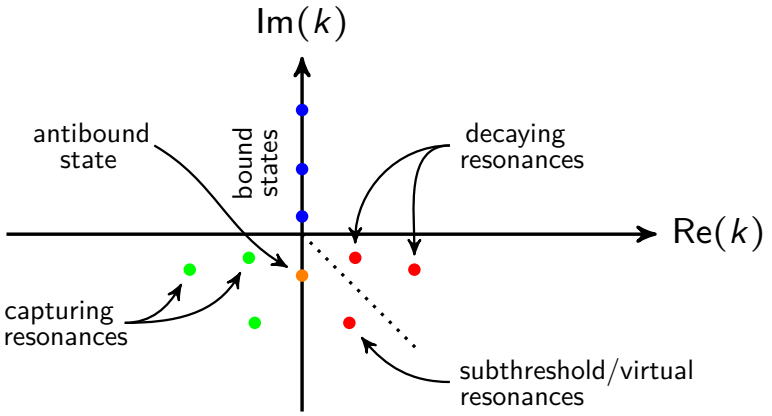

Figure 20: Zoology of S-matrix poles in the complex momentum plane. Bound states are on the positive part of the imaginary axis, while antibound or virtual states are on the negative part. Decaying resonances lie in the fouth quadrant and their time-reversal symmetric, the capturing resonances, lie in the first quadrant. We note that the decaying resonances below the -45 degree line (dotted line) cannot be interpreted as physical states like antibound states (negative energy, positive width), and are usually called subthreshold or virtual resonances.

At that point, a natural question is: Is it possible to use those states to expand any physical state similarly to the Mittag-Lefller expansion? This answer was found by T. Berggren in a groundbreaking work published in 1968 [217] where he demonstrated that a single-particle completeness relation can be built using resonant states and scattering states. He later demonstrated the equivalence with the Mittag-Lefller approach [218].

The proof of the so-called Berggren basis is based on the Cauchy's residue theorem, where the Newton basis [382] that is only made of bound states and positive energy scattering states is deformed, as shown in Fig. 21, to form a complex contour that surrounds selected poles of the S-matrix (resonant states).

In the particular case shown in Fig. 21, only bound states, narrow decaying resonances and scattering states along the contour are considered, but the specific shape of the contour is unimportant providing that the poles inside are properly accounted for in the completeness relation. It is possible to show that if the contour is divided in three parts denoted $\mathcal{S}$, $\mathcal{L}^-$ and $\mathcal{L}^+$ in the Fig. 21, in the limit of an infinite radius only the $\mathcal{L}^+$ contour has a nonzero contribution in the completeness relation as defined in Eq. (42).

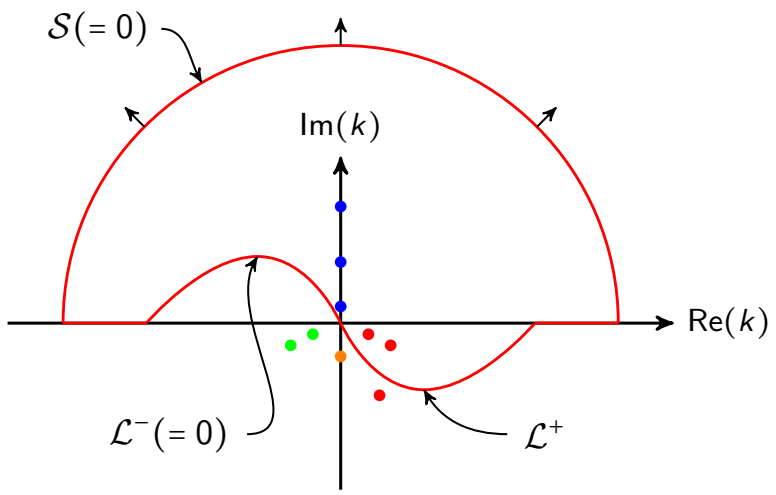

Figure 21: Construction of a typical Berggren basis using Cauchy's residue theorem. The shape of the contour could be changed to go around antibound states, providing that they are accouned for in the completeness relation.

$$\sum_{n\in(b,d)} |u_\ell(k_n)\rangle \langle \tilde{u}_\ell(k_n)| + \int_{\mathcal{L}^+} dk\ |u_\ell(k)\rangle \langle \tilde{u}_\ell(k)| = \hat{1}_{\ell,j}. \tag{42}$$

The sum in Eq. (42) runs over the bound states and decaying resonances (radial part), while the integral along the contour $\mathcal{L}^+$ defines the nonresonant continuum. The tilde over the bras denotes the time reversal operation which is equivalent to the complex conjugate operation. As a consequence, the norm for decaying resonances is the rigged Hilbert space norm (square) as shown in Eq. (43), that reduces to the usual norm for bound states (square modulus).

$$\mathcal{N}^2 = \langle \tilde{u}_{\ell,\eta} | u_{\ell,\eta} \rangle = \int_0^\infty dr\, \tilde{u}^*_{\ell,\eta}(r) u_{\ell,\eta}(r) = \int_0^\infty dr\, u^2_{\ell,\eta}(r). \tag{43}$$

In practice, the Berggren basis is represented as in Fig. 22 and the contour representing the nonresonant continuum is discretized in momentum space using a quadrature technique such as the Gauss-Legendre quadrature with about 30-45 scattering states. The truncation of the contour along the real axis usually requires a maximal momentum of about $k_{\max} = 6\,\mathrm{fm}^{-1}$ to ensure the completeness.

Several methods can be used to generate a single-particle Berggren basis as shown in Fig. 23. The methods shown on the left in Fig. 23 allow to generate a Berggren basis from scratch, while the methods on the right are ways to generate new (improved) Berggren basis if one already has one. Basically, the methods on the left require a one-body potential and a numerical technique to compute Gamow states, while the methods on the right require a many-body result to generate a one-body density whose eigenstates (natural orbits) form a correlated single-particle basis.

The simplest one is based on the analytical continuation of spherical Bessel function in the complex plane. Spherical Bessel functions are solutions of the stationary Shrödinger equation without any potential as shown in Eq. (44).

$$\frac{\partial^2 \psi_\ell(k,r)}{\partial r^2} = \left(\frac{\ell(\ell+1)}{r^2} - k^2 \right) \psi_\ell(k,r). \tag{44}$$

Only the solutions of the first kind $j_\ell(kr)$ that are regular at the origin are of interest to build basis states as defined in Eq. (45).

$$\phi_\ell(kr) = \sqrt{\frac{2}{\pi}} kr j_\ell(kr). \tag{45}$$

These basis states satisfy a special case of the Berggren basis when only positive energy scattering states are involved as in Eq. (46).

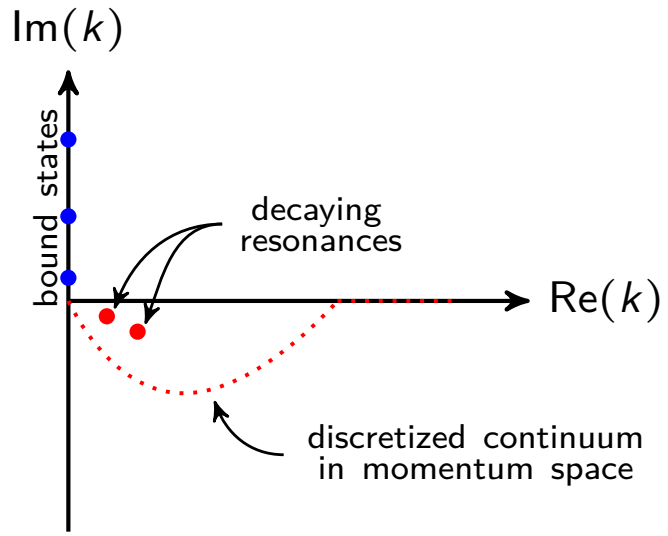

Figure 22: The nonresonant continuum states along the complex contour are discretized in momentum space, which allows to cover relatively high energies in the completeness relation.

$$\int_0^\infty dr\, \phi_\ell(kr)\phi_\ell(k'r) = \delta_{k,k'}. \tag{46}$$

The trick is to deform the real axis to form contour in the complex momentum plane and to compute the basis states in Eq. (45) of complex arguments kr. The analytical continuation of the spherical Bessel functions in the complex plane can be achieved using the recurrence relation refined in Eq. (47) (NIST 10.51(i)) and which is accurate up to $\ell = 6$.

$$f_{n+1}(z) + f_{n-1}(z) = \frac{2n+1}{z} f_n(z) \tag{47}$$

Once the basis states are computed, any one-body potential can be diagonalized, and the resulting eigenstates form a new basis that might include one or more resonant states depending on the potential.

The second method based on the Jost function [382] requires more work but provides smaller bases for the same level of completeness, which is unimportant at that point but can be crucial in many-body applications. There are in fact two equivalent Jost function methods, each one having pros and cons. The first Jost function method presented hereafter is the one used in the Gamow shell model [383, 250, 225], while the second one can be found in Ref. [384].

The first Jost function method is basically a search of the zeroes of the outgoing Jost function for resonant states. One starts with the one-body stationary Schrödinger equation including the Coulomb potential as shown in Eq. (48).

$$\frac{\partial^2 u_{\ell,\eta}(k,r)}{\partial r^2} = \left(\frac{\ell(\ell+1)}{r^2} + \frac{2m}{\hbar^2} V(r) - \frac{2\eta k}{r} + k^2 \right) u_{\ell,\eta}(k,r). \tag{48}$$

One wants the solutions that are regular at the origin and with outgoing boundary conditions, so at large distances, the solutions are the incoming and outgoing Hankel functions:

$$H^{\pm}_{\ell,\eta}(z) = \begin{cases} F_{\ell,\eta}(z) \mp iG_{\ell,\eta}(z) & \text{for } \eta \neq 0, \\ z[j_\ell(z) \mp n_\ell(z)] & \text{for } \eta = 0, \end{cases} \tag{49}$$

which are expressed using either the Coulomb wave functions if there is a Coulomb potential, or the spherical Bessel functions if there is none. Consequently, a general solution of Eq. (48) at large distances can be written as a linear combination of Hankel functions:

$$u_{\ell,\eta}(k,r) = C^+(k)H^+_{\ell,\eta}(kr) + C^-(k)H^-_{\ell,\eta}(kr). \tag{50}$$

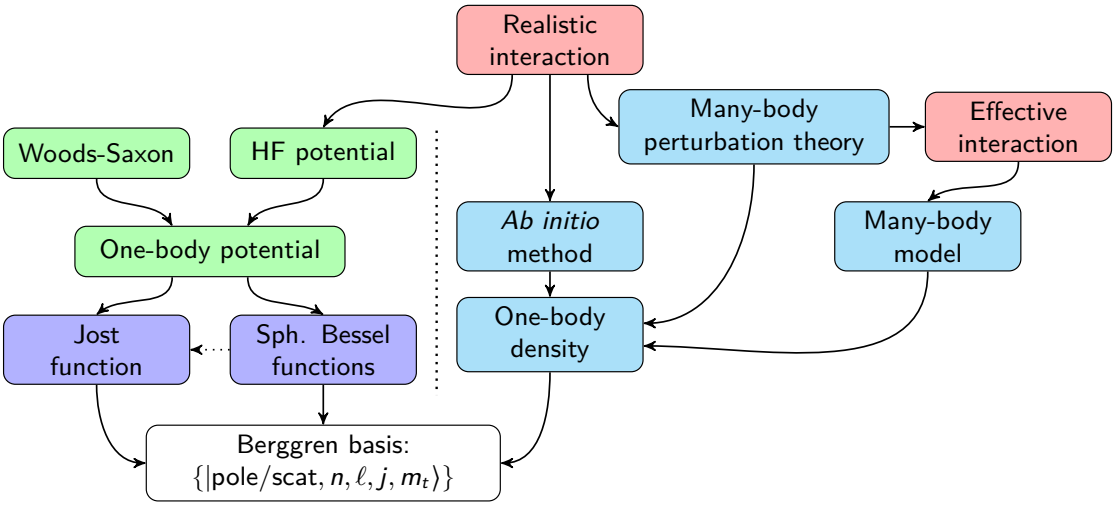

Figure 23: Most common options to generate either a new Berggren basis from scratch, or a better Berggren basis from an existing one. The resulting states are defined by the usual quantum numbers n, ℓ, j and m_t, but in practice one also needs to know whether they correspond to pole states or scattering states.

The solution at large distances must match the solution at intermediate distances, and so the general solution of Eq. (48) can then be written:

$$u_{\ell,\eta}(k,r) = C^+(k)u^+_{\ell,\eta}(k,r) + C^-(k)u^-_{\ell,\eta}(k,r). \tag{51}$$

The goal is then to determine the incoming and outgoing functions $u^\pm_{\ell,\eta}(k,r)$ and the associated coefficients $C^\pm(k)$. The Schrödinger equation can be integrated from zero to $r = R$ with R large enough to reach the asymptotic region, and at that point one can use the matching conditions defined in Eqs. (52,53).

$$\frac{d}{dr}\left(C^+(k)H^+_{\ell,\eta}(kR) + C^-(k)H^-_{\ell,\eta}(kR)\right) = \frac{du_\ell(k,R)}{dr}. \tag{52}$$

$$C^+(k)H^+_{\ell,\eta}(kR) + C^-(k)H^-_{\ell,\eta}(kR) = u_\ell(k,R). \tag{53}$$

While these conditions are sufficient for scattering states, outgoing resonant states (bound states, decaying resonances) satisfy $C^-(k) = 0$ by definition, which means that the differentiability of the wave function is not ensured by Eqs. (52,53). In fact, the additional constrain for outgoing states comes from the outgoing Jost function. The incoming and outgoing Jost functions are defined as [382]:

$$\mathcal{J}^\pm_\ell(k) = W(u^\pm_\ell(k,r), u_\ell(k,r)) = u^\pm_\ell(k,r)\frac{du_\ell(k,r)}{dr} - u_\ell(k,r)\frac{du^\pm_\ell(k,r)}{dr}. \tag{54}$$

The presence of the Wronskian makes the Jost functions independent of r by construction, and so numerically the differentiability of the wave function is enforced by varying k until $\mathcal{J}^+_\ell(k) = 0$, which is just a search of zeroes. The advantage of this method is that the momenta of the resonant states is determined while solving the Schrödinger equation.

The second Jost function method [384] is relatively simpler to implement but requires to know the momenta of the resonant states to include in the Berggren basis beforehand. In practice, this information is obtained by first solving the problem using the method based on spherical Bessel functions, and then just keeping the poles of interest.

The idea of this method is to write the wave function at intermediate distances as a linear combination of Hankel functions as in Eq. (50), except that before the asymptotic region the coefficients $C^\pm(k)$ are replaced by the "r-dependent" Jost functions $\mathcal{F}^+_{\ell,\eta}(r,k)$. The trick is to have an equation for the derivative of the r-dependent Jost functions with initial conditions, which allows to integrate the Schrödinger equation from zero to any desired value as shown in Fig. 24.

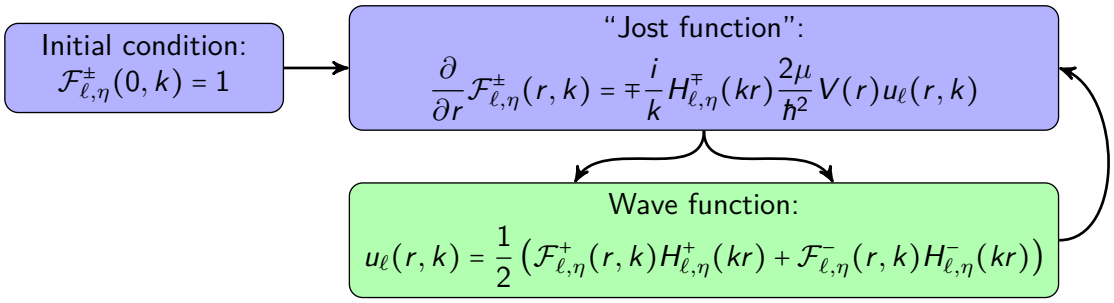

Figure 24: Simple scheme to compute the wave functions of pole and scattering states using the Jost function method. The momenta of the pole states must be known beforehand.

Using the initial conditions for the r-dependent Jost functions and the wave function, the derivatives of the r-dependent Jost functions can be computed, and hence the values of the r-dependent Jost functions at the next point, which can be used to compute the wave function etc. At large distances, the r-dependent Jost functions must become constant and correspond to the Jost functions $\lim_{r\to\infty}\mathcal{F}^{+}_{\ell,\eta}(r,k) = \mathcal{J}^{+}_{\ell,\eta}(k)$, which implies that the incoming and outgoing coefficients are given by: $C^{\pm}(k) = \mathcal{J}^{\pm}_{\ell,\eta}(k)/2$. These coefficients are the asymptotic normalization coefficients (ANCs) and can then be used to compute phase-shifts for instance.

Once all necessary resonant and scattering states have been obtained, the normalization can be achieved for scattering states [385] by satisfying Eq. (55) while for resonant states a regularization method must be used to compute the norm as defined in Eq. (43).

$$C^{+}(k)C^{-}(k) = \frac{1}{2\pi} \tag{55}$$

Several regularization methods can be used in principle to normalized a decaying resonance state, but the exterior complex-scaling method [386, 387, 388] appears as a relatively convenient approach as it can be applied on any wave function. The norm is then computed as follows:

$$\begin{aligned}\mathcal{N}^2 &= \int_0^R dr\, u^2_{\ell,\eta}(r) + \left(C^{+}(k)\right)^2 \int_R^\infty dr\, \left(H^{+}_{\ell,\eta}(kr)\right)^2, \\ &= \mathcal{I}_R + \left(C^{+}(k)\right)^2 \int_0^\infty dx\, \left(H^{+}_{\ell,\eta}(k[R + xe^{i\theta}])\right)^2 e^{i\theta},\end{aligned} \tag{56}$$

where the tail of the wave function is rotated in the asymptotic region by a given angle until the integral is regularized. Once this is achieved, the result does not depend on the angle θ and the position R around which the rotation is done.

As a final remark, one of the biggest difficulty with the Jost function methods is to compute the Hankel functions in the complex plane. So far, it seems that such functions are only available in two publications [389, 390].

A.2 How to build an effective nucleon-nucleus ('optical') potential via Green functions

In principle, Green functions can be generated post-hoc using the many-body method of choice (cf. also Sect. 3.5). Consequently, the effective nucleon-nucleus interaction can be calculated through the inversion of the Dyson equation (26),

$$\Sigma^{\star} = (G^0)^{-1} - G^{-1}, \tag{57}$$

where G^0 and G are the bare and dressed propagators respectively. We outline here some notable points necessary to generate the self-energy from a many-body calculation:

1. Construct the bare single-particle Green function in the given many-body context. That is, consider Eq. (22) and E_0^A as the unperturbed ground state of the system with A particles (e.g. harmonic oscillator filled to *sd* shell closure) and E_n^{A+1} as the possible states of the system with $A+1$ particles (e.g. harmonic oscillator filled to *sd* shell closure, +1 particle in each of the possible states in the space under consideration, $1p_{3/2}$ state, $1p_{1/2}$ ... etc...). Densities are given from the chosen basis states (usually trivially 1, corresponding to occupied hole and particle states, or 0 for unoccupied states).

2. Construct, in the same basis, the dressed single-particle Green function from the given many-body calculation. That is, considering Eq. (22), using the densities (23) and ground A-particles and excited $A+1$-particles states coming from the many-body wavefunction.

3. Invert the Dyson equation (57) to obtain the self-energy, which is the non-local, generalized, nucleon-nucleus optical potential in the chosen basis.

4. Eventually, solve the Dyson equation (26 for the obtained self-energy, at the same many-body expansion to verify convergence of the propagators.

Once the self-energy is obtained, it is possible to exploit its rich content to explore the single-particle spectrum and spectral density, nonlocality, volume integrals of the imaginary part, and to provide a check for dispersion relations.

References

[1] A. Arcones *et al.*, Progress in Particle and Nuclear Physics **94**, 1 (2017).

[2] J. Carlson *et al.*, Progress in Particle and Nuclear Physics **94**, 68 (2017).

[3] M. Mumpower, R. Surman, G. McLaughlin, and A. Aprahamian, Progress in Particle and Nuclear Physics **86**, 86 (2016).

[4] C. R. Brune and B. Davids, Annual Review of Nuclear and Particle Science **65**, 87 (2015).

[5] F. Käppeler, R. Gallino, S. Bisterzo, and W. Aoki, Rev. Mod. Phys. **83**, 157 (2011).

[6] P. Kleinwachter and I. Rotter, Phys. Rev. C **32**, 1742 (1985).

[7] V. Sokolov and V. Zelevinsky, Physics Letters B **202**, 10 (1988).

[8] V. Sokolov and V. Zelevinsky, Nuclear Physics A **504**, 562 (1989).

[9] S. Drożdż, J. Okołowicz, M. Płoszajczak, and I. Rotter, Physical Review C **62**, 024313 (2000).

[10] R. H. Dicke, Physical review **93**, 99 (1954).

[11] N. Auerbach and V. Zelevinsky, Reports on Progress in Physics **74**, 106301 (2011).

[12] A. Baz, Sov. Phys. JETP **6**, 709 (1958).

[13] R. G. Newton, Physical Review **114**, 1611 (1959).

[14] N. Michel, W. Nazarewicz, and M. Płoszajczak, Phys. Rev. C **75**, 031301 (2007).

[15] N. Michel, W. Nazarewicz, and M. Płoszajczak, Phys. Rev. C **82**, 044315 (2010).

[16] Y. V. Fyodorov and B. A. Khoruzhenko, Phys. Rev. Lett. **83**, 65 (1999).

[17] P. E. Koehler, F. Bečvář, M. Krtička, J. A. Harvey, and K. H. Guber, Phys. Rev. Lett. **105**, 072502 (2010).

[18] G. L. Celardo, N. Auerbach, F. M. Izrailev, and V. G. Zelevinsky, Phys. Rev. Lett. **106**, 042501 (2011).

[19] J. Okołowicz, M. Płoszajczak, and W. Nazarewicz, Progress of Theoretical Physics Supplement **196**, 230 (2012).

[20] J. Okołowicz, W. Nazarewicz, and M. Płoszajczak, Fortschritte der Physik **61**, 66 (2013).

[21] K. Ikeda, N. Takigawa, and H. Horiuchi, Progress of Theoretical Physics Supplement **68**, 464 (1968).

[22] J. Okołowicz, M. Płoszajczak, R. J. Charity, and L. G. Sobotka, Phys. Rev. C **97**, 044303 (2018).

[23] H. Witała *et al.*, Phys. Rev. C **63**, 024007 (2001).

[24] R. Lazauskas and J. Carbonell, Phys. Rev. C **70**, 044002 (2004).

[25] R. Lazauskas, Phys. Rev. C **97**, 044002 (2018).

[26] L. Hlophe, J. Lei, C. Elster, A. Nogga, and F. M. Nunes, Phys. Rev. C **96**, 064003 (2017).

[27] A. Kievsky, S. Rosati, M. Viviani, L. E. Marcucci, and L. Girlanda, Journal of Physics G: Nuclear and Particle Physics **35**, 063101 (2008).

[28] A. Deltuva and A. C. Fonseca, Phys. Rev. C **75**, 014005 (2007).

[29] K. M. Nollett, S. C. Pieper, R. B. Wiringa, J. Carlson, and G. M. Hale, Phys. Rev. Lett. **99**, 022502 (2007).

[30] F. Nunes and N. Upadhyay, J. Phys. G: Conf. Ser. **403**, 012029 (2012).

[31] C. Elster and L. Hlophe, J.Phys.Conf.Ser. **403**, 012025 (2012).

[32] I. J. Thompson and F. M. Nunes, *Nuclear Reactions for Astrophysics* (Cambridge University Press, 2009).

[33] E. O. Alt, P. Grassberger, and W. Sandhas, Nucl. Phys. **B2**, 167 (1967).

[34] A. Deltuva and A. C. Fonseca, Phys. Rev. C **79**, 014606 (2009).

[35] A. Deltuva, Phys.Rev. **C79**, 054603 (2009).

[36] E. Cravo, R. Crespo, A. M. Moro, and A. Deltuva, Phys. Rev. C **81**, 031601 (2010).

[37] Nunes, F.M. *et al.*, EPJ Web Conf. **178**, 03001 (2018).

[38] A. Mukhamedzhanov, V. Eremenko, and A. Sattarov, Phys.Rev. **C86**, 034001 (2012).

[39] TORUS Collaboration, N. J. Upadhyay *et al.*, Phys. Rev. C **90**, 014615 (2014).

[40] TORUS Collaboration, L. Hlophe *et al.*, Phys. Rev. C **90**, 061602 (2014).

[41] N. Austern *et al.*, Physics Reports **154**, 125 (1987).

[42] N. J. Upadhyay, A. Deltuva, and F. M. Nunes, Phys. Rev. C **85**, 054621 (2012).

[43] K. Ogata and K. Yoshida, Phys. Rev. C **94**, 051603 (2016).

[44] J. Lei and A. M. Moro, Phys. Rev. C **95**, 044605 (2017).

[45] A. Gómez Camacho, B. Wang, and H. Q. Zhang, Phys. Rev. C **97**, 054610 (2018).

[46] M. Gómez-Ramos and N. K. Timofeyuk, Phys. Rev. C **98**, 011601 (2018).

[47] Y. Chazono, K. Yoshida, and K. Ogata, Phys. Rev. C **95**, 064608 (2017).

[48] R. C. Johnson and P. J. R. Soper, Phys. Rev. C **1**, 976 (1970).

[49] R. Johnson and P. Tandy, Nuclear Physics A **235**, 56 (1974).

[50] F. Nunes and A. Deltuva, Phys.Rev. **C84**, 034607 (2011).

[51] K. T. Schmitt *et al.*, Phys. Rev. Lett. **108**, 192701 (2012).

[52] J. Yang and P. Capel, Phys. Rev. C **98**, 054602 (2018).

[53] A. Kankainen *et al.*, Physics Letters B **769**, 549 (2017).

[54] J. A. Tostevin and A. Gade, Phys. Rev. C **90**, 057602 (2014).

[55] T. Aumann, C. A. Bertulani, F. Schindler, and S. Typel, Phys. Rev. Lett. **119**, 262501 (2017).

[56] P. Capel, D. Baye, and Y. Suzuki, Phys. Rev. C **78**, 054602 (2008).

[57] C. Hebborn and P. Capel, Phys. Rev. C **98**, 044610 (2018).

[58] N. C. Summers, F. M. Nunes, and I. J. Thompson, Phys. Rev. C **74**, 014606 (2006).

[59] N. C. Summers, F. M. Nunes, and I. J. Thompson, Phys. Rev. C **89**, 069901 (2014).

[60] A. M. Moro and J. A. Lay, Phys. Rev. Lett. **109**, 232502 (2012).

[61] R. de Diego, J. M. Arias, J. A. Lay, and A. M. Moro, Phys. Rev. C **89**, 064609 (2014).

[62] M. Gómez-Ramos, A. M. Moro, J. Gómez-Camacho, and I. J. Thompson, Phys. Rev. C **92**, 014613 (2015).

[63] R. Crespo, A. Deltuva, and A. M. Moro, Phys. Rev. C **83**, 044622 (2011).

[64] A. Deltuva, Phys. Rev. C **91**, 024607 (2015).

[65] T. Matsumoto *et al.*, Phys. Rev. C **73**, 051602 (2006).

[66] M. Rodríguez-Gallardo *et al.*, Phys. Rev. C **80**, 051601 (2009).

[67] P. Descouvemont, Phys. Rev. C **97**, 064607 (2018).

[68] A. E. Lovell and F. M. Nunes, Phys. Rev. C **97**, 064612 (2018).

[69] G. B. King, A. E. Lovell, and F. M. Nunes, Phys. Rev. C **98**, 044623 (2018).

[70] A. V. Manohar, Introduction to Effective Field Theories, in *Les Houches summer school: EFT in Particle Physics and Cosmology Les Houches, Chamonix Valley, France, July 3-28, 2017*, 2018, arXiv:1804.05863.

[71] D. B. Kaplan, Five lectures on effective field theory, 2005, arXiv:nucl-th/0510023.

[72] J. Polchinski, Effective field theory and the Fermi surface, in *Proceedings, Theoretical Advanced Study Institute (TASI 92): From Black Holes and Strings to Particles: Boulder, USA, June 1-26, 1992*, pp. 0235–276, 1992, arXiv:hep-th/9210046.

[73] S. Weinberg, Phys. Lett. **B251**, 288 (1990).

[74] S. Weinberg, Nucl. Phys. **B363**, 3 (1991).

[75] I. Tanihata et al., Phys. Lett. **B160**, 380 (1985).

[76] I. Tanihata et al., Phys. Rev. Lett. **55**, 2676 (1985).

[77] P. G. Hansen and B. Jonson, Europhys. Lett. **4**, 409 (1987).

[78] C. A. Bertulani, H. W. Hammer, and U. Van Kolck, Nucl. Phys. **A712**, 37 (2002).

[79] P. F. Bedaque, H. W. Hammer, and U. van Kolck, Phys. Lett. **B569**, 159 (2003).

[80] G. Rupak, Int. J. Mod. Phys. **E25**, 1641004 (2016).

[81] H. W. Hammer, C. Ji, and D. R. Phillips, J. Phys. **G44**, 103002 (2017), arXiv:1702.08605.

[82] R. Higa, G. Rupak, and A. Vaghani, Eur. Phys. J. **A54**, 89 (2018), arXiv:1612.08959.

[83] U. van Kolck, Nucl. Phys. **A645**, 273 (1999), arXiv:nucl-th/9808007.

[84] J.-W. Chen, G. Rupak, and M. J. Savage, Nucl. Phys. **A653**, 386 (1999), arXiv:nucl-th/9902056.

[85] L. Fernando, R. Higa, and G. Rupak, Eur. Phys. J A **48**, 24 (2012).

[86] E. Ryberg, C. Forss'en, H. W. Hammer, and L. Platter, Annals Phys. **367**, 13 (2016), arXiv:1507.08675.

[87] S. Typel, Private communication.

[88] B. Davids and S. Typel, Phys. Rev. C **68**, 045802 (2003).

[89] T. Tombrello, Nucl. Phys. **71**, 459 (1965).

[90] M. Butler, J.-W. Chen, and X. Kong, Phys. Rev. **C63**, 035501 (2001), arXiv:nucl-th/0008032.

[91] C. Mahaux and R. Sartor, Single-particle motion in nuclei, in *Adv. Nucl. Phys.* Vol. 20, p. 1, Springer US, 1991.

[92] M. H. Mahzoon, R. J. Charity, W. H. Dickhoff, H. Dussan, and S. J. Waldecker, Phys. Rev. Lett. **112**, 162503 (2014).

[93] W. H. Dickhoff, R. J. Charity, and M. H. Mahzoon, J. Phys G **44**, 033001 (2017).

[94] M. H. Mahzoon, M. C. Atkinson, R. J. Charity, and W. H. Dickhoff, Phys. Rev. Lett. **119**, 222503 (2017).

[95] H. Feshbach, Ann. Phys. **5**, 357 (1958).

[96] F. Capuzzi and C. Mahaux, Ann. Phys. (N.Y.) **281**, 223 (2000).

[97] J. Escher and B. K. Jennings, Phys. Rev. C **66**, 034313 (2002).

[98] S. J. Waldecker, C. Barbieri, and W. H. Dickhoff, Phys. Rev. C **84**, 034616 (2011).

[99] N. B. Nguyen, S. J. Waldecker, F. M. Nunes, R. J. Charity, and W. H. Dickhoff, Phys. Rev. C **84**, 044611 (2011).

[100] G. Potel *et al.*, The European Physical Journal A **53**, 178 (2017).

[101] M. C. Atkinson, H. P. Blok, L. Lapikás, R. J. Charity, and W. H. Dickhoff, ArXiv e-prints (2018), arXiv:1808.08895.

[102] L. Lapikás, Nucl. Phys. A **553**, 297 (1993).

[103] P. F. Bedaque and U. van Kolck, Annual Review of Nuclear and Particle Science **52**, 339 (2002).

[104] E. Epelbaum *et al.*, Phys. Rev. C **66**, 064001 (2002).

[105] D. R. Entem and R. Machleidt, Phys. Rev. C **68**, 041001 (2003).

[106] E. Epelbaum, Prog. Part. Nucl. Phys. **57**, 654 (2006).

[107] R. Machleidt, Phys. Rev. C **63**, 024001 (2001).

[108] A. Shirokov, J. Vary, A. Mazur, S. Zaytsev, and T. Weber, Physics Letters B **621**, 96 (2005).

[109] A. Shirokov, J. Vary, A. Mazur, and T. Weber, Phys. Lett. B **644**, 33 (2007).

[110] R. Roth and P. Navrátil, Phys. Rev. Lett. **99**, 092501 (2007).

[111] T. Abe *et al.*, Phys. Rev. C **86**, 054301 (2012).

[112] A. F. Lisetskiy *et al.*, Phys. Rev. C **78**, 044302 (2008).

[113] S. Quaglioni and P. Navrátil, Phys. Rev. Lett. **101**, 092501 (2008).

[114] S. Quaglioni and P. Navrátil, Phys. Rev. C **79**, 044606 (2009).

[115] P. Navratil, R. Roth, and S. Quaglioni, Physics Letters B **704**, 379 (2011).

[116] K. Wildermuth and Y. Tang, *A Unified Theory of The Nucleus* (Braunschweig, Vieweg, 1977).

[117] D. Baye and E. Brainis, Phys. Rev. C **61**, 025801 (2000).

[118] P. Descouvemont and D. Baye, Rep. Prog. Phys. **73**, 3 (2010).

[119] P. Descouvemont, Comp. Phys. Comm. **200**, 199 (2016).

[120] S. Baroni, P. Navrátil, and S. Quaglioni, Phys. Rev. Lett. **110**, 022505 (2013).

[121] S. Baroni, P. Navrátil, and S. Quaglioni, Phys. Rev. C **87**, 034326 (2013).

[122] G. Hupin, S. Quaglioni, and P. Navrátil, Phys. Rev. Lett. **114**, 212502 (2015).

[123] E. J. Heller and H. A. Yamani, Phys. Rev. A **9**, 1201 (1974).

[124] H. A. Yamani and L. Fishman, Journal of Mathematical Physics **16**, 410 (1975).

[125] G. Filippov and I. Okhrimenko, Sov. J. Nucl. Phys.(Engl. Transl.);(United States) **32** (1980).

[126] I. Okhrimenko, Nuclear Physics A **424**, 121 (1984).

[127] Y. Smirnov and Y. Nechaev, Kinam **4**, 445 (1982).

[128] Y. I. Nechaev and Y. F. Smirnov, Soviet Journal of Nuclear Physics **35**, 808 (1982).

[129] J. Bang, A. Mazur, A. Shirokov, Y. F. Smirnov, and S. Zaytsev, Annals of Physics **280**, 299 (2000).

[130] A. Shirokov, Y. F. Smirnov, and S. Zaytsev, Modern problems in quantum theory, 1998.

[131] S. Zaitsev, Y. F. Smirnov, and A. Shirokov, Theoretical and mathematical physics **117**, 1291 (1998).

[132] Y. A. Lurie and A. M. Shirokov, Annals of Physics **312**, 284 (2004).

[133] V. Vasilevsky, A. V. Nesterov, F. Arickx, and J. Broeckhove, Phys. Rev. C **63**, 034606 (2001).

[134] V. Vasilevsky, A. V. Nesterov, F. Arickx, and J. Broeckhove, Phys. Rev. C **63**, 034607 (2001).

[135] V. Vasilevsky, A. V. Nesterov, F. Arickx, and J. Broeckhove, Phys. Rev. C **63**, 064604 (2001).

[136] Y. A. Lashko, G. Filippov, and V. Vasilevsky, Nuclear Physics A **958**, 78 (2017).

[137] A. Solovyev and S. Y. Igashov, Physics of Atomic Nuclei **80**, 890 (2017).

[138] S. Zaytsev, Teoreticheskaya i Matematicheskaya Fizika **115**, 263 (1998).

[139] S. Zaytsev, Teoreticheskaya i Matematicheskaya Fizika **121**, 424 (1999).

[140] S. Zaitsev and E. Kramar, Journal of Physics G: Nuclear and Particle Physics **27**, 2037 (2001).

[141] A. Shirokov, A. Mazur, S. Zaytsev, J. Vary, and T. Weber, Physical Review C **70**, 044005 (2004).

[142] A. M. Shirokov, A. I. Mazur, J. P. Vary, and E. A. Mazur, Phys. Rev. C **79**, 014610 (2009).

[143] A. Shirokov, A. Mazur, E. Mazur, and J. Vary, Applied Mathematics & Information Sciences **3**, 245 (2009).

[144] A. Shirokov, A. Mazur, J. Vary, and I. Mazur, Oscillator basis, scattering and nuclear structure, in *Journal of Physics: Conference Series* Vol. 403, p. 012021, IOP Publishing, 2012.

[145] A. M. Shirokov, A. I. Mazur, I. A. Mazur, and J. P. Vary, Phys. Rev. C **94**, 064320 (2016).

[146] I. Mazur, A. Shirokov, A. Mazur, and J. Vary, Physics of Particles and Nuclei **48**, 84 (2017).

[147] L. Blokhintsev, A. Mazur, I. Mazur, D. Savin, and A. Shirokov, Physics of Atomic Nuclei **80**, 226 (2017).

[148] L. Blokhintsev, A. Mazur, I. Mazur, D. Savin, and A. Shirokov, Physics of Atomic Nuclei **80**, 1093 (2017).

[149] A. M. Shirokov *et al.*, Phys. Rev. Lett. **117**, 182502 (2016).

[150] K. Kravvaris and A. Volya, Phys. Rev. C **100**, 034321 (2019).

[151] T. Dytrych, K. D. Sviratcheva, J. P. Draayer, C. Bahri, and J. P. Vary, J. Phys. G: Nucl. Part. Phys. **35**, 123101 (2008).

[152] K. D. Launey, T. Dytrych, and J. P. Draayer, Prog. Part. Nucl. Phys. **89**, 101 (2016).

[153] T. Dytrych *et al.*, (2018), 1810.05757.

[154] T. Dytrych *et al.*, Phys. Rev. Lett. **111**, 252501 (2013).

[155] T. Dytrych *et al.*, Comput. Phys. Commun. **207** (2016).

[156] T. Dytrych *et al.*, Phys. Rev. C **91**, 024326 (2015).

[157] K. D. Launey *et al.*, AIP Conference Proceedings **2038**, 020004 (2018).

[158] A. Bohr and B. R. Mottelson*Nuclear Structure* Vol. 1 (Benjamin, New York, 1969).

[159] J. P. Elliott, Proc. Roy. Soc. A **245**, 128 (1958).

[160] J. P. Elliott, Proc. Roy. Soc. A **245**, 562 (1958).

[161] J. P. Elliott and M. Harvey, Proc. Roy. Soc. A **272**, 557 (1962).

[162] G. Rosensteel and D. J. Rowe, Phys. Rev. Lett. **38**, 10 (1977).

[163] D. J. Rowe, Reports on Progr. in Phys. **48**, 1419 (1985).

[164] D. J. Rowe, G. Thiamova, and J. L. Wood, Phys. Rev. Lett. **97**, 202501 (2006).

[165] A. C. Dreyfuss, K. D. Launey, T. Dytrych, J. P. Draayer, and C. Bahri, Phys. Lett. B **727**, 511 (2013).

[166] J. Draayer, K. Weeks, and G. Rosensteel, Nucl. Phys. **A419**, 1 (1984).

[167] G. K. Tobin *et al.*, Phys. Rev. C **89**, 034312 (2014).

[168] O. Castaños, P. Hess, J. Draayer, and P. Rochford, Nucl. Phys. A **524**, 469 (1991).

[169] M. Jarrio, J. L. Wood, and D. J. Rowe, Nucl. Phys. A **528**, 409 (1991).

[170] C. Bahri and D. J. Rowe, Nucl. Phys. A **662**, 125 (2000).

[171] B. J. Verhaar, Nucl. Phys. **21**, 508 (1960).

[172] K. T. Hecht, Nucl. Phys. A **170**, 34 (1971).

[173] A. Ekström *et al.*, Phys. Rev. Lett. **110**, 192502 (2013).

[174] Y. Akiyama and J. P. Draayer, Comput. Phys. Commun. **5**, 405 (1973).

[175] J. P. Draayer, Y. Leschber, S. C. Park, and R. Lopez, Comput. Phys. Commun. **56**, 279 (1989).

[176] K. D. Launey, T. Dytrych, J. P. Draayer, G.-H. Sun, and S.-H. Dong, Int. J. Mod. Phys. E **24**, 1530005 (review) (2015).

[177] E. J. Reske, *Sp(6,R) symmetry and the giant quadrupole resonance of 24Mg*, PhD thesis, University of Michigan, 1984.

[178] Y. Suzuki and K. T. Hecht, Nucl. Phys. A **455**, 315 (1986).

[179] Y. Suzuki, Nucl. Phys. A **448**, 395 (1986).

[180] J. Escher and J. P. Draayer, J. Math. Phys. **39**, 5123 (1998).

[181] T. Dytrych, K. D. Sviratcheva, C. Bahri, J. P. Draayer, and J. P. Vary, Phys. Rev. Lett. **98**, 162503 (2007).

[182] A. E. McCoy, *Ab initio multi-irrep symplectic no-core configuration interaction calculations*, PhD thesis, University of Notre Dame, 2018.

[183] A. E. McCoy, M. A. Caprio, and T. Dytrych, Ann. Acad. Rom. Sci. Ser. Chem. Phys. Sci. **3**, 17 (2018).

[184] E. Epelbaum, H.-W. Hammer, and U.-G. Meißner, Rev. Mod. Phys. **81**, 1773 (2009).

[185] R. Machleidt and D. Entem, Phys. Rept. **503**, 1 (2011).

[186] R. Machleidt and F. Sammarruca, Physica Scripta **91**, 083007 (2016).

[187] U.-G. Meißner, Physica Scripta **91**, 033005 (2016).

[188] K. Hebeler, Phys. Rev. C **85**, 021002 (2012).

[189] M. Wang *et al.*, Chin. Phys. C **36**, 1603 (2012).

[190] D. Gazit, S. Quaglioni, and P. Navrátil, Phys. Rev. Lett. **103**, 102502 (2009).

[191] T. Duguet, H. Hergert, J. D. Holt, and V. Somà, Phys. Rev. C **92**, 034313 (2015).

[192] R. J. Furnstahl and A. Schwenk, Journal of Physics G: Nuclear and Particle Physics **37**, 064005 (2010).

[193] R. Furnstahl, Nucl. Phys. B (Proc. Suppl.) **228**, 139 (2012).

[194] S. N. More, S. König, R. J. Furnstahl, and K. Hebeler, Phys. Rev. C **92**, 064002 (2015).

[195] S. N. More, S. K. Bogner, and R. J. Furnstahl, Phys. Rev. C **96**, 054004 (2017).

[196] H. Hergert, S. K. Bogner, T. D. Morris, A. Schwenk, and K. Tsukiyama, Physics Reports **621**, 165 (2016).

[197] H. Hergert, Phys. Scripta **92**, 023002 (2017).

[198] M. Hjorth-Jensen, M. P. Lombardo, and U. van Kolck, *An Advanced Course in Computational Nuclear Physics*, Springer Lecture Notes in Physics Vol. 936 (Springer, 2017).

[199] N. M. Parzuchowski, T. D. Morris, and S. K. Bogner, Phys. Rev. C **95**, 044304 (2017).

[200] S. R. Stroberg *et al.*, Phys. Rev. Lett. **118**, 032502 (2017).

[201] E. Gebrerufael, K. Vobig, H. Hergert, and R. Roth, Phys. Rev. Lett. **118**, 152503 (2017).

[202] I. Shavitt and R. J. Bartlett, *Many-Body Methods in Chemistry and Physics: MBPT and Coupled-Cluster Theory* (Cambridge University Press, 2009).

[203] G. Hagen, T. Papenbrock, M. Hjorth-Jensen, and D. J. Dean, Reports on Progress in Physics **77**, 096302 (2014).

[204] K. G. Wilson, Phys. Rev. D **10**, 2445 (1974).

[205] H. M. Muller, S. E. Koonin, R. Seki, and U. van Kolck, Phys. Rev. **C61**, 044320 (2000), arXiv:nucl-th/9910038.

[206] D. Lee, Prog. Part. Nucl. Phys. **63**, 117 (2009), arXiv:0804.3501.

[207] B. Borasoy, H. Krebs, D. Lee, and U. G. Meissner, Nucl. Phys. **A768**, 179 (2006), arXiv:nucl-th/0510047.

[208] T. A. Lähde *et al.*, (2013), [PoSLATTICE2013,231(2014)].

[209] E. Epelbaum, H. Krebs, D. Lee, and U.-G. Meissner, Phys. Rev. Lett. **106**, 192501 (2011), arXiv:1101.2547.

[210] M. Pine, D. Lee, and G. Rupak, Eur. Phys. J. **A49**, 151 (2013).

[211] S. Elhatisari *et al.*, Nature **528**, 111 (2015), arXiv:1506.03513.

[212] S. Elhatisari *et al.*, Phys. Rev. Lett. **119**, 222505 (2017), arXiv:1702.05177.

[213] L. Schaller *et al.*, Nuclear Physics A **379**, 523 (1982).

[214] J. J. Thomson, Proc. London Math. Soc. , 197 (1884).

[215] G. Gamow, Z. Physik **51**, 204 (1928).

[216] A. F. J. Siegert, Phys. Rev. **56**, 750 (1939).

[217] T. Berggren, Nuclear Physics A **109**, 265 (1968).

[218] T. Berggren and P. Lind, Phys. Rev. C **47**, 768 (1993).

[219] T. Vertse, K. F. Pal, and Z. Balogh, Computer Physics Communications **27**, 308 (1982).

[220] G. L. Ixaru, M. Rizea, and T. Vertse, Computer Physics Communications **85**, 217 (1995).

[221] A. Baran, C. Noszaly, and T. Vertse, Computer Physics Communications **228**, 185 (2018).

[222] I. M. Gel'fand, G. E. Shilov, N. Y. Vilenkin, and M. I. Graev, *Generalized Functions. Vol. 1: Properties and Operations*, 1st ed. ed. (Academic Press, New York, 1964).

[223] I. M. Gel'fand and G. E. Shilov, *Generalized Functions. Vol. 2: Spaces of Fundamental and Generalized Functions*, 1st ed. ed. (Academic Press, New York, 1968).

[224] K. Maurin, *Generalized Eigenfunction Expansions and Unitary Representations of Topological Groups*, 1st ed. ed. (Polish Scientific, Warsaw, 1968).

[225] R. Id Betan, R. J. Liotta, N. Sandulescu, and T. Vertse, Phys. Rev. Lett. **89**, 042501 (2002).

[226] J. Rotureau, N. Michel, W. Nazarewicz, M. Płoszajczak, and J. Dukelsky, Phys. Rev. Lett. **97**, 110603 (2006).

[227] J. Rotureau, N. Michel, W. Nazarewicz, M. Płoszajczak, and J. Dukelsky, Phys. Rev. C **79**, 014304 (2009).

[228] K. Fossez, W. Nazarewicz, Y. Jaganathen, N. Michel, and M. Płoszajczak, Phys. Rev. C **93**, 011305(R) (2016).

[229] S. M. Wang, N. Michel, W. Nazarewicz, and F. R. Xu, Phys. Rev. C **96**, 044307 (2017).

[230] P. Navrátil, S. Quaglioni, G. Hupin, C. Romero-Redondo, and A. Calci, Phys. Scr. **91**, 053002 (2016).

[231] Y. Jaganathen, N. Michel, and M. Płoszajczak, Weakly bound systems, continuum effects and reactions, in *Journal of Physics: Conference Series* Vol. 403, p. 012022, IOP Publishing, 2012.

[232] Y. Jaganathen, N. Michel, and M. Płoszajczak, Phys. Rev. C **89**, 034624 (2014).

[233] F. De Grancey *et al.*, Physics Letters B **758**, 26 (2016).

[234] K. Fossez, N. Michel, M. Płoszajczak, Y. Jaganathen, and R. M. Id Betan, Phys. Rev. C **91**, 034609 (2015).

[235] G. Dong *et al.*, Journal of Physics G: Nuclear and Particle Physics **44**, 045201 (2017).

[236] A. Kumar *et al.*, Phys. Rev. Lett. **118**, 262502 (2017).

[237] A. Idini, C. Barbieri, and P. Navrátil, Acta Phys. Pol. B **48**, 273 (2017).

[238] J. Rotureau, P. Danielewicz, G. Hagen, F. M. Nunes, and T. Papenbrock, Phys. Rev. C **95**, 024315 (2017).

[239] M. Burrows *et al.*, Phys. Rev. C **99**, 044603 (2019), arXiv:1810.06442.

[240] M. Gennari, M. Vorabbi, A. Calci, and P. Navrátil, Phys. Rev. C **97**, 034619 (2018).

[241] W. H. Dickhoff and D. V. Neck, *Many-Body Theory Exposed! Propagator Description of Quantum Mechanics in Many-Body Systems*, 2nd ed. (World Scientific, New Jersey, 2008).

[242] H. Feshbach, Annals of Physics **5**, 357 (1958).

[243] H. Feshbach, Annals of Physics **19**, 287 (1962).

[244] C. Mahaux and H. A. Weidenmüller, (1969).

[245] H.-W. Barz, I. Rotter, and J. Höhn, Nuclear Physics A **275**, 111 (1977).

[246] K. Bennaceur, F. Nowacki, J. Okołowicz, and M. Płoszajczak, Nuclear Physics A **671**, 203 (2000).

[247] J. Rotureau, J. Okołowicz, and M. Płoszajczak, Phys. Rev. Lett. **95**, 042503 (2005).

[248] J. Rotureau, J. Okołowicz, and M. Płoszajczak, Nuclear Physics A **767**, 13 (2006).

[249] J. Okołowicz, M. Płoszajczak, and I. Rotter, Physics Reports **374**, 271 (2003).

[250] N. Michel, W. Nazarewicz, M. Płoszajczak, and K. Bennaceur, Phys. Rev. Lett. **89**, 042502 (2002).

[251] R. Id Betan, R. J. Liotta, N. Sandulescu, and T. Vertse, Phys. Rev. Lett. **89**, 042501 (2002).

[252] N. Michel, W. Nazarewicz, M. Płoszajczak, and J. Okołowicz, Phys. Rev. C **67**, 054311 (2003).

[253] N. Michel, W. Nazarewicz, M. Płoszajczak, and T. Vertse, Journal of Physics G: Nuclear and Particle Physics **36**, 013101 (2008).

[254] Y. Suzuki and K. Ikeda, Phys. Rev. C **38**, 410 (1988).

[255] S. R. White, Phys. Rev. B **48**, 10345 (1993).

[256] J. Rotureau, N. Michel, W. Nazarewicz, M. Płoszajczak, and J. Dukelsky, Phys. Rev. Lett. **97**, 110603 (2006).

[257] J. Rotureau, N. Michel, W. Nazarewicz, M. Płoszajczak, and J. Dukelsky, Physical Review C **79**, 014304 (2009).

[258] A. Mercenne, N. Michel, and M. Płoszajczak, Phys. Rev. C **99**, 044606 (2019).

[259] G. Papadimitriou, J. Rotureau, N. Michel, M. Płoszajczak, and B. R. Barrett, Phys. Rev. C **88**, 044318 (2013).

[260] K. Fossez, J. Rotureau, N. Michel, and M. Płoszajczak, Phys. Rev. Lett. **119**, 032501 (2017).

[261] J. Bardeen, J. N. Cooper, and J. R. Schrieffer, Physical Review **106**, 162 (1957).

[262] A. Bohr, M. B. R., and D. Pines, Physical Review **110**, 936 (1958).

[263] S. T. Belyaev, Mat. Fys. Medd. Dan. Vid. Selsk. **31**, 11 (1959).

[264] R. W. Richardson, Physics Letters **3**, 277 (1963).

[265] G. Sierra, J. Dukelsky, G. G. Dussel, J. von Deft, and F. Braun, Physical Review B **61**, 11890 (2000).

[266] D. M. Brink and R. A. Broglia, *Nuclear superfluidity. Pairing in Finite System* (Cambridge University Press, 2005).

[267] X. Guan *et al.*, Phys. Rev. C **86**, 024313 (2012).

[268] J. Dukelsky and S. Pittel, *Fifty Years of Nuclear BCS* (Eds R. Broglia and V. Zelevinsky. Singapore, World Scientific Publishing Company, 2013).

[269] M. Hasegawa and K. Kaneko, Physical Review C **67**, 024304 (2003).

[270] R. Id Betan, Physical Review C **85**, 064309 (2012).

[271] A. Mercenne, N. Michel, and M. Płoszajczak, Acta Phys. Pol. B **47**, 967 (2016).

[272] R. M. Id Betan, IOP Conf. Series: Journal of Physics: Conf. Series **839**, 012033 (2017).

[273] R. G. Thomas, Prog. Theor. Phys. **12**, 253 (1954).

[274] H. J. Mang, Phys. **148**, 582 (1957).

[275] G. Dodig-Crnkovic, F. A. Janouch, R. J. Liotta, and Z. Xiaolin, Phys. Scr. **37**, 523 (1988).

[276] D. S. Delion and J. Suhonen, Phys. Rev. C **61**, 024304 (2000).

[277] R. Id Betan and W. Nazarewicz, Physical Review C **86**, 034338 (2012).

[278] Y. Jaganathen, R. M. Id Betan, N. Michel, W. Nazarewicz, and M. Płoszajczak, Physical Review C **96**, 054316 (2017).

[279] K. Auranen, D. Seweryniak, M. Albers, and et al., Physical Review Letters **121**, 182501 (2018).

[280] B. S. Hu, Q. Wu, Z. H. Sun, and F. R. Xu, Phys. Rev. C **99**, 061302(R) (2019).

[281] R. D. Lawson and R. D. Lawson, *Theory of the nuclear shell model* (Clarendon Press Oxford, 1980).

[282] H. Masui, K. Katō, N. Michel, and M. Płoszajczak, Phys. Rev. C **89**, 044317 (2014).

[283] G. Källén, Helvetica Physica Acta **25**, 417 (1952).

[284] H. Lehmann, Il Nuovo Cimento (1943-1954) **11**, 342 (1954).

[285] W. Dickhoff and C. Barbieri, Progress in Particle and Nuclear Physics **52**, 377 (2004).

[286] C. Barbieri and A. Carbone, *Self-Consistent Green's Function Approaches* (Springer International Publishing, Cham, 2017), pp. 571–644.

[287] A. Idini, F. Barranco, and E. Vigezzi, Phys. Rev. C **85**, 014331 (2012).

[288] B. Holm and U. von Barth, Phys. Rev. B **57**, 2108 (1998).

[289] A. Rios, A. Polls, and W. H. Dickhoff, Phys. Rev. C **89**, 044303 (2014).

[290] D. Ding *et al.*, Phys. Rev. C **94**, 025802 (2016).

[291] J. Schirmer, Phys. Rev. A **26**, 2395 (1982).

[292] M. Bender, P.-H. Heenen, and P.-G. Reinhard, Rev. Mod. Phys. **75**, 121 (2003).

[293] R. Navarro Pérez, N. Schunck, A. Dyhdalo, R. J. Furnstahl, and S. K. Bogner, Phys. Rev. **C97**, 054304 (2018), arXiv:1801.08615.

[294] M. Piarulli *et al.*, Phys. Rev. **C91**, 024003 (2015), arXiv:1412.6446.

[295] M. Kortelainen *et al.*, Phys. Rev. **C89**, 054314 (2014), arXiv:1312.1746.

[296] K. M. Nollett and R. B. Wiringa, Phys. Rev. C **83**, 041001 (2011).

[297] A. C. Fonseca and A. Deltuva, Few Body Syst. **58**, 46 (2017).

[298] A. Deltuva and A. C. Fonseca, Phys. Rev. **C95**, 024003 (2017), arXiv:1702.01034.

[299] M. Viviani *et al.*, Phys. Rev. **C95**, 034003 (2017), arXiv:1610.09140.

[300] A. Deltuva and A. Fonseca, Phys.Rev. **C79**, 014606 (2009).

[301] T. Furumoto, K. Tsubakihara, S. Ebata, and W. Horiuchi, Phys. Rev. **C99**, 034605 (2019).

[302] S. Weppner, R. Penney, G. Diffendale, and G. Vittorini, Phys.Rev. **C80**, 034608 (2009).

[303] A. Koning and J. Delaroche, Nucl.Phys. **A713**, 231 (2003).

[304] R. Varner, W. Thompson, T. McAbee, E. Ludwig, and T. Clegg, Phys.Rept. **201**, 57 (1991).

[305] K. M. Watson, Phys. Rev. **89**, 575 (1953).

[306] N. C. Francis and K. M. Watson, Phys. Rev. **92**, 291 (1953).

[307] A. K. Kerman, H. McManus, and R. M. Thaler, Ann. Phys. **8**, 551 (1959).

[308] E. R. Siciliano and R. M. Thaler, Phys. Rev. **C16**, 1322 (1977).

[309] A. Idini, G. Potel, F. Barranco, E. Vigezzi, and R. A. Broglia, Phys. Rev. C **92**, 031304 (2015).

[310] R. J. Bartlett and M. Musiał, Rev. Mod. Phys. **79**, 291 (2007).

[311] A. Koning and J. Delaroche, Nuclear Physics A **713**, 231 (2003).

[312] A. Ekström *et al.*, Phys. Rev. C **91**, 051301 (2015).

[313] G. Hagen *et al.*, Nature Physics **12**, 186 (2016).

[314] R. F. Garcia Ruiz *et al.*, Nature Physics (2016), 1602.07906.

[315] J. Rotureau, P. Danielewicz, G. Hagen, G. R. Jansen, and F. M. Nunes, Phys. Rev. C **98**, 044625 (2018).

[316] C. R. Chinn, C. Elster, and R. M. Thaler, Phys. Rev. **C47**, 2242 (1993).

[317] M. Burrows *et al.*, Phys. Rev. **C97**, 024325 (2018), arXiv:1711.07080.

[318] C. R. Chinn, C. Elster, R. M. Thaler, and S. P. Weppner, Phys. Rev. **C52**, 1992 (1995).

[319] M. L. Goldberger and K. M. Watson, *Collision Theory/* (John Wiley and Sons, Inc.„ New York, London, Sydney :, 1964).

[320] R. Crespo, R. C. Johnson, and J. A. Tostevin, Phys. Rev. **C46**, 279 (1992).

[321] G. A. Moss *et al.*, Phys. Rev. **C21**, 1932 (1980).

[322] C. W. Glover *et al.*, Phys. Rev. **C31**, 1 (1985).

[323] V. D. Efros, W. Leidemann, and G. Orlandini, Physics Letters B **338**, 130 (1994).

[324] V. D. Efros, W. Leidemann, G. Orlandini, and N. Barnea, Journal of Physics G: Nuclear and Particle Physics **34**, R459 (2007).

[325] S. Bacca, N. Barnea, G. Hagen, G. Orlandini, and T. Papenbrock, Phys. Rev. Lett. **111**, 122502 (2013).

[326] R. B. Baker *et al.*, AIP Conference Proceedings **2038**, 020006 (2018).

[327] G. Hagen *et al.*, Nature Phys **12**, 186 (2016).

[328] M. Miorelli *et al.*, Phys. Rev. C **94**, 034317 (2016).

[329] C. Ji, S. Bacca, N. Barnea, O. J. Hernandez, and N. N. Dinur, Journal of Physics G: Nuclear and Particle Physics **45**, 093002 (2018).

[330] E. Dagotto, Rev. Mod. Phys. **66**, 763 (1994).

[331] N. Nevo Dinur, N. Barnea, C. Ji, and S. Bacca, Phys. Rev. C **89**, 064317 (2014).

[332] N. Auerbach and B. Minh Loc, Phys. Rev. C **98**, 064301 (2018).

[333] S. Elhatisari, D. Lee, U.-G. Meißner, and G. Rupak, Eur. Phys. J. A **52**, 174 (2016), arXiv:1603.02333.

[334] M. Luscher, Commun. Math. Phys. **104**, 177 (1986).

[335] S. N. More, A. Ekström, R. J. Furnstahl, G. Hagen, and T. Papenbrock, Phys. Rev. C **87**, 044326 (2013), arXiv:1302.3815.

[336] R. J. Furnstahl, T. Papenbrock, and S. N. More, Phys. Rev. **C89**, 044301 (2014), arXiv:1312.6876.

[337] R. J. Furnstahl, G. Hagen, T. Papenbrock, and K. A. Wendt, J. Phys. G **42**, 034032 (2015), arXiv:1408.0252.

[338] K. A. Wendt, C. Forssén, T. Papenbrock, and D. Sääf, Phys. Rev. C **91**, 061301 (2015), arXiv:1503.07144.

[339] S. Koenig, D. Lee, and H. W. Hammer, Phys. Rev. Lett. **107**, 112001 (2011), arXiv:1103.4468.

[340] S. Koenig, D. Lee, and H. W. Hammer, Annals Phys. **327**, 1450 (2012), arXiv:1109.4577.

[341] S. König and D. Lee, Phys. Lett. B **779**, 9 (2018), arXiv:1701.00279.

[342] T. Busch, B.-G. Englert, K. Rzażewski, and M. Wilkens, Foundations of Physics **28**, 549 (1998).

[343] E. L. Bolda, E. Tiesinga, and P. S. Julienne, Phys. Rev. A **66**, 013403 (2002).

[344] M. Block and M. Holthaus, Phys. Rev. A **65**, 052102 (2002).

[345] A. Suzuki, Y. Liang, and R. K. Bhaduri, Phys. Rev. A **80**, 033601 (2009).

[346] T. Luu, M. J. Savage, A. Schwenk, and J. P. Vary, Phys. Rev. **C82**, 034003 (2010), arXiv:1006.0427.

[347] J. Rotureau, I. Stetcu, B. R. Barrett, and U. van Kolck, Phys. Rev. **C85**, 034003 (2012), arXiv:1112.0267.

[348] X. Zhang *et. al.,*, in preparation (2018).

[349] Private communication with James P. Vary (2018).

[350] R. Furnstahl, D. Phillips, and S. Wesolowski, J.Phys. **G42**, 034028 (2015), arXiv:1407.0657.

[351] M. Luscher, Nucl. Phys. **B354**, 531 (1991).

[352] M. T. Hansen and S. R. Sharpe, Phys. Rev. **D90**, 116003 (2014), arXiv:1408.5933.

[353] H. W. Hammer, J. Y. Pang, and A. Rusetsky, JHEP **10**, 115 (2017), arXiv:1707.02176.

[354] X. Zhang, K. M. Nollett, and D. R. Phillips, Phys. Rev. **C89**, 051602 (2014), arXiv:1401.4482.

[355] X. Zhang, K. M. Nollett, and D. R. Phillips, EPJ Web Conf. **113**, 06001 (2016), arXiv:1508.06935.

[356] X. Zhang, K. M. Nollett, and D. R. Phillips, Phys. Lett. **B751**, 535 (2015), arXiv:1507.07239.

[357] X. Zhang, K. M. Nollett, and D. R. Phillips, (2017), arXiv:1708.04017.

[358] A. Mukhamedzhanov and F. Nunes, Nucl.Phys. **A708**, 437 (2002), arXiv:nucl-th/0205045.

[359] D. Baye and E. Brainis, Phys.Rev. **C61**, 025801 (2000).

[360] D. Baye, Phys.Rev. **C62**, 065803 (2000).

[361] H. Esbensen, Phys. Rev. C **70**, 047603 (2004).

[362] P. Yin, W. Du, W. Zuo, X. Zhao, and J. P. Vary, arXiv:1910.10586 (2019).

[363] S. Koonin, D. Dean, and K. Langanke, Phys. Rept. **278**, 1 (1997).

[364] Y. Alhassid, D. Dean, S. Koonin, G. Lang, and W. Ormand, Phys. Rev. Lett. **72**, 613 (1994), arXiv:nucl-th/9310026.

[365] Y. Alhassid, Auxiliary-field quantum Monte Carlo methods in nuclei, in *Emergent phenomena in atomic nuclei from large-scale modeling: a symmetry-guided perspective*, edited by K. D. Launey, p. 229, World Scientific Publishing Co., 2017.

[366] V. Zelevinsky, B. Brown, N. Frazier, and M. Horoi, Phys. Reports **276**, 315 (1996).

[367] M. Horoi, A. Volya, and V. Zelevinsky, Phys. Rev. Lett. **82**, 2064 (1999).

[368] M. Horoi, M. Ghita, and V. Zelevinsky, Phys. Rev. C **69**, 041307(R) (2004).

[369] M. Horoi and V. Zelevinsky, Phys. Rev. Lett. **98**, 262503 (2007).

[370] R. Sen'kov, M. Horoi, and V. Zelevinsky, Phys. Lett. B **702**, 413 (2011).

[371] R. Sen'kov, M. Horoi, and V. Zelevinsky, Computer Physics Communications **184**, 215 (2013).

[372] R. Sen'kov and V. Zelevinsky, Phys. Rev. C **93**, 064304 (2016).

[373] M. Horoi, J. Kaiser, and V. Zelevinsky, Phys. Rev. C **67**, 054309 (2003), Reprinted in: V.K.B. Kota and R.U. Haq, eds., "Spectral Distributions in Nuclei and Statistical Spectroscopy" (World Scientific, Singapore, 2010), p. 633.

[374] V. K. B. Kota and R. U. Haq, *Spectral Distributions in Nuclei and Statistical Spectroscopy* (World Scientific Publishing Co., 2010).

[375] K. D. Sviratcheva, J. P. Draayer, and J. P. Vary, Nucl. Phys. A **786**, 31 (2007).

[376] C. W. Johnson, Physics Letters B **750**, 72 (2015).

[377] S. Karampagia, R. Sen'kov, and V. Zelevinsky, Atomic Data and Nuclear Data Tables **120**, 1 (2018).

[378] S. Karampagia and V. Zelevinsky, Phys. Rev. C **94**, 014321 (2016).

[379] S. Karampagia, A. Renzaglia, and V. Zelevinsky, Nucl. Phys. A **962**, 46 (2017).

[380] V. Zelevinsky, S. Karampagia, and A. Berlaga, Phys. Lett. B **783**, 428 (2018).

[381] T. Duguet and G. Hagen, Phys. Rev. C **85**, 034330 (2012).

[382] R. G. Newton, *Scattering Theory of Waves and Particles*, 2nd ed. ed. (Springer-Verlag, New York, 1982).

[383] R. M. Id Betan, R. J. Liotta, N. Sandulescu, and T. Vertse, Phys. Rev. Lett. **89**, 042501 (2002).

[384] H. Masui, M. Aoyama, and D. Baye, Prog. Theor. Exp. Phys. **2013**, 123A02 (2013).

[385] N. Michel, J. Math. Phys. **49**, 022109 (2008).

[386] A. M. Dykhne and A. V. Chaplik, Sov. Phys. JETP **13**, 1002 (1961).

[387] B. Gyarmati and T. Vertse, Nucl. Phys. A **160**, 523 (1971).

[388] B. Simon, Phys. Lett. A **71**, 211 (1979).

[389] I. J. Thompson and A. R. Barnett, J. Comp. Phys. **64**, 490 (1986).

[390] N. Michel, Comp. Phys. Comm. **176**, 232 (2007).